공학박사 학위논문

Lifetime - Configurable Material Systems for Soft Robotics

수명제어가 가능한
소프트 로봇용 재료 시스템 연구

2023 년 8 월

서울대학교 대학원
재료공학부 재료공학전공
오 민 하

Lifetime - Configurable Material Systems for Soft Robotics

지도 교수 강 승 균

이 논문을 공학박사 학위논문으로 제출함
2023 년 8 월

서울대학교 대학원
재료공학부 재료공학전공
오 민 하

오민하의 공학박사 학위논문을 인준함
2023 년 5 월

위 원 장 안 철 희 (인)

부위원장 강 승 균 (인)

위 원 권 민 상 (인)

위 원 김 상 엽 (인)

위 원 고 제 성 (인)

Abstract

Min-Ha Oh

Department of Material Science and Engineering

The Graduate School

Seoul National University

Soft materials refer to a variety of materials with relatively soft mechanical properties among various material groups. Owing to these soft mechanical properties, soft materials have been studied by many scientists and engineers in various fields such as engineering plastics, biomaterials, electronic devices, and robotics. Recently, research on soft robots, which utilize these soft materials, has been actively conducted.

Soft robots have the advantage of having a wide range of motion due to their high deformability, and they can also make seamless contact with external objects and surfaces. Moreover, they can be made of materials that are relatively similar texture and mechanical properties to those found in the human body, making it possible to mimic biological structures. Additionally, they can be manufactured at a low cost and in large quantities through various processes, such as 3D printing. These various advantages and

potential applications in diverse fields have led to the rapid growth of the soft robotics market worldwide, with several companies established and operating in the production of soft robots.

The ultimate goal of soft robot research lies in the sophisticated mimicry of humans or living organisms. Currently, various biomimetic soft robots are being studied and developed. Among them are representative examples that imitate the movements of living organisms, such as cheetah mimic robots that mimic the way animals walk, saltwater mimetic robots, and caterpillar mimetic robots. Furthermore, recent studies have reported research that imitates the growth of robots by embedding small 3D printers into them, as well as soft robots that imitate the wound healing of living organisms using self-healing polymers. However, these studies are currently limited to mimicking only one function at a time. Therefore, the future of soft robots aims to simulate the entire life of living organisms.

We focused on the study of decomposable soft robots that mimic robot death by progressing towards an irreversible transition to an unrecoverable state, either when the robot's functionality is no longer required or when its function cannot be performed. In the course of this research, the standard material that constitutes most of the robot's body, silicon-based crosslinked polymers, posed the

biggest challenge. Silicon crosslinked polymers have excellent mechanical properties due to strong chemical bonding and are highly resistant to high temperatures and chemicals, making them widely used in the field of soft robots. However, their structural characteristics have made decomposition difficult. To overcome this, people have focused on researching biodegradable polymers that dissolve in water. These polymers have a weakness in being vulnerable to water and a fatal disadvantage of having to determine the material's lifespan by adjusting its thickness due to decomposition reactions during use.

In this study, we developed a material that has excellent mechanical properties and ensures operational stability without undergoing decomposition reactions during operation by adding various photoresponsive agents that generate acids when exposed to light to various polymers that already have good mechanical properties. In addition, we conducted qualitative and quantitative characterization of the decomposition reaction through chemical and thermodynamic analysis of these materials and presented the mechanism of the decomposition reaction. Furthermore, we added and synthesized self-diagnostic molecules that change color in response to external stimuli and self-healing molecules that can be healed with low energy to develop state-of-the-art soft robotic

materials.

Keyword: soft material, soft robotics, soft electronics, polymer engineering, organic analysis

Student Number: 2019-35593

Table of Contents

Chapter 1. Introduction 6

1.1 Objective of the Thesis 7

1.2 Outline of the Thesis 10

Chapter 2. Research Background 11

2.1 Soft Robotics 12

2.1.1 Soft Robotics Characteristics 12

2.1.2 Biomimic Soft Robotics 17

2.2 Soft Materials for Transient Soft Robotics.....19

2.2.1 Passive Transient Soft Materials 19

2.2.2 Active Transient Soft Materials 21

Chapter 3. Photodegradable Pneumatic Soft Robots

..... 24

3.1 Introduction 25

3.2 Overall strategy of research 30

3.3 Material Degradation Analysis 33

3.3.1 Structural Analysis 33

3.3.2 Kinetics Analysis 43
3.4 Robotic Applications.....54
3.4.1 Transformable Soft Actuators 54
3.4.2 Gaiting Soft Robots with Electronics 64
3.5 Experimental Verification 76
3.6 Chapter Summary 82

Chapter 4. Photodegradable Magnetic Soft Robots 84

4.1 Introduction 85
4.2 Overall strategy of research 89
4.3 Material Degradation Analysis 93
4.3.1 Structural Analysis 93
4.3.2 Kinetics Analysis 96
4.4 Robotic Applications.....101
4.4.1 SAM capsulized magnetic particles 101
4.4.2 Magnetically actuated trigger transient actuators.107
4.5 Experimental Verification 112
4.6 Chapter Summary 116

Chapter 5. Lifecycle Configurable Soft Robots .. 117

5.1 Introduction 118
5.2 Overall strategy of research 122

5.3 Material design 126

5.3.1 Self Reporting System 126

5.3.2 Self Healing System 129

5.3.3 Self Healing, Reporting and Degrading combined System 131

5.4 Application to Soft Robotics.....134

5.4.1 Soft Robot demonstration.....134

5.4.2 Soft Electronics Integration 135

5.5 Chapter Summary 137

Chapter 6. Conclusion..... 139

References 143

Abstract in Korean 165

Curriculum Vitae 168

Acknowledgement 169

LIST OF FIGURES

Figure 1. Key characteristics of soft robotics.

Figure 2. Global emerging field–soft robotics

Figure 3. Present and future biomimicry of soft robotics.

Figure 4. Passive transient materials for soft robotics.

Figure 5. Active transient materials for soft robotics.

Figure 6. Overview of transient DPI–HFP/silicone composites and a –lifetime configurable soft robot.

Figure 7. Decomposition chemistry of DPI–HFP/ecoflex 00–30 composites that utilizes photoinduced fluoride.

Figure 8. Decomposition chemistry of DPI–HFP/sylgard–184 composites that utilizes photoinduced fluoride.

Figure 9. ^{29}Si-NMR analysis of DPI-HFP/linear PDMS and DPI-HFP/sylgard-184 composites that utilizes photoinduced fluoride.

Figure 10. FT-IR and GPC analysis of DPI-HFP/linear composites that utilizes photoinduced fluoride.

Figure 11. Decomposition kinetics of the DPI-HFP/ecoflex 00-30 composite.

Figure 12. Decomposition sequential images of the DPI-HFP/sylgard-184 composite.

Figure 13. DSC analysis of DPI-HFP/ecoflex 00-30 composite.

Figure 14. Decomposition kinetics of the DPI-HFP/Sylgard-184 composite.

Figure 15. On-demand motion transformation by triggering the decomposition of DPI-HFP/silicone.

Figure 16. Remotely laser-induced triggering the decomposition of DPI-HFP/silicone and its analysis.

Figure 17. Laser induced decomposition chemistry of DPI-HFP/silicone composites that utilizes photoinduced fluoride.

Figure 18. On-demand motion transformation by laser-induced triggering the decomposition of DPI-HFP/silicone.

Figure 19. Demonstration of pneumatic gaiting robot developed using flexible and stretchable DPI-HFP/silicone.

Figure 20. Integration and characterization of electronics for temperature, strain, and photo sensing.

Figure 21. Autonomic operation of a life-time controlled gaiting robot.

Figure 22. Overall strategy of magnetically actuated trigger transient polymer composite and a lifetime controllable soft actuator.

Figure 23. Structural analysis of photo-triggered decomposition of PPC polymer by PAG.

Figure 24. Decomposition reaction kinetic analysis of PPC polymer by PAG using TGA analysis.

Figure 25. Magnetic particle modifications for embedding in PPC polymer and various analyses for confirming decomposition of PPC polymer.

Figure 26. Application of trigger transient composites to kirigami soft robot.

Figure 27. Photo-induced degradation of kirigami soft robot.

Figure 28. Scheme of autonomous lifetime-configurable soft material.

Figure 29. Overall strategy of autonomous lifetime-configurable soft material.

Figure 30. Working mechanism of self-reporting material and polymerization strategy.

Figure 31. Healing mechanism of dynamic bond-based self-healing

materials and real images.

Figure 32. Integration strategy of self-healing materials and self-reporting material via PDMS linker.

Chapter 1.

INTRODUCTION

Contents

1.1 Objective of the Thesis 7

1.2 Outline of the Thesis 10

1.1. Objective of the Thesis

Soft materials generally refer to various materials with soft mechanical properties. Due to their mechanical properties, which include plastics, electronic components, medical devices, biomedical materials, and energy storage systems, soft materials have been widely used in various fields. Building upon these diverse applications, recent research in the field of soft robotics, which uses soft materials, has emerged and is currently being actively pursued.

The development and application of soft materials are closely related to the advancement of soft robotics technology. Soft materials are flexible, bendable, and stretchable, making them suitable as components of soft robots. Thus, the development of soft materials is driving the development of soft robotics technology. Soft robots are made up of flexible and elastic components, rather than traditional building blocks. These components include various soft materials, such as elastomers, fiber-reinforced elastomers, and flexible conductive polymers. The development and application of soft materials have led to innovative technological advances in various fields of soft robotics. For example, research is underway in the medical field to develop robots that can explore and treat internal organs using soft robotics technology. Furthermore, soft

robotics technology is being applied to develop flexible robot systems that allow humans and robots to work together in the manufacturing industry. Additionally, research is also being conducted in various fields, such as earthquake response robots, structural robots, and space exploration robots. The development and application of soft materials in these areas have led to the recognition of soft robotics technology as a versatile technology that can be used in everyday life and in industrial fields.

The objective of this paper is to increase the lifespan and functionality of soft robots through the development and application of polymer composite materials used in the field of soft robotics. To achieve this, the paper focuses on the development of new polymer composite materials and their application to soft robot components, in order to investigate ways to control the lifespan of soft robots. Thus, the paper presents research results on the development and application of new materials in the field of soft robotics and contributes to the development of more reliable soft robots. Additionally, the paper provides a detailed analysis of the mechanical properties and chemical/kinetic analysis of the newly developed materials and how they can be optimized for soft robotics applications. Ultimately, this research aims to promote the development of soft robotics technology by providing a foundation

for the development and application of new materials in the field of soft robotics.

1.2. Outline of the Thesis

The present study comprises six distinct chapters which delve into various aspects of soft robotics and transient soft robotic materials. The introductory chapter briefly outlines the thesis, while the second chapter provides a comprehensive overview of the aforementioned topics, including both passive and active materials. Furthermore, past research on soft robotics and soft materials is presented in this section. Chapter 3 presents a pioneering photodegradable pneumatic soft robot that employs on-demand transient soft materials. In Chapter 4, a magnetically actuated photodegradable soft robot is detailed, with a thorough discussion of the results obtained. The fifth chapter highlights a lifecycle configurable soft robot, which represents a significant contribution to the field of soft robotics. Finally, Chapter 6 offers a compelling conclusion about the developments of this study. The reference section is presented at the end of the thesis, documenting the sources used for this research.

Chapter 2.

RESEARCH BACKGROUND

Contents

2.1 Soft Robotics 12

2.1.1 Soft Robotics Characteristics 12

2.1.2 Biomimic Soft Robotics 17

2.2 Soft Materials for Transient Soft Robotics 19

2.2.1 Passive Transient Soft Materials 19

2.2.2 Active Transient Soft Materials 21

2.1. Soft Robotics

2.1.1 Soft Robotics Characteristics

The development of robots in various fields has been highlighted due to the advancement of the fourth industrial revolution, leading to rapid progress in the field of robotics. Starting with the development of industrial robots, advanced robots equipped with features such as sensors and image recognition technology that enable interaction with humans have been developed since the late 1990s. The development of robot technology has also led to the emergence of robots that can be applied to human daily life, such as surgical robots, household robots, military robots, and space exploration robots. Recently, the combination of artificial intelligence and robot technology has led to the development of even more advanced robots, such as artificial intelligence robots with human-like intelligence, drones that can operate in real environments, and robots capable of supporting human body weight. Thanks to these various developments, the field of robotics is used in various industries such as industry, military, medicine, and home, and is expected to further develop in the future.

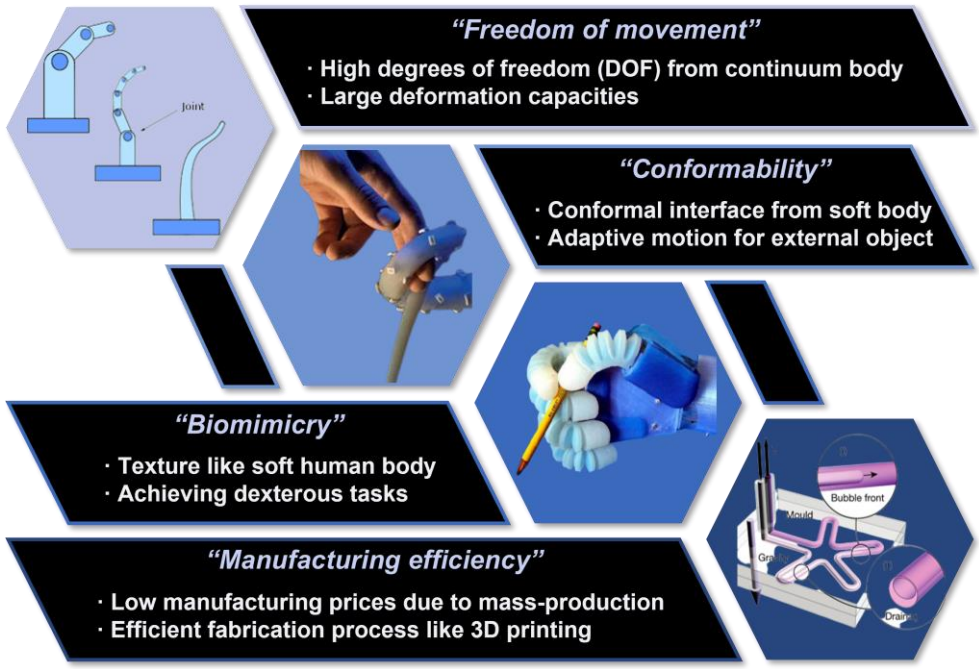

Figure 1. Key characteristics of soft robotics.

As robots have evolved in various ways, researchers have proposed a new research field called "soft robotics" based on soft materials rather than traditional rigid materials.

Figure 1 illustrates the characteristics of soft robotics. Soft robots made from such materials have a high degree of freedom and can perform movements similar to those of the human body and have the advantage of being suitable for performing fine and complex tasks. Furthermore, traditional robots can be difficult to work in narrow spaces because they are made of rigid structures. However, soft robots have the advantage of being able to move freely in narrow spaces because they are made of flexible structures and can achieve conformal contact with complex objectives. In addition, because the material has a texture similar to that of the human body, it is advantageous for biomimicry. Soft robots also use minimal power to operate, which can lead to longer battery life and energy efficiency and can be easily mass-produced due to the low cost and various fabrication processes such as 3D printing.

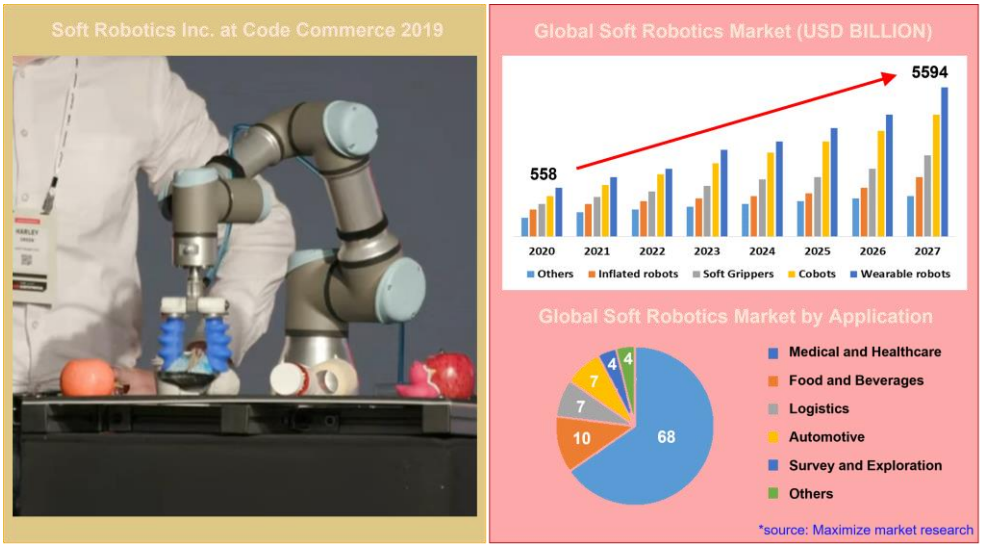

Figure 2. Global emerging field-soft robotics

Based on these diverse features, there has been a significant increase in demand for soft robots in the global market, and companies that produce and sell soft robots have been established and are operating. (Figure 2) The demand for soft robots can be seen in various fields in the global market, especially in the medical and healthcare fields where there is a lot of interface with humans and demand is increasing significantly, and steady demand is also observed in industries such as food, logistics, and automotive. With this growth in the industry, the need for education and training for researchers, engineers, and technicians in the field of soft robotics is also increasing.

2.1.2 Biomimicry Soft Robotics

Currently, research on biomimicry soft robotics aims to design soft robots that mimic the movement and structure of animals, with the goal of creating robots with exceptional movement abilities and functionality. Previous studies have primarily focused on developing soft robots by mimicking animals such as snakes, octopuses, fish, and insects. For instance, research has been conducted to create legless robots that mimic the movement of snakes, or robots that perform complex tasks by mimicking the arms of octopuses. Furthermore, recent research has also been conducted to develop

humanoid robots by mimicking the structure and function of the human body, which could be utilized as surgical robots or assistive devices in the medical field.

These various studies have predominantly focused on investigating individual functions (Figure 3, left). For example, cheetah-inspired robots that mimic the movement of animals, growth robots that gradually grow by embedding 3D printers, and self-healing soft robots created by mimicking the regenerative abilities of living organisms are prime examples. However, it is anticipated that future soft robots will move towards mimicking the entire life cycle of an organism (Figure 3, right). For instance, this refers to robots that are born, grow, learn on their own, and engage in activities in society with both robots and humans. They then heal themselves if injured and ultimately die like humans. To achieve such robots, it is essential to conduct research on materials that possess diverse functionalities from a materials engineering standpoint. However, research in this area has yet to be fully activated, with most studies still focusing on improving performance by concentrating on a single function. In this research, we aim to develop future-oriented, lift-cycle configurable soft materials through materials engineering approaches and apply them to soft robots.

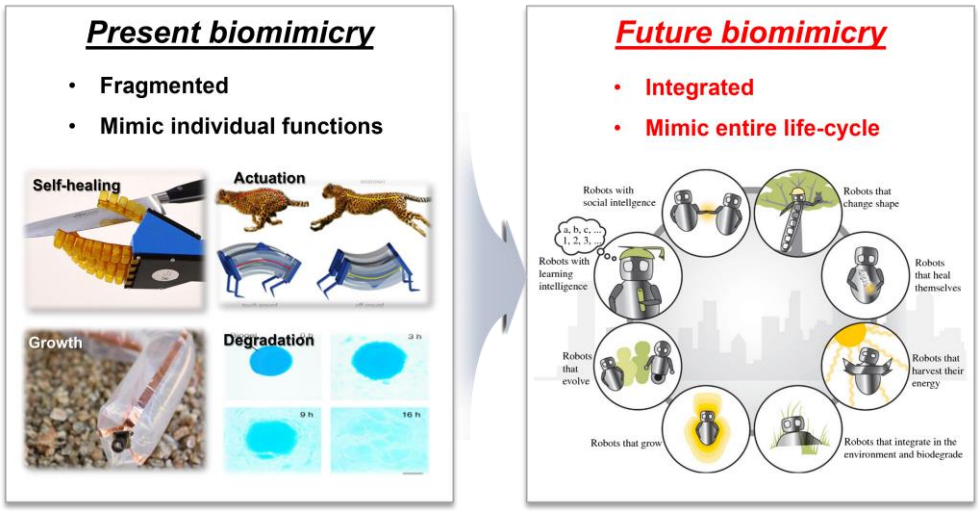

Figure 3. Present and future biomimicry of soft robotics.

2.2. Soft Materials for Transient Soft Robotics

2.2.1 Passive Transient Soft Materials

Soft robots exhibit significant deformations during actuation, and many of the highly deformable materials with transient characteristics are passive transient materials. These materials undergo degradation reactions through hydrolysis or enzymes. Typically, these materials contain a polymer backbone with carboxylic groups that experience cleavage upon the addition of water from external sources, as shown in Figure 4. The Kaltenbrunner group in Austria has implemented soft actuators using gelatin and included the degradation of this material in their design, as demonstrated in Figure 4 (left bottom).

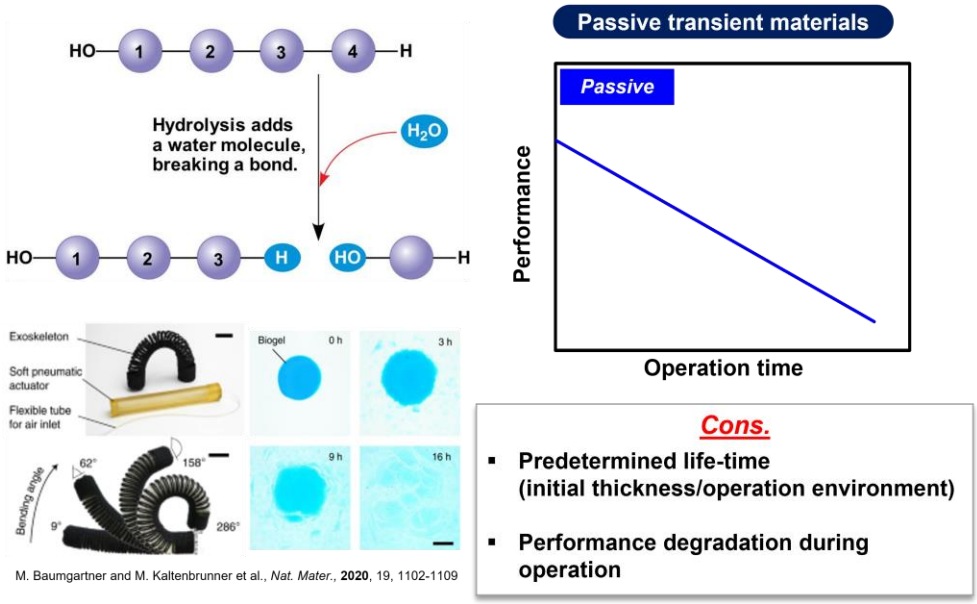

Figure 4. Passive transient materials for soft robotics.

Passive transient materials possess excellent mechanical properties that make them suitable for applications in soft robotics. However, their major drawback is the degradation of material performance during operation in the usage environment. This issue is particularly significant for biomedical applications that are readily exposed to moisture. To overcome this limitation, a prevalent approach is to calculate the decomposition rate of the material and control the thickness of the material required for operation to predetermine the lifetime of the soft robot. Recently, research has also focused on developing a passivation layer, such as a bag-like cover, that can be attached to the material to control the lifetime of the soft robot.

2.2.2 Active Transient Soft Materials

The concept that opposes the aforementioned passive transient soft material is active transient soft material. Active transient soft material is a substance in which the degradation reaction occurs by a specific external stimulus and is typically designed or synthesized through molecular engineering. (Figure 5) Unlike passive materials, active transient soft materials initiate degradation reactions at a desired time through specific stimuli, eliminating the need to predetermine the material's lifetime. Furthermore, in theory,

performance degradation does not occur during the material's operation time, providing an advantage.

However, when designing and producing such materials, various limitations are observed. First, active transient soft materials often exhibit brittle and poor mechanical properties due to the nature of the synthesized polymers. There is a limit to increasing the molecular weight of the synthesized polymer, and cyclic polymers designed to be structurally unstable exhibit a lack of entanglement between chains, resulting in even greater brittleness. Additionally, such materials are also prone to instability in ambient conditions caused by weak bonding energy, chemical structure, and unstable moieties. For these reasons, there are no known cases of active transient materials applied to soft robots. Therefore, the ideal transient soft robotic material is one that possesses both the on-demand lifetime controllability of active soft transient materials and the excellent mechanical properties of passive soft transient materials. This study presents various methods to achieve this ideal material.

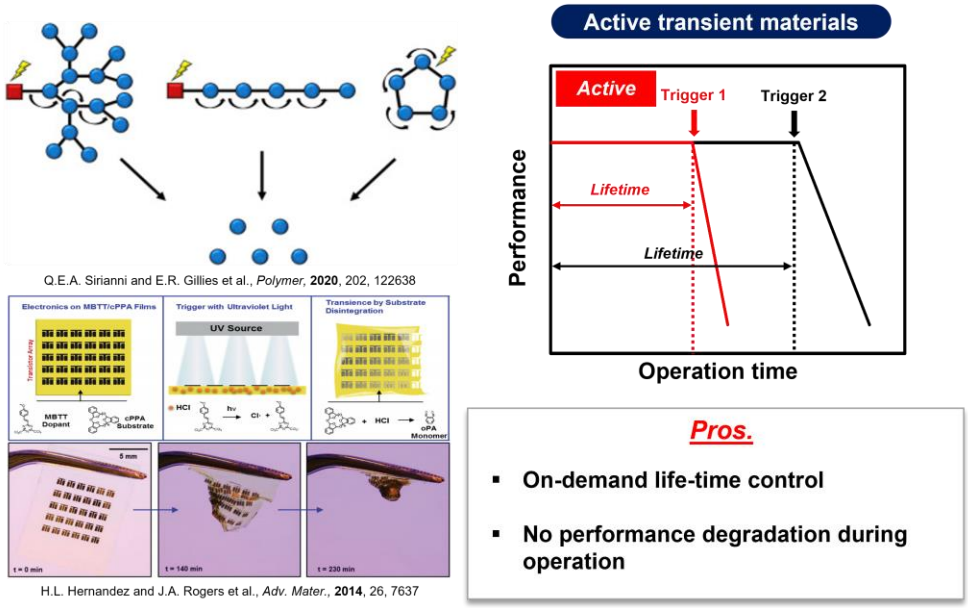

Figure 5. Active transient materials for soft robotics.

Chapter 3

PHOTODEGRADABLE PNEUMATIC SOFT ROBOTS

Contents

3.1 Introduction 25

3.2 Overall strategy of research 30

3.3 Material Degradation Analysis 33

3.3.1 Structural Analysis 33

3.3.2 Kinetics Analysis 43

3.4 Robotic Applications 54

3.4.1 Transformable Soft Actuators 54

3.4.2 Gaiting Soft Robots with Electronics 64

3.5 Experimental Verification 76

3.6 Chapter Summary 82

3.1. Introduction

Soft robotics have been developed by robotic materials with hyper-elasticity and tunable functionalities, a vital component of the field [1, 2]. Soft robots offer advanced functional adaptability and enable intricate movements, such as handling delicate objects or adapting to unpredictable environments, a capability that is not possible with conventional robots with limited degrees of freedom [3, 4]. Soft robots are becoming increasingly sophisticated and can mimic the lifecycle of living organisms, demonstrating growth [5], healing [6], transition [7], transformation [8], and even death [9]. For instance, robots with an integrated 3D printer can incrementally add self-generated material system to the original platform, demonstrating the "growth" capability [10]. Another study utilized the Diels-Alder reaction of thermo-reversible polymer networks to demonstrate the "self-healing" capability of robots [11].

Recently, attention has turned to the "death" and "disposal" of soft robots after their operational lifespan to ensure sustainable environments for future robotic systems [12]. With the growing demand for and supply of soft robots in various fields, such as prosthetics, emotional robots, and intelligent manufacturing robots, there is a growing concern about robotic waste [13]. A promising

solution to tackle these issues involves the use of transient soft robots that are designed to degrade or dissolve in a controlled manner. Transient soft robots have unique applications, including hardware security in the military, where unrecoverable and vanishing robots can ensure secure military operations such as scouting, invasion, or transport without being exposed to enemies [14, 15]. In addition, transient soft robots can explore dangerous locations such as deep sea or radioactive areas where retrieval methods are costly or unavailable [16-20]. Temporary biomedical implants such as urinary catheters, surgical forceps, and functional stents can also benefit from transient soft robots, as they require no secondary removal surgeries and can discharge degraded residues via excretory organs [21-24].

Prior studies have focused on developing fully biodegradable soft robots utilizing biodegradable elastomers, including poly(glycol sebacate) (PGS) and gelatin-based biogels. Walker et al. [25] have produced accordion-style pneumatic actuators based on PGS-CaCo3, exhibiting multiple actuations and complete degradability when buried in compost. Meanwhile, Kaltenbrunner et al. [26] have demonstrated the efficacy of gelatin biogel-based soft actuators, electronic sensor patches, and e-skins with remarkable tunability, mechanical properties, and biodegradability in deionized water. In

particular, the gelatin-based electronic sensor patches have successfully integrated temperature, strain, and humidity sensors, revealing their ability to be integrated into electronic systems.

Passive degradation, which is based on the hydrolysis rate of materials, is still the norm for biodegradable soft robots. However, this approach has two major drawbacks: the materials' performance continuously degrades as they decompose, and the system's lifetime is predetermined by factors like initial thickness and environmental conditions, with limited controllability. To overcome these drawbacks, on-demand transient materials that are highly stable yet rapidly degradable under specific external stimuli offer a solution. On-demand transient robots can initiate degradation when disposed of without functional deterioration during operation, unlike passive transient robots that undergo immediate degradation upon interaction with the surrounding environment. On-demand degradation offers several benefits, such as high and stable robot performance during their operation period, self-directed disappearance of temporary biomedical actuators after treatment, and programmable lifecycles for special-purpose robots.

Self-immolative polymers are a potential option for on-demand transient robotics, as their chains disintegrate under external conditions due to their weak chemical bonding energy. [27,28]

However, their low ceiling temperature (T_c) and poor flexibility and stretchability make them unsuitable under ambient conditions. [29,30] For instance, polyphthalaldehydes (PPAs) possess a Young's modulus of 2.5−4.5 GPa, fracture strain of 1.5%−2%, and a low T_c of −45℃. [31] Some studies have attempted to enhance the stimuli−responsiveness of composite materials by adding a photo−responsive acid generator (PAG) to the polymer matrix, which generates acids to degrade the polymer matrix when triggered with a light source. This is commonly used for photo−responsive patterning, but the resulting mechanical properties are unsuitable for soft robotics due to their narrow elastic range. An example of such a composite is polypropylene carbonate (PPC) and photo acid generator (PAG; Rhodorsil−FABA). [32,33]

Our study introduces on−demand transient materials for soft robots through the incorporation of a photo−induced fluoride−generating diphenyliodonium hexafluorophosphate (DPI−HFP) into silicone resin. This DPI−HFP/silicone composite maintains the hyper−elasticity of pure silicone but undergoes degradation into an oily liquid form upon exposure to ultraviolet (UV) light. We analyzed the degradation mechanism and kinetics of the Si−O−Si backbone cleavage initiated by hydrofluoric acid (HF) generated when exposed to UV light. By utilizing this transient composite, we

were able to showcase various types of on-demand soft robots and their practical applications in the field of robotics. For example, we achieved transformable soft robotics by selectively triggering strain limiters for grippers and actuators, and we demonstrated a highly deformable and fully degradable gaiting robot by using transient materials for the entire platform of a soft robot. Additionally, we integrated electronic devices to monitor self-movement, sense arbitrary conditions, and determine the trigger time point along with the disintegration of the entire robotic system into a non-restorable form. Our proposed system has the potential to address sustainability issues by reducing soft robotics waste and ensuring hardware security with on-demand destructible devices, as well as being applicable in biomedical settings.

3.2. Overall Strategy of Research

Soft robots made with transient silicone composites possess desirable mechanical properties and a configurable lifetime based on their disintegration when subjected to specific external stimuli. To this end, we have developed a comprehensive strategy for designing such transient silicone composites, encompassing their fabrication, application, and disintegration (as illustrated in Figure 6). In the fabrication step (as shown in Figure 6A), we added fluoride ion-emitting diphenyliodonium hexafluorophosphate (DPI-HFP) to commercial silicone resin (Ecoflex 00-30 and Sylgard-184) and molded the mixture using a polylactic acid (PLA) mold, followed by curing at 60°C for 30 minutes to obtain the desired morphology of the DPI-HFP/silicone composite. Upon exposure to UV light, the DPI-HFP releases F^- ions, resulting in cleavage of the Si-O backbone and the conversion of the composite into an oily liquid. As an example of the application of this on-demand transient material, we constructed a gating robot using DPI-HFP/silicone (as shown in Figure 6B), which can disintegrate when exposed to UV light in situations requiring such an outcome (e.g., mission completion, discovery by enemies, or disposal requiring volume reduction). The sequential images depicted in Figure 6C

demonstrate the on-demand transient behavior of the DPI-HFP/silicone gating robot when subjected to UV light and heat, resulting in complete decomposition into an oily liquid state.

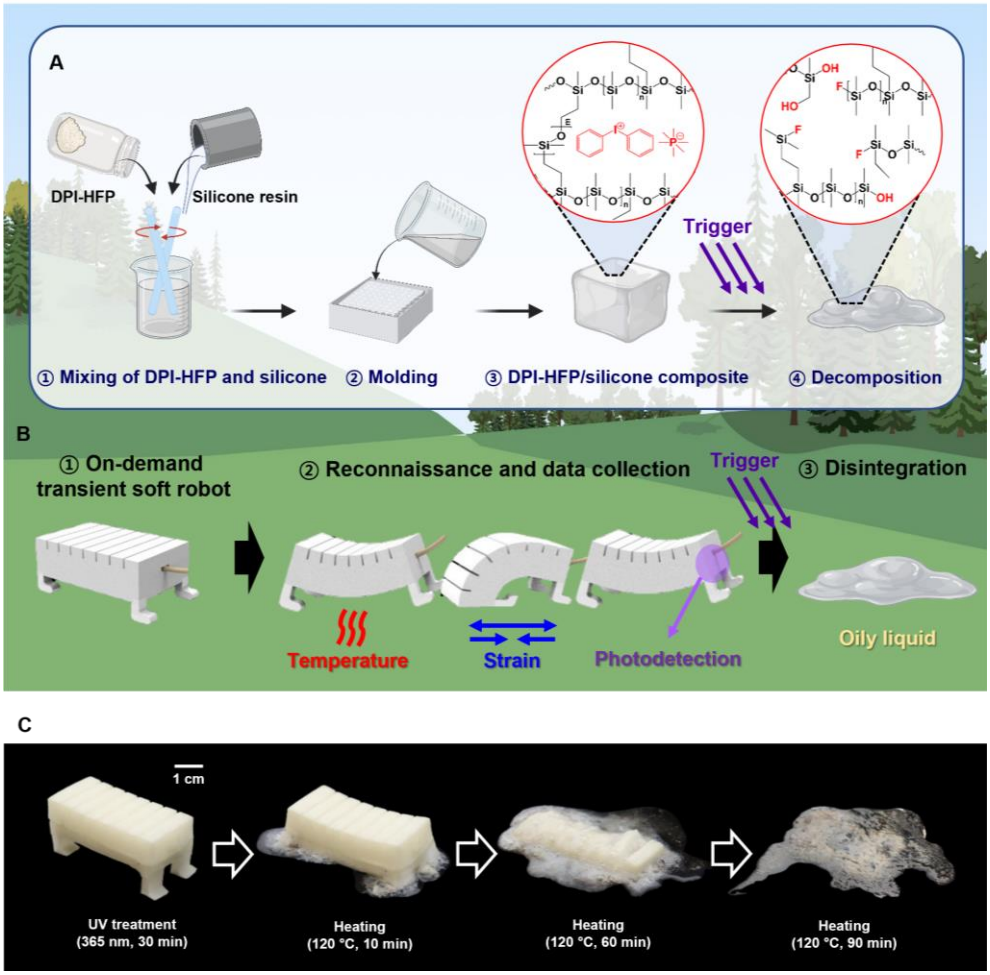

Figure 6. Overview of transient DPI-HFP/silicone composites and a lifetime-configurable soft robot.

3.3. Material Degradation Analysis

3.3.1. Structural Analysis

Through structural and thermodynamic analyses of the decomposition reactions of the hyper-elastic photo-degradable silicone composite comprising the frame of the robot, it is possible to elucidate the conditions and mechanisms underlying the degradation of the robot. Figure 7A illustrates the mechanism underlying the decomposition reaction of the material. Upon exposure to UV light, DPI-HFP, which contains an iodonium group, undergoes decomposition to form radicals that scavenge protons from the environment. [34] These protons subsequently react with PF_6^- ions to form HPF_6, which is highly unstable at room temperature and decomposes into hydrofluoric acid (HF) and PF_5. The resulting fluorine ion reacts with the Si atom, breaking the Si-O bond that forms the backbone of the silicone elastomer due to the greater bonding energy of the Si-F bond (565 KJ/mol) relative to the Si-O bond (452 KJ/mol). The broken Si-O bonds then undergo two main reaction pathways: they can react with the protons generated in the photo-induced fluoride generation reaction to form Si-OH bonds, or they can be attacked by O^- ions on the same chain to form cyclic dimethyl siloxane. [35] These reactions were

analyzed through structural analysis.

Figures 7B and 8C display the T_2 relaxation times of DPI-HFP/Ecoflex 00-30 composite and DPI-HFP/Sylgard-184 composite, respectively, before and after degradation, as measured by proton nuclear magnetic resonance (NMR). T_2 relaxation time is an indicator of the cross-linking density of polymers, which is indirectly determined by the difference in relaxation time according to the spacing between polymer chains in organic chemistry analysis. As the cross-linking density decreases, the degree of freedom of the movement of the polymer chain increases, resulting in an increase in the spacing between the chains and an increase in relaxation time. [36] Before degradation, the T_2 relaxation time of DPI-HFP/Ecoflex 00-30 composite was 41.3 ms, but the T_2 relaxation time of the residue after degradation increased significantly to 73.3 ms, confirming that the polymer degradation occurred and resulted in a decrease in cross-linking density. Similarly, for DPI-HFP/Sylgard-184 composite, the T_2 relaxation time before degradation was 28.1 ms, but the T_2 relaxation time of the residue after degradation increased significantly to 178 ms, confirming that the polymer degradation occurred and resulted in a decrease in cross-linking density.

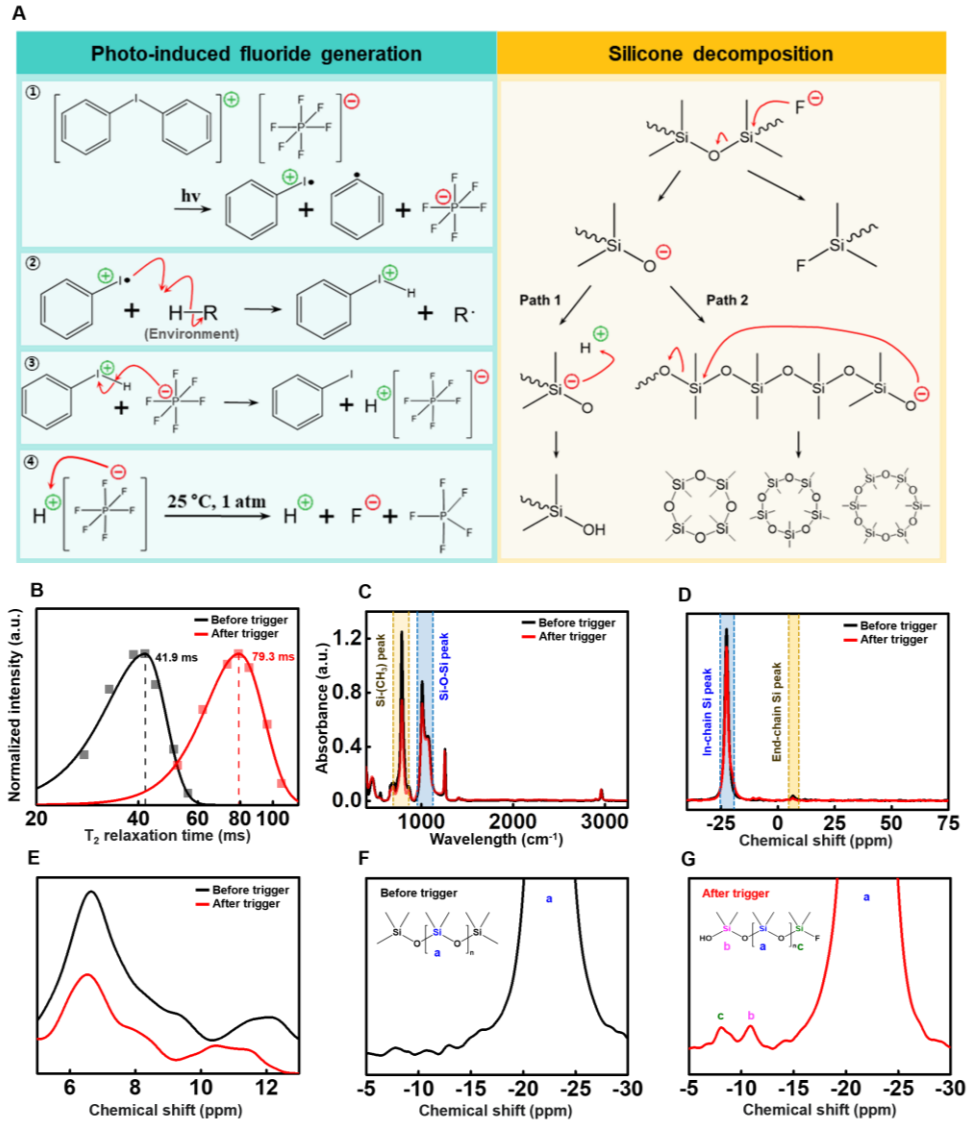

Figure 7. Decomposition chemistry of DPI-HFP/ecoflex 00-30 composites that utilizes photoinduced fluoride.

Figures 7C and 8A illustrate Fourier-transform infrared spectroscopy (FT-IR) data of the polymer composites before and after the degradation reaction. The presence or absence of the degradation reaction was indirectly confirmed by the difference in absorbance peak intensity before and after degradation. For DPI-HFP/Ecoflex 00-30 (Figure 7C), the intensity of the Si-(CH_3) peak (792 cm^{-1}) and the Si-O-Si peak (1013 cm^{-1}) before degradation were approximately 1.2 a.u. and 0.9 a.u., respectively, whereas after degradation, the intensity of the Si-(CH_3) peak and the Si-O-Si peak decreased to 0.8 a.u. and 0.8 a.u., respectively. [37, 38] Similarly, for DPI-HFP/Sylgard-184 (Figure 8A), the intensity of the Si-(CH_3) peak and the Si-O-Si peak before degradation were approximately 1.0 a.u. and 0.8 a.u., respectively, whereas after degradation, the intensity of the Si-(CH_3) peak and the Si-O-Si peak decreased to 0.6 a.u. and 0.6 a.u., respectively. The reduction in peak intensity in this data confirmed the occurrence of the degradation reaction in the various bonds that make up the silicone. Figures 7D and 8B present solid state ^{29}Si-NMR analysis data of these polymer composites before and after degradation. For both DPI-HFP/Ecoflex 00-30 (Figure 7D) and DPI-HFP/Sylgard-184 (Figure 8B) composites, there was a clear difference in the intensity of the In-chain peak and the end-chain

peak before and after the degradation reaction, and in both types of composites, the intensity of these two peaks decreased after the reaction. Figures 7E-7G depict the difference in peaks by chemical shift region of the solid state ^{29}Si-NMR data. Figure 7E presents an enlarged data of the end-chain peak, clearly indicating a significant decrease in peak intensity after decomposition. Figures 7F, 7G, and Figure 8B, on the other hand, are enlarged data of the chemical shift area near the in-chain Si peak. The pre-decomposition data clearly depicts only the in-chain Si peak (Figure 7F). However, post-decomposition data reveals the emergence of Si-F bond peaks (-8 ppm) and Si-OH bond peaks (-11.6 ppm). The same Si-F bond peaks (-8 ppm) and Si-OH bond peaks (-11.6 ppm) are also evident in Figure 9B, providing direct evidence of the silicone decomposition mechanism illustrated in Figure 7A.

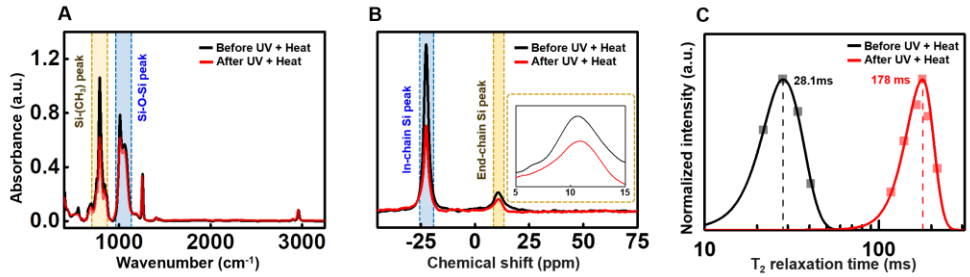

Figure 8. Decomposition chemistry of DPI-HFP/sylgard-184 composites that utilizes photoinduced fluoride.

The ingredients and compositions of Ecoflex 00-30 and Sylgard-184 are proprietary, and the residue after the decomposition reaction is substantial, but it is difficult to analyze due to the inclusion of uncertain amounts of additives such as silica, which makes it insoluble in organic solvents. [39] Therefore, in this study, a DPI-HFP/PDMS (linear) model system similar to DPI-HFP/Ecoflex 00-30 and DPI-HP/Sylgard-184 was used, considering the difficulty in analyzing the residue. Upon examining the ^{29}Si-NMR analysis of linear PDMS (M_n = 139,000) before and after the decomposition reaction (Figure 9A), a similar trend was observed to that of DPI-HFP/Ecoflex 00-30 and DPI-HP/Sylgard-184 analyzed earlier. Moreover, various peaks, including those known as cyclic compound peaks, such as octamethyl cyclotetrasiloxane (D4), decamethyl cyclopentasiloxane (D5), and dodecamethyl cyclopentasiloxane (D6) peaks, were observed. These peaks, which were not observed in DPI-HFP/Ecoflex 00-30 and DPI-HP/Sylgard-184 due to the resolution limitation of solid-NMR, were confirmed to occur as residues through the linear model, and this is also an analytical result that supports the decomposition mechanism presented in Figure 7A. [40]

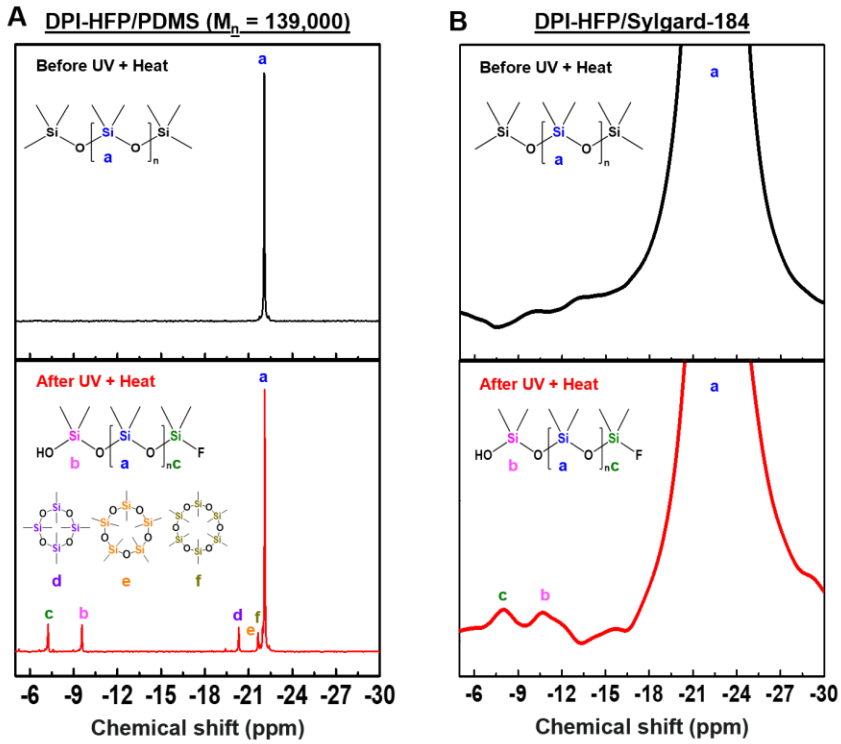

Figure 9. ^{29}Si-NMR analysis of DPI-HFP/linear PDMS and DPI-HFP/sylgard-184 composites that utilizes photoinduced fluoride.

Figure 10A presents the FT-IR spectra of the polymer before and after degradation. It was observed that the intensity of the Si-(CH_3) and Si-O-Si peaks decreased after the degradation reaction. Figure 10B shows the gel permeation chromatography (GPC) analysis of the polymer before and after degradation. The polymer had a molecular weight of M_n=64,980 and M_w=117,300 before degradation, but oligomer peaks were observed at M_n=1,351 and M_w=1,641, as well as peaks in the M_n<500 and M_w<500 region after analyzing the residue post-degradation. This indicates a significant decrease in the molecular weight of the polymer due to the degradation reaction. The structural analysis of this linear PDMS model provides an indication of the degradation mechanism of DPI-HFP/Ecoflex 00-30 and DPI-HP/Sylgard-184, which involves the cleavage of Si-O bonds by fluoride ions released from DPI-HFP. Conversely, while cyclic siloxane compounds have the capacity to be recycled [39, 41], and fragmented PDMS chains are deemed appropriate for degradation by soil or clay minerals [42, 43], the present study has shown that DPI-HFP, upon reacting with Ecoflex 00-30 and Sylgard-184, experienced Si-O bond cleavage, as demonstrated by the spectroscopic findings (Fig. 2B-G and figs. S1A-C). The fluoride ion generated from DPI-HFP was found to be responsible for this reaction.

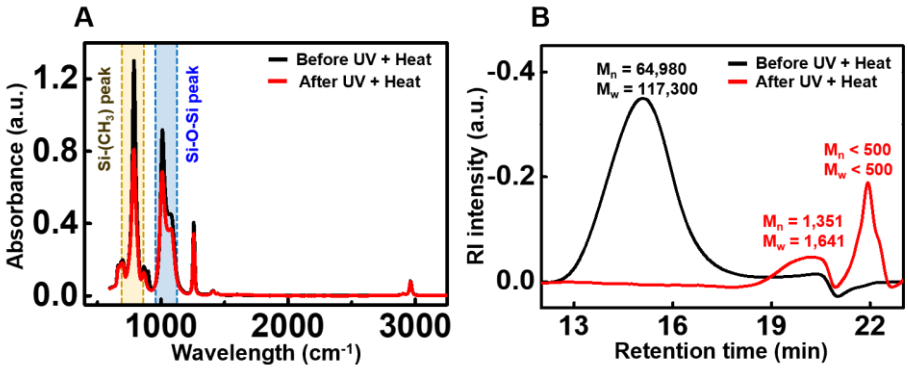

Figure 10. FT-IR and GPC analysis of DPI-HFP/linear silicone composites that utilizes photoinduced fluoride.

3.3.2. Kinetics Analysis

Verification of the kinetics parameters of the decomposition reaction is necessary to predict the decomposition reaction profile of DPI-HFP/silicone composites. Therefore, characterization of the decomposition reaction of polymer composites can be achieved through kinetics analysis under various thermal conditions. Sequential images of the DPI-HFP/Ecoflex 00-30 decomposition are presented in Figure 11A. The decomposition reaction was initiated by 365 nm UV light for 30 min, and the decomposition rate was accelerated by heat (120℃), resulting in a phase change from a crosslinked solid elastomer to a de-crosslinked oily liquid.

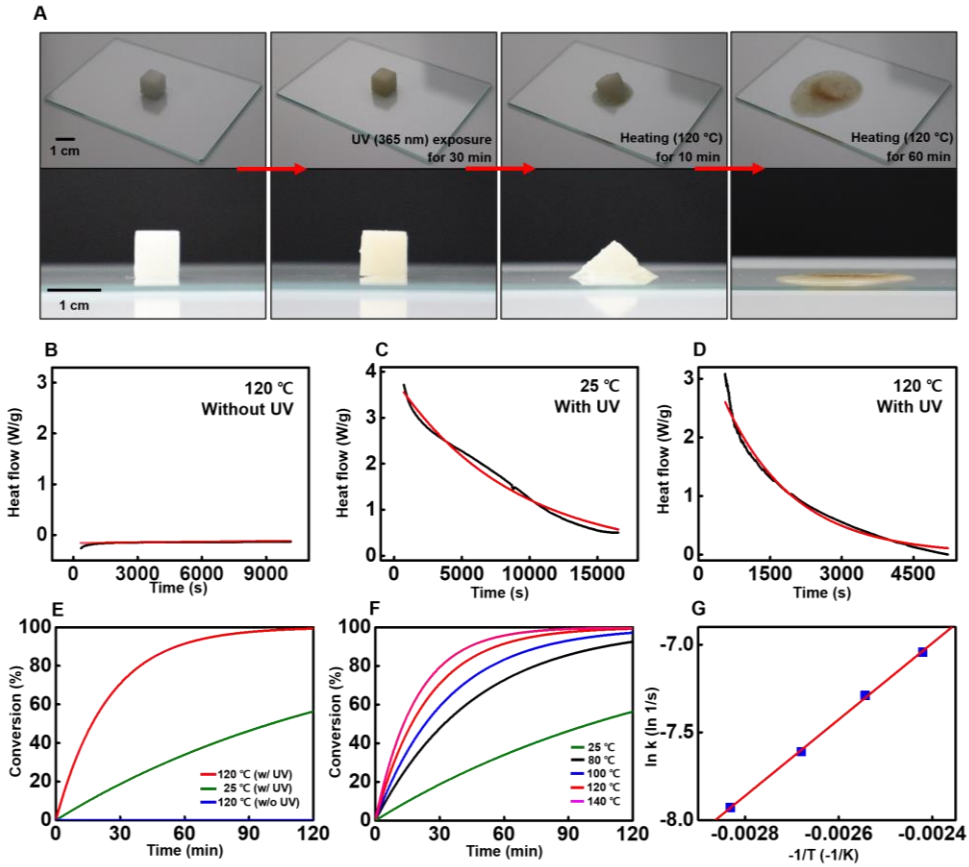

Figure 11. Decomposition kinetics analysis of the DPI-HFP/ecoflex 00-30 composite.

Prior to thermal analysis, the kinetics of the reaction (photolysis) that generated HF in DPI−HFP under UV light was calculated. For a first−order kinetic reaction from DPI−HFP to HF,

$$v = k[DPI\text{-}HFP] = -\frac{d[DPI\text{-}HFP]}{dt} = \frac{d[HF]}{dt}$$

where v is the reaction rate, k is the DPI−HFP photolysis rate constant, t is the time, and [DPI−HFP] is the concentration at time point. By arranging the above equation based on the variable [DPI−HFP],

$$-kdt = \frac{d[DPI\text{-}HFP]}{[DPI\text{-}HFP]}$$

$$[\text{DPI-HFP}] = [DPI\text{-}HFP]_0 e^{-kt}$$

where $[\text{DPI−HFP}]_0$ is the initial concentration. Considering one DPI−HFP yields a stoichiometric amount of HF, the equation can be rearranged as:

$$[\text{DPI-HFP}] = [DPI\text{-}HFP]_0 e^{-kt} = [\text{DPI-HFP}]_0 - [\text{HF}]$$

$$[\text{HF}] = [\text{DPI-HFP}]_0 (1 - e^{-t})$$

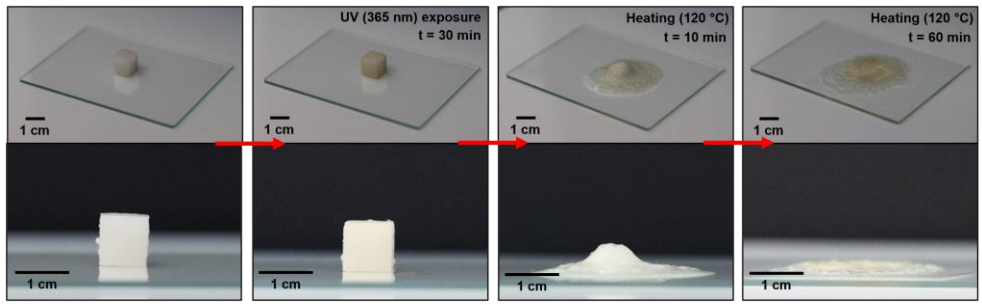

Figure 12. Decomposition sequential images of the DPI-HFP/sylgard-184 composite.

To perform thermal analysis of DPI-HFP/silicone composite, we measured the enthalpy required for composite decomposition using photo-differential scanning calorimetry (photo-DSC) and calculated the acceleration of decomposition reaction rate under various temperature conditions based on this (Figures 11B-11D and Figures 13A-13E). When no UV light was applied to the composite, no heat flow was observed even when heat was applied at 120℃ (Figure 11B). On the other hand, when only UV light was applied at room temperature (25℃), heat flow was observed due to exothermic Si-O cleavage reaction (~15,000 s, Figure 11C). When both UV light and 120℃ heat were applied together, heat flow was observed to accelerate (~4,500 s, Figure 11D). The extent of phase conversion (α) of DPI-HFP/silicone can be measured through thermal analysis using photo-DSC, as decomposition of DPI-HFP/silicone refers to exothermic Si-O cleavage. [44]

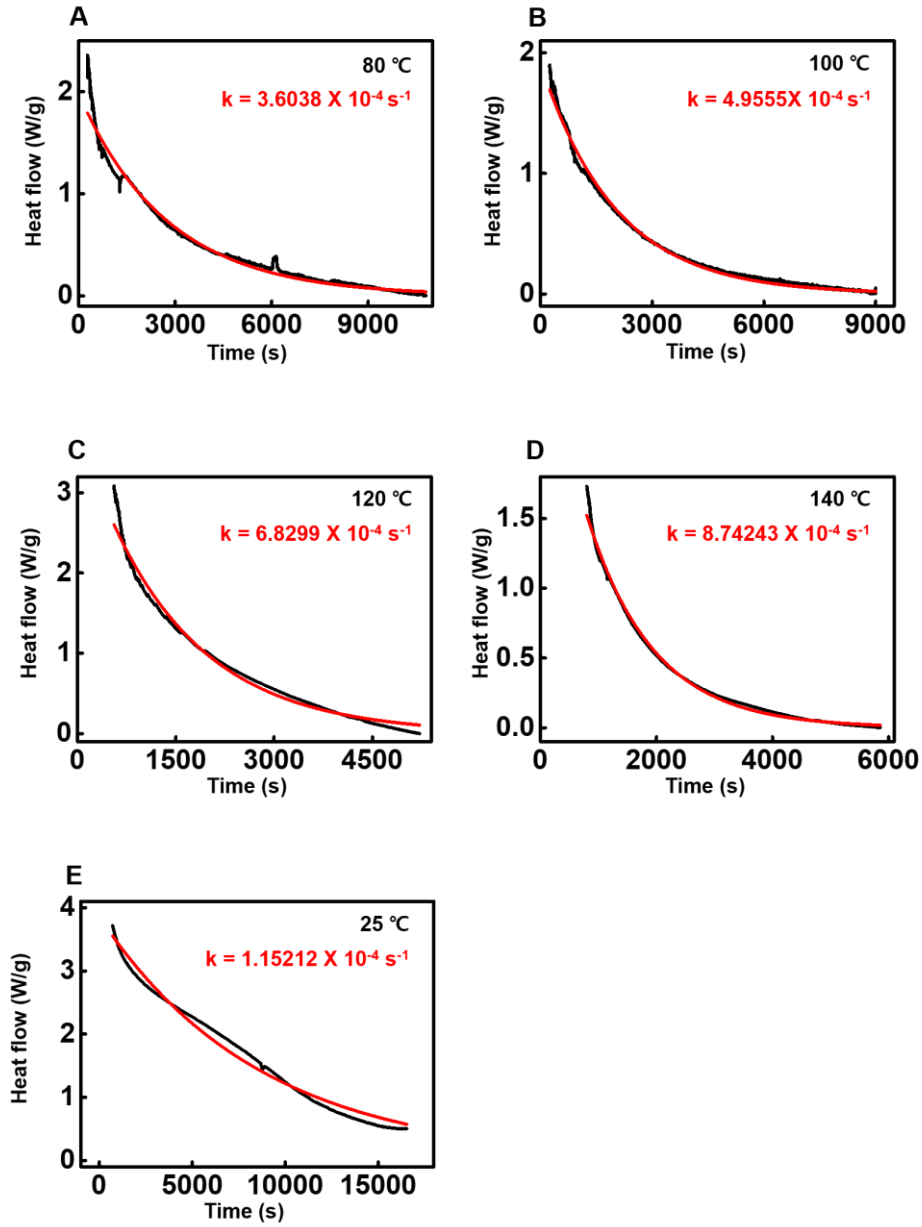

Figure 13. DSC analysis of DPI-HFP/ecoflex 00-30 composite.

Here, at time t, the value of α is empirically quantified as:

$$\alpha = \frac{\Delta H_t}{\Delta H_{total}}$$

In this context, ΔH_{total} refers to the total heat emitted during the decomposition process, while ΔHt represents the amount of heat emitted until time t. Through photo-DSC analysis, the decomposition profiles of DPI-HFP/Ecoflex 00-30 were obtained by applying various temperatures to the aforementioned equation (Figures 11E and 11F). Since the decomposition reaction of DPI-HFP/Ecoflex 00-30 is initiated by UV light irradiation, no phase conversion occurs when only heat at 120℃ is applied without UV light irradiation. When heat at various temperatures is applied to the sample irradiated with UV light, the initial slope of the decomposition profile increases with higher temperatures. This indicates that thermal energy accelerates the decomposition reaction, and higher temperatures result in a faster decomposition rate. Moreover, this indicates that after photolysis of DPI-HFP, sufficient energy is made available to overcome the activation energy barrier required for fluoride ion to cleave the Si-O bond, when external thermal energy is applied. In Vyazovkin's model, the

kinetics of the solid–to–liquid transition are expressed as:

$$\frac{d\alpha}{dt} = k(T) \times f(\alpha)$$

where α is the extent of phase conversion, k(T) is the rate constant as a function of temperature, and f(α) is a function dependent on the extent of phase conversion. Because Si—O cleavage occurs with a finite amount of fluoride and is a decelerating reaction, f(α) can be expressed for the decomposition reaction as:

$$f(\alpha) = (1 - \alpha)^n$$

where n is the reaction order. As the reaction order of Si—O cleavage with HF is 1, $f(\alpha) = (1 - \alpha)$ in this case. Furthermore, combining Eqs. $\alpha = \frac{\Delta H_t}{\Delta H_{total}}$ and $\alpha = 1 - e^{-kt}$ from the main text yields

$$\Delta H_t = \Delta H_{total}(1 - e^{-kt}).$$

Differentiating Eq. $\Delta H_t = \Delta H_{total}(1 - e^{-kt})$ by variable *t* leads to

$$\frac{d(\Delta H_t)}{dt} = k\Delta H_{total} \times e^{-kt},$$

Because the isothermal photo-DSC curve is a plot of $\frac{d(\Delta H_t)}{dt}$ over time *t*, fitting the DSC curve with Eq. $\frac{d(\Delta H_t)}{dt} = k\Delta H_{total} \times e^{-kt}$ yields the *k* value. Figure 11 shows the photo-DSC curve and *k* values obtained for DPI-HFP/Ecoflex 00-30 at varying temperatures. Moreover, Vyazovkin's model [45] provides a theoretical expression relating α to the rate constant k.

$$\alpha = 1 - e^{-kt}$$

The measurement of α using photo-DSC and its application in Eq. $\alpha = 1 - e^{-kt}$ enables the determination of k at different temperatures, as depicted in Figure 13, thus allowing the construction of an Arrhenius plot (Figure 11G). This Arrhenius plot of the conversion rate, which is indicative of the activation energy-based process of decomposition rate, yielded an Arrhenius pre-exponential factor A = 0.1703 and an activation energy E_a = 18.09 kJ/mol. These values can aid in predicting the degradation profile of DPI-HFP/Ecoflex 00-30 at arbitrary temperatures under UV radiation. Supplementary Figure 14 displays the phase conversion

datasets and Arrhenius plot for DPI-HFP/Sylgard-184. The kinetic analysis of DPI-HFP/Ecoflex 00-30 (Figure 11) and DPI-HFP/Sylgard-184 demonstrates that these materials exhibit similar decomposition behavior. To evaluate the decomposition behavior of identical DPI-HFP/Ecoflex 00-30 composite cubes (0.8 × 0.8 × 0.8 cm^3) under normal sunlight and UV-triggered conditions without any additional heat exposure was analyzed. However, the energy transferred from sunlight was insufficient to surmount the activation energy barrier and induce decomposition, and as a result, DPI-HFP/Ecoflex 00-30 did not undergo a phase change in the absence of the designated trigger of UV light. This highlights the vital role of UV light in designing reliable soft robots for real-world applications.

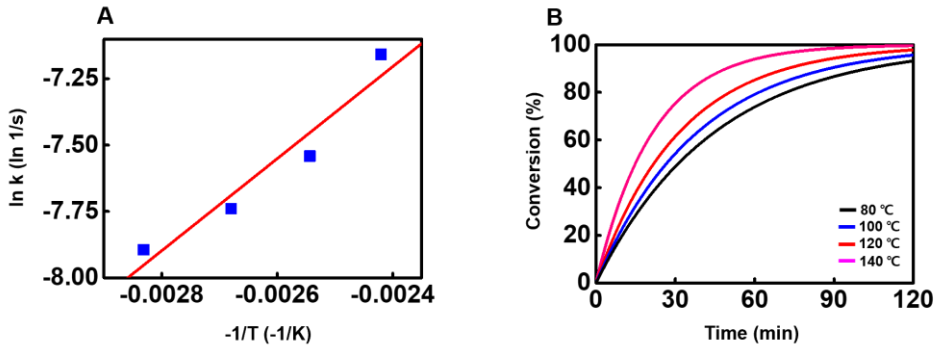

Figure 14. Decomposition kinetics of the DPI-HFP/Sylgard-184 composite.

3.4. Robotic Applications

3.4.1 Transformable Soft Actuators

Pneumatic soft actuators function by controlling actuation in the desired direction through the use of substances with differing moduli or thicknesses attached to the actuator as strain limiters. By utilizing an optimized on-demand transient soft material, a transformable soft actuator can be achieved by partially decomposing the strain limiter.

Figure 15A serves as a simple example of this concept. By attaching a strain limiter composed of DPI-HFP/Ecoflex 00-30, which is much thicker than the Ecoflex 00-30 that constructs the actuator frame, to one side of the actuator and performing pneumatic actuation, a motion of approximately 35 degrees, resembling that of a banana, can be achieved, as seen in the leftmost picture. When actuated after partially decomposing half of the actuator's strain limiter (middle picture), the upper portion exhibits similar actuation behavior to before, while the lower portion only inflates, resulting in a decrease in the angle of actuation to approximately 20 degrees. Finally, when the entire strain limiter is reacted to remove it completely, a linear actuation motion is observed, as seen in the rightmost picture.

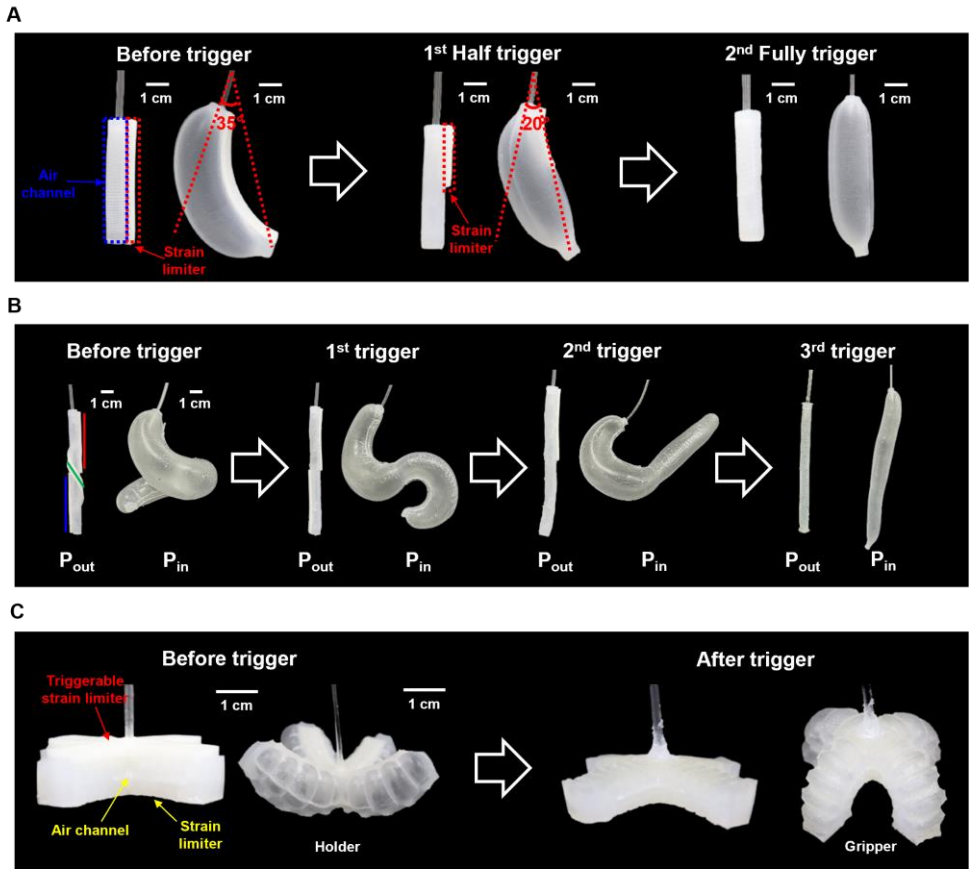

Figure 15. On-demand motion transformation by triggering the decomposition of DPI-HFP/silicone.

Figure 15B shows the multi-step transformation of the Ecoflex 00-30 actuator using the DPI-HFP/Sylgard-184 strain limiter at multiple positions. The balloon initially shows a helix-shaped actuation (location of strain limiter; top right side, red; bottom left side, blue; center, green). Triggering the center of the DPI-HFP/Sylgard-184 strain limiter (green) results in motion changes from helix-type to S-type (second images). The decomposition of the bottom left-side strain limiter (blue) leads to a transformation into the J-type (third image). The final triggering of the right-side strain limiter (red) generates a pure Ecoflex 00-30 balloon. Figure 15C shows photographic images of an one-step on-demand transformable robot from a holder to a gripper. The robot comprises an actuator with an air channel, a thin strain limiter at the bottom (Ecoflex 00-30), and a thick degradable strain limiter (DPI-HFP/Ecoflex 00-30) on top of the actuator. The robot initially operates as a holder using the thickness difference between the thin bottom and the thick top strain limiter. The application of UV (365 nm, 30 min) followed by heating (120℃, 60 min) led to the decomposition of the top destructible strain limiter and the transformation of the function of the robot from holder to gripper.

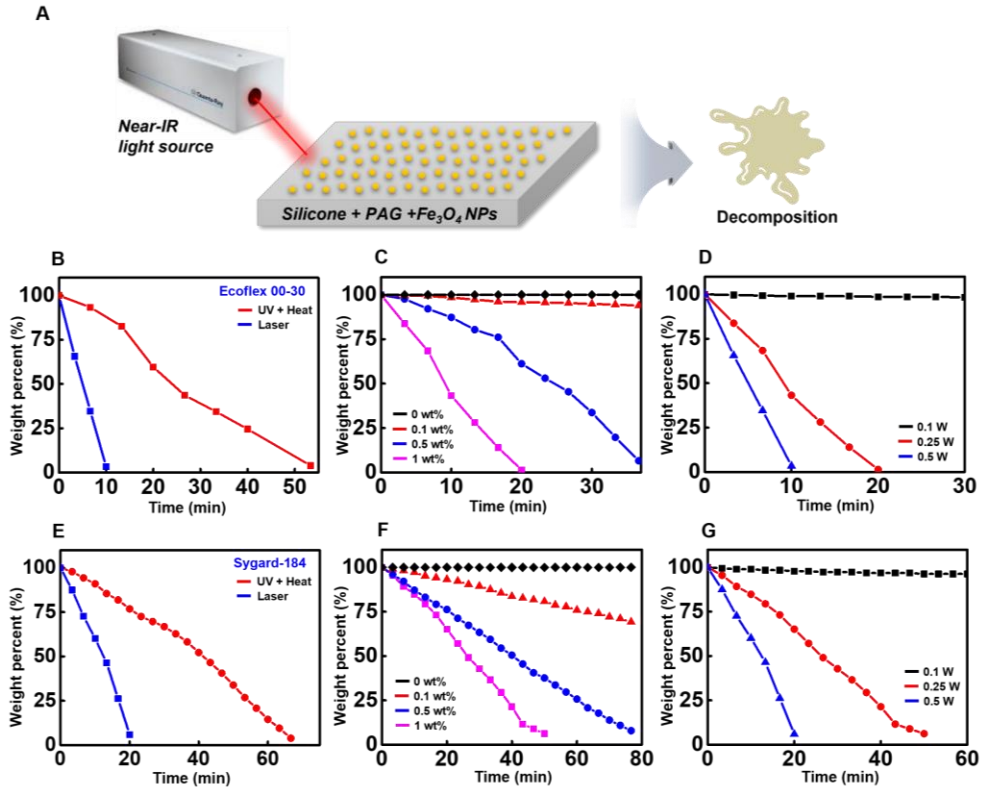

Figure 16. Remotely laser-induced triggering the decomposition of DPI-HFP/silicone and its analysis.

The actuators can be transformed by remotely decomposing the strain limiter using laser and iron oxide nanoparticles (Fe_3O_4 NPs). The application of indirect heat energy to DPI-HFP/Fe_3O_4 NPs/silicone composites using a femtosecond pulsed laser (λ=800 nm, pulse width=~100 fs) leads to the decomposition of the strain limiter owing to the photothermal effect of Fe_3O_4 NPs (Figure 16A). The reaction without UV exposure is possible, owing to the sufficiently high energy of the femtosecond pulsed laser, which can overcome the decomposition activation energy.

Figure 16B-16G illustrate the weight changes of DPI-HFP/Fe_3O_4 NPs/Ecoflex 00-30 (Figure 16B-16D) and DPI-HFP/Fe_3O_4 NPs/Sylgard-184 (Figure 16E-16G) resulting from the heat generation from femtosecond pulsed laser adsorption (λ=800 nm, pulse width=~100 fs, 0.5 W). Figure 16B illustrates the difference in decomposition rates between the conventional thermal and UV-induced decomposition steps and the newly proposed pulsed laser-induced decomposition step. It is observed that the sample undergoes decomposition in approximately 55 minutes when exposed to UV and heat, while the use of pulsed laser induces decomposition in a significantly shorter time of 10 minutes. Figure 16C shows the differences in the decomposition behavior of the DPI-HFP/Fe_3O_4 NPs/Ecoflex 00-30 composites with various Fe_3O_4

NPs concentrations. The DPI-HFP/Ecoflex 00-30 composites without Fe_3O_4 NPs did not absorb the pulsed laser. The decomposition rates of the DPI-HFP/Fe_3O_4 NPs/Ecoflex 00-30 composites accelerated, owing to an increase in the number of photothermal heating sites with an increase in Fe_3O_4 NPs concentration. Increasing the laser power input enhanced the decomposition of DPI-HFP/Fe_3O_4 NPs/Ecoflex 00-30 composites (Figure 16D). DPI-HFP/Fe_3O_4 NPs/Sylgard-184 (Figure 16E-11G) also exhibited a similar trend, as shown in Figure 16E. It was observed that Sylgard-184 required approximately one hour to undergo decomposition through UV and heat, whereas pulsed laser irradiation allowed for efficient decomposition in a short time of 20 minutes. Moreover, as the Fe_3O_4 NPs concentration increased, the site where heat was generated to induce decomposition also increased, leading to faster decomposition, as observed in Figure 16F. Furthermore, it was observed that an increase in the power of the pulsed laser resulted in a faster decomposition reaction.

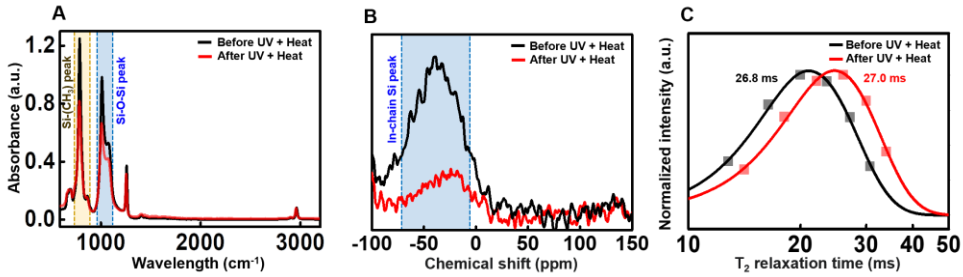

Figure 17. Laser induced decomposition chemistry of DPI-HFP/silicone composites that utilizes photoinduced fluoride.

FT-IR, ^{29}Si-NMR, and ^{1}H-NMR T_2 relaxometry data of silicone composite residue with iron oxide indicated that the photothermal effect using Fe_3O_4 nanoparticles followed the same decomposition mechanism as the UV + heat triggering method (Figure 17A-17C). Figure 17A shows before and after decomposition FT-IR data of DPI-HFP/Fe_3O_4 NPs/Ecoflex 00-30 composites. Upon comparing the FT-IR data before and after the decomposition reaction, it was observed that both the Si-O-Si bond peak and the Si-CH_3 bond peak decreased significantly. Figure 17B shows the solid-state ^{29}Si-NMR data. Due to the measurement characteristics of NMR, the peak became broad and noisy with the addition of magnetic particles such as Fe_3O_4, but a significant decrease in the intensity of the in-chain Si peak was still observed. The T_2 relaxometry data showed that the T_2 relaxation time, which was 27 ms before the decomposition reaction, decreased to 26.8 ms. (Figure 17C) This provides evidence that the cross-linking density of the polymer composite decreased due to the decomposition reaction. Through these data, it was confirmed that the pulsed laser induced trigger decomposition reaction occurred smoothly in the polymer composite. By utilizing these polymer composites as the strain limiter of the actuator, we were able to achieve remote transformation of the actuator.

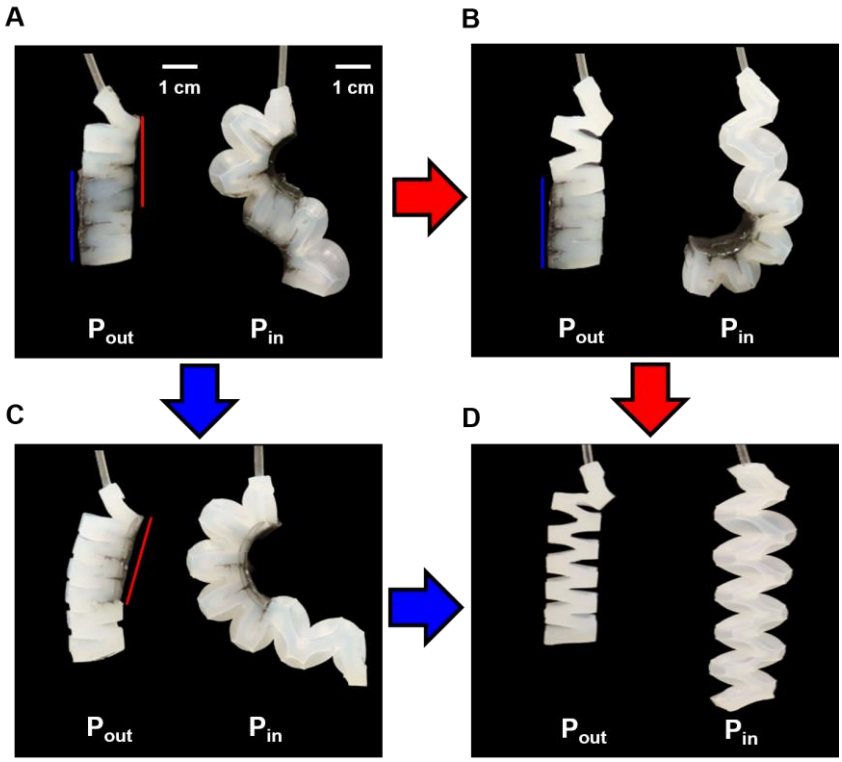

Figure 18. On-demand motion transformation by laser-induced triggering the decomposition of DPI-HFP/silicone.

Figure 18A-18D shows the remotely and selectively triggerable transformations of soft actuators via the application of DPI-HFP/Fe_3O_4 NPs/Ecoflex 00-30 composite and a femtosecond pulsed laser. The strain limiter of DPI-HFP/Fe_3O_4 NPs/ Ecoflex 00-30 is located at the top right and bottom left sides of the zigzag-shaped actuators (Figure 18A). Applying pneumatic pressure to the air channel results in an S-type motion. After the decomposition of the top-right strain limiter using a femtosecond pulsed laser (λ=800 nm, pulse width=~100 fs, 0.5 W), the actuator shows a J-type motion (Figure 18B). This is followed by triggering of the bottom-left strain limiter, leading to the transformation of the actuator from J-type to I-type (bottom right images). The change in the sequence of the strain limiter provides a different path for motion transformation. Decomposing the bottom-right strain limiter transforms the actuator motion into a C-type motion (Figure 18C). Subsequently, triggering the decomposition of the strain limiter located on the top right-side leads to the transformation of the actuator from C-type to I-type (Figure 18D). Through these experiments, we were able to verify the possibility of using a partially remote trigger soft actuator for transformation applications.

3.4.2 Gaiting Soft Robots with Electronics

In this study, we aimed to create a fully degradable soft robot using a DPI-HFP/silicone composite and equip it with electronics to enable sensing of the surrounding environment and trigger decomposition reaction when necessary. To create a highly deformable walking soft robot, the applicability of the DPI-HFP/silicone composite material as a soft robot was assessed, particularly its hyper-elastic mechanical properties were required. To this end, various deformations were applied to the material, including shaping, uniaxial, twisting, and biaxial deformations, as shown in Figure 19A. The hyper-elastic silicone-based material exhibited deformation-resistance properties, returning to its original shape even after various deformations were applied. To quantify the mechanical properties of the material, strain-stress curves were measured using an instron tensile tester, as shown in Figure 19B. The ecoflex 00-30 without any additives showed a fracture stress of 0.4251 MPa and an elongation range of 683.72%. The addition of 10 wt% DPI-HFP to ecoflex 00-30 resulted in a fracture stress of 0.1453 MPa and an elongation range of 571.67%, while 20 wt% DPI-HFP resulted in a fracture stress of 0.1897 MPa and an elongation range of 493.34 %. Nevertheless, the presence of stress concentration at the silicone and DPI-HFP interface induces

the generation of internal voids within the material, which function as crack initiation sites, and in turn, reduce the fracture strain [46,47]. The addition of DPI-HFP to the silicone matrix polymer resulted in a reduction in fracture strain value in areas where DPI-HFP was present, while the elastic modulus did not change significantly (400 % elastic limit, 40.02 ± 1.65 kPa elastic modulus). [48] This indicates that the polymer is a superior stimuli-responsive polymer with excellent mechanical properties, confirming its applicability as a soft robot material.

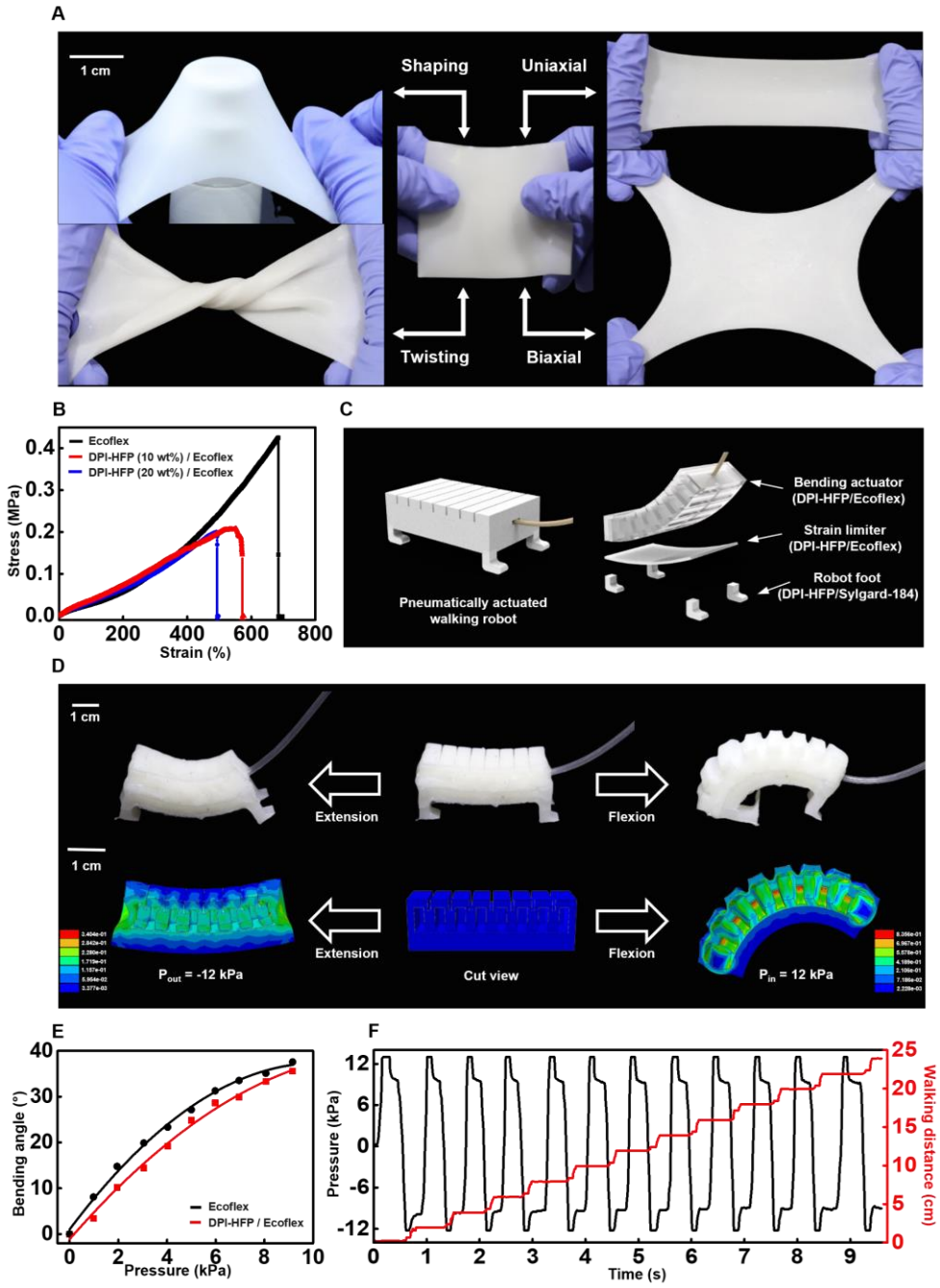

Figure 19. Demonstration of pneumatic gaiting robot developed using flexible and stretchable DPI-HFP/silicone.

We have created a pneumatically actuated gaiting soft robot that can be intentionally decomposed. Our design takes advantage of the hyper-elastic properties of DPI-HFP/silicone composites. A schematic of the robot and its actuation components are shown in Figere 4C. The robot is made up of a bending actuator with an air channel (DPI-HFP/Ecoflex 00-30), a strain limiter (DPI-HFP/Ecoflex 00-30), and four supporting feet (DPI-HFP/Sylgard-184). We have included photographs and finite element analysis (FEA) strain profiles in Figure 19D to illustrate the robot's motion under pressures ranging from 12 kPa to −12 kPa. The bending motion of the robot was a result of applying pneumatic pressure to the air channel, which was due to the difference in thickness and stiffness between the bending actuator and strain limiter. The robot was able to move forward with the support of the relatively rigid feet during movement, with the rear feet showing higher frictional force in a flexed state compared to the front feet. This allowed the robot to transition into an extended state with greater displacement at the front feet, resulting in forward movement. [49] The actuation mechanism was quantitatively evaluated through FEA, as shown in Figure 19D (cut view). Upon pressurization, the distribution of principal strains indicated that the top wall of the air channel experienced a maximum strain of 83.56% when the robot was in a

flexed state. To demonstrate that adding DPI-HFP does not affect the original performance of pure Ecoflex 00-30, we experimentally measured the bending angles of the pressurized Ecoflex 00-30 and DPI-HFP/Ecoflex 00-30 actuators (Fig. 4E), which exhibited similar bending angles at the same pressure. The displacement of the DPI-HFP/silicone gaiting robot was observed under cyclic pressure between 12 kPa to -12 kPa (Fig. 4F), and the robot steadily moved at a velocity of 2.5 cm/s through repeated extension and flexion.

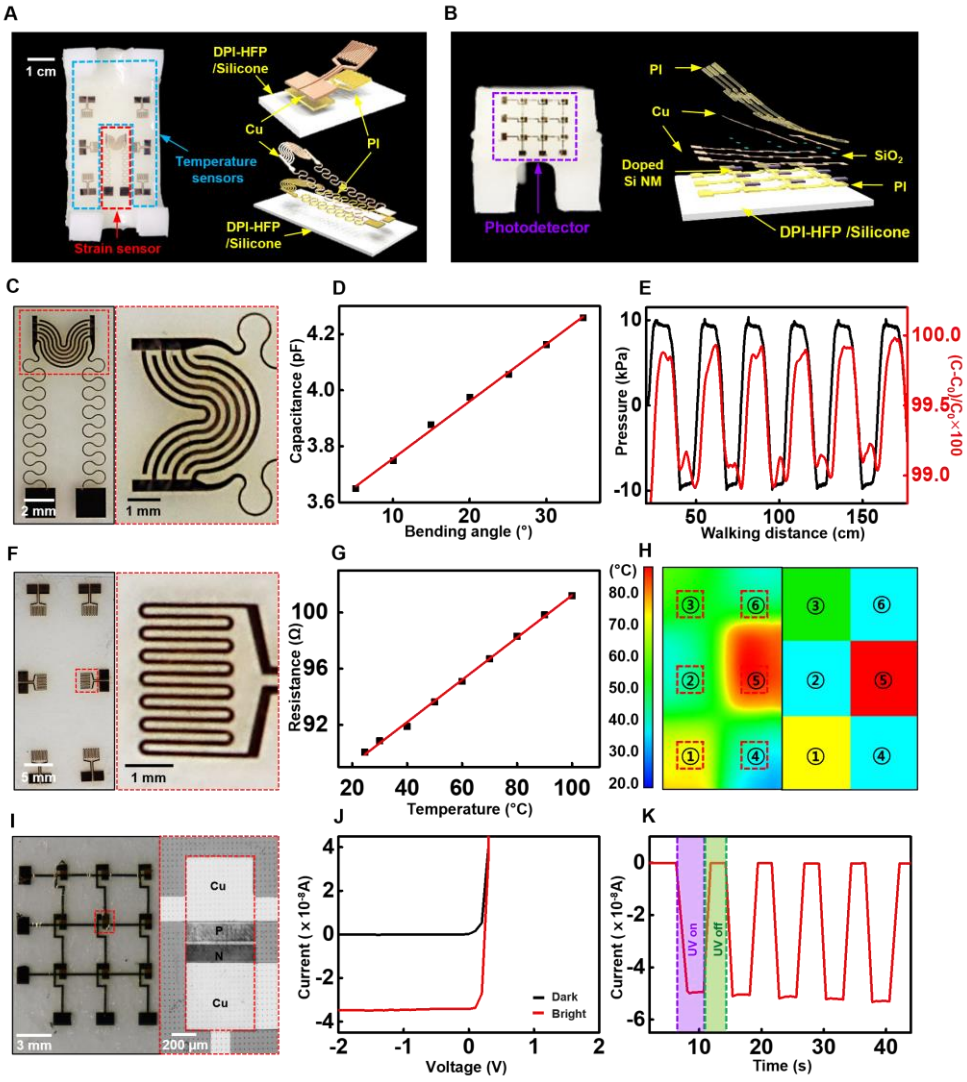

Figure 20. Integration and characterization of electronics for temperature, strain, and photo sensing.

By integrating a pneumatic soft robot with a soft electronic system, we have expanded its functionality to include ambient condition monitoring, destructive condition detection, self-alarm, and actuation control. To achieve this, we incorporated a temperature sensor array, strain sensor, and photodetector array with our on-demand transient robot made of DPI-HFP/silicone composites. The strain sensor allowed us to gather data on the strain induced during the robot's walking motion, which we could then use to control the robot's movement. Meanwhile, the temperature sensor provided information about the ambient temperature, and the photodetectors monitored for the presence of ultraviolet (UV) light during normal operating conditions. Both the temperature sensor and photodetector were crucial for detecting triggering conditions that could initiate the destruction of the robot. An image in Figure 20A illustrates the strain sensor and temperature sensor array, which were integrated into the strain limiter of the robot, and its exploded view schematics. These sensors included a copper layer with a thickness of around 300 nm deposited on a supportive polyimide (PI) dielectric film of approximately 10 μm thickness. Figure 20B presents the UV sensor array, installed on the forehead of the robot, along with its exploded view schematic. The array was made up of PIN photodiodes and

featured a monocrystalline silicon membrane, approximately 1500 nm thick, with a channel length of 20 μm and width of 625 μm, as well as Cu electrodes with a thickness of roughly 300 nm.

In Fig. 5C, the strain sensor and its magnified view are presented, which utilizes interdigitated electrodes to measure capacitance and determine strain. The capacitance measurement obtained during a single cycle of robot walking with bending angles ranging from 0−35° is displayed in Fig. 5D. The sensor was designed to detect an increase in capacitance as the distance between neighboring electrodes increased, [50] and FEM analysis was used to examine the strain induced in the region where the sensor was located. Experimental data of capacitance changes was compared to FEM data of strain changes at varying bending angles (fig. S13A), and the capacitance was then converted to strain, as shown in fig. 13B. Continuous capacitance measurements were taken during robot walking, and the capacitance change remained constant at 1 pF under cyclical pneumatic pressurization between −10 kPa and 10 kPa, as depicted in Fig. 5E.

In Figure 20F, a magnified view of the temperature sensor array is presented, which utilizes the thermal resistivity of the material. [51] The copper's measured temperature coefficient of resistance (TCR) in the temperature range of 25−100℃ was 2

$m\Omega \cdot ℃^{-1}$ (Figure 20G). This value is comparable to the one reported in the literature (3.69 $m\Omega \cdot ℃^{-1}$) [52]. To evaluate the temperature sensor array's performance, joule-heated rods with temperatures of 50, 70, and 100℃ were placed under sensors 1, 3, and 5, respectively. The temperatures across the surface resulting from heat diffusion were measured using an infrared camera (Figure 20H, left) and the temperature sensor array (Figure 20H, right). The temperature variations throughout the robot body measured via the integrated temperature sensor array corresponded to the calibrated temperature measurement shown in Figure 20H [53].

Figure 20I indicates a Si PIN photodiode array and a magnified photodiode. These photodiodes operate based on the photoelectric current generated by a p-n junction to detect the UV light that triggers the robot's disintegration [54]. The current-voltage (I-V) characteristics in both dark (without UV light) and bright (365 nm UV light) modes are presented in Figure 20J. Under the applied voltage sweep from −2 V to 2 V, the induced currents in dark and bright modes were 0 A and 3.4×10^{-8} A, respectively. The photocurrent induced by cycling the UV light on and off modes (0 V to −2V) remained consistently at -5×10^{-8} A at −2 V, as shown in Figure 20K.

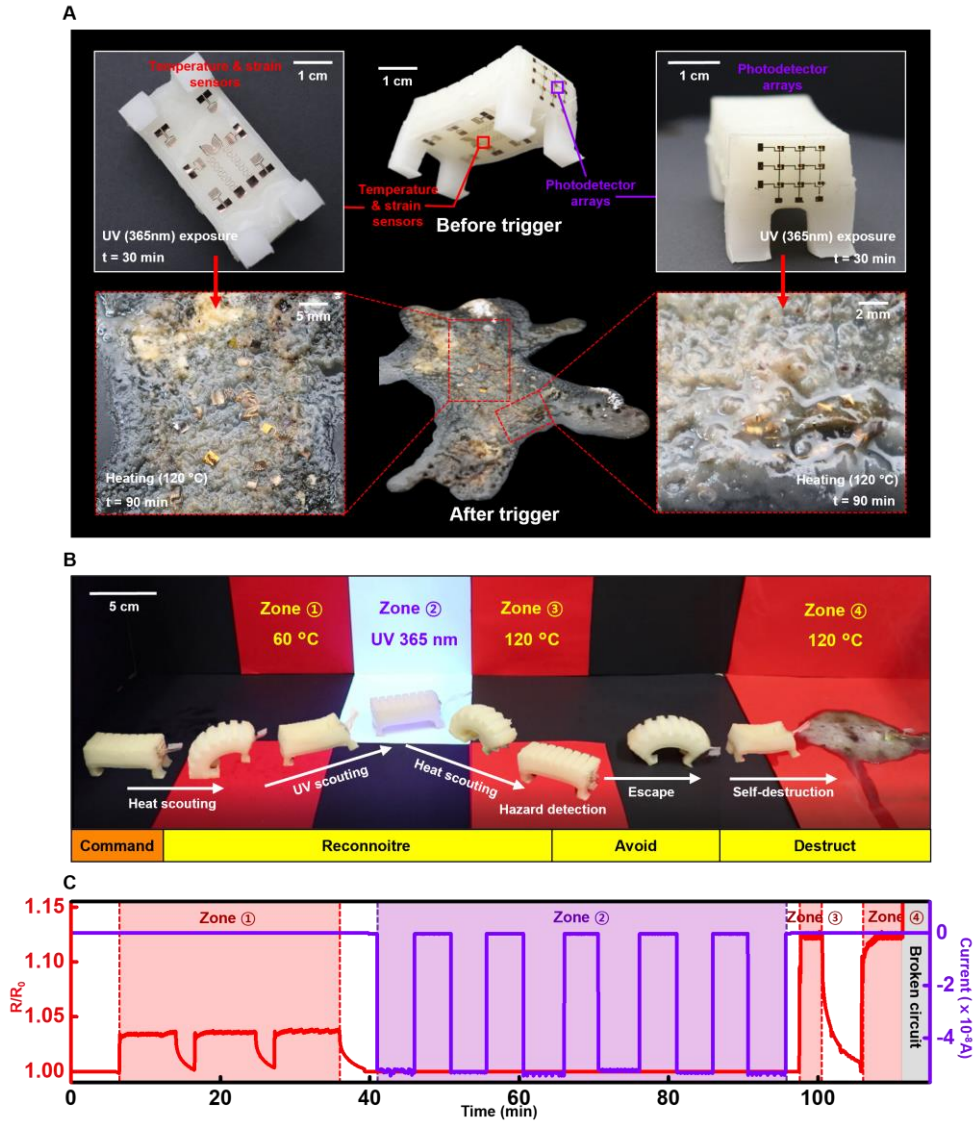

Figure 21. Autonomic operation of a life-time controlled gaiting robot.

The gaiting soft robot was tested under various conditions and its disintegration was ultimately triggered to demonstrate its functionality. It was tested in hypothetical military missions, such as scouting an unknown environment without being detected, detecting the risk factors for decomposition, escaping to avoid destruction, and finding a suitable environment to trigger the robot's self-disintegration (Figsures 6B and C). In Zone 1, the robot was exposed to a heat gun and collected data about the environment's temperature. In Zone 2, the robot was exposed to 365 nm UV light, which triggered the material's transience. The robot noted the hazardous risk of decomposition due to high temperature in Zone 3 (120℃ via hot plate) and warned the operator to leave quickly. After completing the mission, the robot entered the final zone (120℃ via a hot plate) and disintegrated into an oily liquid state within 1 hour with no chance of recovery.

The destruction of the robot after the trigger (365 nm UV light, 120℃ heating) is depicted in Figure 21A. The top row displays an integrated view of each sensor in the DPI-HFP/silicone robot, while the bottom row shows images of the strain sensor, temperature sensors, and photodetectors that collapsed and entangled in an unusable and non-restorable form with the destruction of the robot body. In addition, the electronic failure was

facilitated by the dissolution of the Cu used for the metal electrodes, which was caused by the production of F^- ions during decomposition [55]. Before failure, a robust change in the strain sensor capacitance was observed due to robot body instability during decomposition. Before the robot was triggered, the temperature sensor displayed a stable resistance reading of 0 Ω, which rapidly exceeded 106 Ω as the robot was triggered with UV light and heat. Additionally, the induction of photocurrent (-5×10^{-8} A at −2 V) was disabled as the robot collapsed.

3.5 Experimental Verification

Preparation of DPI-HFP/silicone composite

To make the DPI-HFP/Ecoflex 00-30 resin, we added a specific amount of diphenyl iodonium hexafluorophosphate (DPI-HFP; TCI, Japan) to Ecoflex 00-30 prepolymer (Smooth-On, USA) in a 1:1 mass ratio. Next, we stirred the mixture manually with a metal stick and placed it in a vacuum desiccator for 5 minutes to remove air bubbles. We poured the mixture into a 3D-printed mold and cured it in an oven at 60℃ for 30 minutes. The same process was repeated to create the DPI-HFP/Sylgard-184 composite, using Sylgard-184 (Dow Corning, USA) in a 20:1 ratio and curing for 60 minutes. For the DPI-HFP/PDMS composite used for residue analysis, we mixed trimethyl-terminated PDMS (M.W. = 139,000; Alfa Aesar, USA) with 20 wt% DPI-HFP.

Characterization and decomposition analysis of DPI-HFP/silicone composites

We conducted uniaxial tensile tests using an Instron 3343 universal testing machine (Instron, USA) with a fixed receding strain rate of 10%/s to determine the mechanical properties of the

DPI-HFP/silicone composites. The decomposition reaction required a UV lamp, and we used a VL-215L model (Vilber Lourmat, France) that emits an intensity of 2300 μW/cm^2 at a distance of 15 cm. To analyze the decomposition chemistry, we used a Nicolet iS50 FT-IR spectrophotometer (Thermo-Fisher Scientific, USA). We obtained ^{29}Si and ^{1}H solid-state NMR data using a 500 MHz Avance III system (Bruker, Germany), and solution-state ^{29}Si-NMR data were obtained using a 600 MHz Avance 600 system (Bruker, Germany) with THF as the solvent. We measured the decomposition kinetics using a photo-DSC system that included a DSC-Q200 (TA Instruments, USA) and an Omnicure-s2000 spot-cure light source (Excelitas, USA). For GPC measurements, we used a Shodex SEC LF-804 column with a Wyatt OptiLab T-rEx refractive index (RI) detector, with chloroform as the solvent.

Photo-triggered degradation experiments

Initially, a 365 nm UV lamp (VL-215L, Viber Lourmat, France) with an intensity of 2300 μW/cm^2 was used to irradiate UV light for the necessary duration. Next, a hot plate (MSH-20D, DAIHAN-Science, Korea) and a heat oven (SOF-W305, DAIHAN-Science, Korea) were employed to apply heat at the appropriate temperature and duration to cause the degradation of DPI-HFP/silicone. For

kinetic measurements, a spot-cure light source with the same intensity and wavelength was used to irradiate UV light, followed by heating in a DSC furnace. The femtosecond pulse laser (Mai-Tai-HP, Spectra-Physics, USA) was utilized in laser-induced decomposition experiments with DPI-HFP/silicone/Fe_3O_4 without any UV or heat treatment.

Fabrication of on-demand transformable robots

Applying uncured Ecoflex 00-30 to a 3D printed mold and integrating each part yielded a gripper and actuators. DPI-HFP/Ecoflex 00-30 and DPI-HFP/Sylgard-184 strain limiters were also fabricated in the 3D printed mold. The uncured DPI-HFP/Ecoflex 00-30 was applied to the interface between the DPI-HFP/Ecoflex 00-30 strain limiter and gripper-integrated transformable holder at 60℃ for 30 min as an adhesive. The DPI-HFP/Sylgard-184 strain limiter of the transformable cylindrical actuator was also attached to the actuator using uncured DPI-HFP/Sylgard-184 and by applying heat at 60℃ for 1 h. Laser-induced triggering robots were fabricated using an Ecoflex 00-30 actuator and DPI-HFP/Sylgard-184/Fe3O4 NP strain limiters. Uncured DPI-HFP/Sylgard-184/Fe3O4 NPs were applied between each side of the zigzag actuators. After curing at 60℃ for 1 h, it

acted as a strain limiter.

Fabrication, characterization, and simulation of soft robots

The robot's bending actuator and feet were created using 3D printed PLA molds, which were filled with DPI-HFP/Ecoflex 00-30 and DPI-HFP/Sylgard-184, and then cured. Uncured DPI-HFP/Ecoflex 00-30 was applied as an adhesive at the interfaces between the different parts of the robot and cured at 60℃ for 30 min. To enable pneumatic actuation, a tube was inserted into a small hole drilled in the body using a needle. The displacement and bending angle of the robot were measured with image analysis software (Tracker 5.1.5, Open Source Physics), and pneumatic pressure was measured using a customized Arduino setup that included a pressure sensor and microcontroller.

The motions of the transformable robot were simulated using 3D finite element analysis (FEA) software (ABAQUS, Dassault Systemes, France). The main body part of the robot had an inner empty space that was modeled to represent air pressure. A uniform pressure was applied to the walls perpendicular to the inner surface without air injection holes. The element type used in the simulation was a 4-node linear tetrahedron (C3D4), and the elastic modulus, Poisson's ratio, and density were set to 40 kPa, 0.43, and 1.07 g/cc,

respectively, corresponding to the mechanical properties of DPI-HFP/Ecoflex 00-30.

Fabrication of multipurpose electronic sensors

To create the temperature and strain sensors, a polyimide (PI) film (10 μm, Goodfellow) was first laminated onto a DPI-HFP/Ecoflex 00-30 (~500 μm)-coated glass slide. Next, a thin film of copper (Cu, 300 nm) was deposited on the PI via sputtering, and laser cutting of the PI-Cu bilayer defined the resistive structure for the temperature sensor and capacitive structure for the strain sensor. The DPI-HFP/Ecoflex 00-30 with embedded sensors was then removed from the glass slide and attached to the DPI-HFP/Ecoflex 00-30 robot.

To fabricate the photodiode array, a SiO_2 diffusion mask was deposited on an SOI wafer (top Si thickness ~1500 nm, p-type, Soitec) using plasma-enhanced chemical vapor deposition (PECVD). The Si membrane PIN diodes were produced by diffusing boron (spin-on-dopant 20B, Filmtronics; tube furnace at 1050℃ with N_2 flow) and phosphorous (spin-on-dopant P509, Filmtronics; tube furnace at 1000℃ with N_2 flow) through the SiO_2 diffusion mask. The removal of the buried oxides allowed the top monocrystalline Si membrane to be released and transferred onto a diluted PI (D-PI)

membrane (converted from poly(pyromellitic dianhydride co-4,4-oxydianiline), ~1.5 μm, Sigma-Aldrich) on a sacrificial PMMA-coated (poly(methyl methacrylate), ~600 nm, Microchem) silicon wafer. Electrical connections and contact pads (Cu, ~300 nm) were formed by sputtering and lift-off procedures. D-PI was spin-coated over the diode array and photopatterned to dry etch the excessive D-PI layout. The PIN diode array was released and transferred onto the DPI-HFP/Ecoflex 00-30 robot body after the PMMA was removed through immersion in acetone.

3.6 Chapter Summary

The composites of DPI-HFP and silicone described in this study possess excellent stretchable mechanical properties while also allowing for UV-initiated decomposition as needed. According to FT-IR and NMR analyses, the silicone composites undergo backbone cleavage as a result of fluoride generated from DPI-HFP, with temperature-dependent kinetics based on the Arrhenius equation. By combining DPI-HFP/Ecoflex 00-30 and DPI-HFP/Sylgard-184 composites, a highly flexible and destructible pneumatic robot can be created, while incorporating flexible electronics in the form of strain, temperature, and UV light sensors enables the robot to have multiple functions, including environmental sensing, motion control, and self-diagnosis for self-protection or self-destruction. The use of decomposable silicone composite strain limiters and Fe_3O_4 NPs added to the composite also allows for remote laser-induced transformation and on-demand actuator transformations in various scenarios.

To summarize, this study demonstrates the potential of on-demand degradation of silicone elastomers for several applications, including the creation of disposable soft robotic systems and the

integration of electronics for multifunctional use. The proposed mechanism enables the decomposition of standard soft robotics materials without affecting their mechanical properties. This concept and materials have broad applications in fields such as military hardware security, exploration of hazardous locations, and waste processing. Future studies could focus on developing fully degradable, remote-controlled, and advanced soft robots for military use. Additionally, research into reducing trigger time scales and exploring the re-polymerization of residual liquid could expand the field of on-demand transient robotics. It is important to note that further studies are necessary to assess in-vivo cytotoxicity and excretion pathways for biomedical applications. Fabrication of fully degradable, remote-controlled, and elaborated soft robots for military applications also remains a challenge. Additionally, further studies on the chemical approach to reduce the trigger time scale or the actual re-polymerization of residual liquid can expand the field of on-demand transient robotics.

Chapter 4

PHOTODEGRADABLE MAGNETIC SOFT ROBOTS

Contents

4.1 Introduction 85

4.2 Overall strategy of research 89

4.3 Material Degradation Analysis 93

4.3.1 Structural Analysis 93

4.3.2 Kinetics Analysis 96

4.4 Robotic Applications.....101

4.4.1 SAM capsulized magnetic particles 101

4.4.2 Magnetically actuated trigger transient actuators.....107

4.5 Experimental Verification 112

4.6 Chapter Summary 116

4.1. Introduction

Soft actuators have become a subject of intense interest due to their potential to overcome the limitations of conventional hard actuators. [56–58] These actuators possess biomimetic properties, making them capable of performing functions similar to those found in living organisms [59–60], such as adapting to unpredictable environments [61] and delicately manipulating fragile objects. [62, 63] Consequently, numerous research studies have been conducted on soft actuation using a range of techniques. In addition to the initial pneumatic actuation,[64] researchers have explored magnetic,[65,66] electric,[67] thermal,[68] photo,[69], and hydraulic actuation.[70] Of particular interest are magnetic soft actuators that offer remote controllability and can function in hazardous, difficult–to–reach, or unprecedented spaces, noninvasively, for potential applications.[71–74] Moreover, the magnetic field characteristics of the soft actuators enable precise modulation of their size, direction, and frequency, which ensures their effective operation and precise manipulation.[75–77]

Soft actuators have seen a surge in demand and supply across various applications, driving the need for functional soft actuators such as transience. Transient soft actuators, which can degrade

on-demand, have emerged as a promising alternative to conventional soft actuators with fixed lifetimes. Transience offers several benefits, including simplification of waste disposal processes and elimination of removal steps in difficult-to-access or hazardous situations. Moreover, transient soft actuators may enable new functionalities in military and security devices. For example, in military operations, they can be used for scouting, invasion, or transportation, without raising enemy suspicions. In security devices, the transient properties of soft actuators may facilitate unique evidence-free applications by irreversibly decomposing the actuator at the desired time.

However, soft actuators present a significant challenge when it comes to disposal, particularly due to their small size and diverse range of materials, such as polymers and particles, that are used for actuation. While recent research has focused on biodegradable materials for transient soft actuators, they can be unreliable in moist environments due to the hydrolysis-based decomposition and dissolution mechanism of the materials. [78, 79] Additionally, some dissolution strategies do not break the chemical bonds, leading to recoverable residue. [80] There are still significant challenges that need to be addressed as research on soft actuators made from degradable materials is not yet extensive. Stimuli-responsive

materials offer a solution by enabling transient soft actuators that disintegrate in response to a designated stimulus. [81] However, synthesizing decomposition-initiating moieties in the polymer chain or designing metastable polymer structures [82-84] is not ideal for precise control of the actuator's lifetime since decomposition reactions easily occur with a small amount of applied energy due to the thermodynamically unstable state. As a result, the application of trigger transient materials to soft actuators has been limited.

This study describes the development of trigger transient soft materials for magnetic actuators that offer precise control over their lifetime and irreversibility. The researchers used a polymer composite consisting of poly(propylene carbonate) (PPC) and 4-Isopropyl-4'-methyldiphenyliodonium tetrakis(pentafluorophenyl)borate (Rhodorsil-FABA) photo-acid generator (PAG) additives, which can be rapidly decomposed under ultraviolet (UV, 365 nm wavelength) light, leaving only a small amount of residue. [85] The decomposition mechanism and kinetics of the polymer composite were investigated using spectroscopic and thermal analyses, which revealed that the photo-induced acid generated from PAG cleaves the backbone of PPC polymer. Additionally, surface-treated ferromagnetic particles were designed using self-assembled monolayer (SAM) treatment [86]

and Sr-ferrite particles to prevent chemical bond formation between the Sr-ferrite and PPC polymer during the decomposition reaction. The researchers demonstrated the magnetically actuated gripper and kirigami actuators based on the designed polymer composites. The system presented in this study has potential applications in soft actuator waste reduction and hardware security with on-demand destructible devices.

4.2. Overall Strategy of Research

This paper introduces a novel soft actuator made of trigger transient composite materials that can exhibit various actuation functions and be degraded on demand via external stimulus control. The research strategy is depicted in Figure 22, which outlines the components of the composite material used to fabricate the trigger transient soft actuator, the actuation principle of the magnetic soft actuator, and the concept of decomposition after final use. Figure 22A illustrates the magnetically actuated trigger transient composite soft actuator, which consists of a poly(propylene carbonate) (PPC) polymer matrix with the addition of 4-isopropyl-4'-methyldiphenyliodonium tetrakis(pentafluorophenyl)borate (Rhodorsil-FABA) as a photo-acid generator (PAG). This composite can be decomposed under ultraviolet (UV) light. To produce the magnetically actuated trigger transient composite, the surface-treated self-assembled monolayer (SAM) ferromagnetic particle Sr-ferrite is mixed with dissolved PPC/PAG polymer composite in ethyl acetate (EA) solvent, then poured into the designed silicone molds for the solvent casting process. Figure 22B explains the magnetization, actuation, and decomposition of the trigger transient polymer composite. The aligned magnetic particles

embedded in the composite are magnetized in a strong and uniform magnetic field, [87] allowing the spin-aligned soft composite materials to actuate in a programmed direction with external magnetic fields. [88,89] After performing all functions or actuations, the actuator can be decomposed by initiating the trigger degradation of the PPC/PAG composite under 365 nm wavelength UV light. The applied thermal energy accelerates the decomposition reaction, and most of the polymers vaporize, leaving only a small amount of liquid residue and SAM-treated magnetic particles. The proposed research strategy aims to trigger the decomposition of the soft actuators using stimuli-responsive materials to control their lifetime in response to specific external destructive conditions.

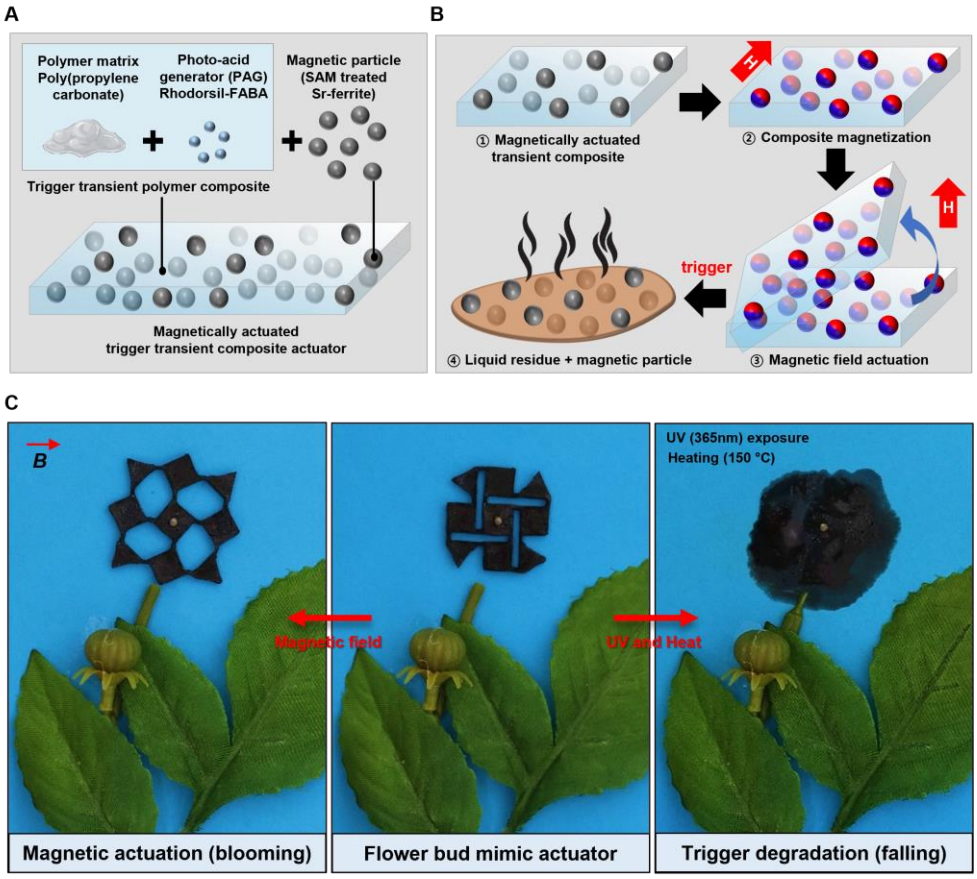

Figure 22. Overall strategy of magnetically actuated trigger transient polymer composite and a lifetime controllable soft actuator.

The utilization of a magnetic field for the actuation of the trigger transient soft actuator, which exhibits a flower's lifespan through the kirigami structure and transience via UV initiation and heat acceleration, is demonstrated in Figure 22C. The bud-shaped kirigami soft actuator in the center was produced and programmed using a sequence of processes outlined in the Experimental Section. Upon application of a magnetic field of approximately 300 mT to the actuator in the middle, it blossoms into a full flower on the left, with each composite actuator part aligned along the magnetic field. The transient property of the polymer composites is employed to mimic the falling flower. Upon exposure of the polymer composite to a UV lamp for 15 minutes and heating at 150° C for 15 minutes using a hot plate, the PPC/PAG layer degrades initially due to external heat. Subsequently, the PPC/SAM-treated Sr-ferrite layer at the top disintegrates, and finally, the entire body of the actuator decomposes. As depicted in the image on the right of Figure 22C, the kirigami soft actuator vaporizes and completely breaks down, leaving behind a magnetic particle and a minimal amount of liquid residue.

4.3. Material Degradation Analysis

4.3.1 Structural Analysis

Figure 23 depicts the characterization of trigger transient materials, including sequential images and chemical reactions during the decomposition process. As presented in Figures 23A and 23B, the trigger transient composite materials undergo a phase transition from solid to gas and a small amount of liquid during decomposition, accompanied by a change in color from transparent to translucent light brown after exposure to UV light. Figure 23B details the depolymerization mechanism of the trigger transient composite material. Upon UV irradiation, the 4−isopropyl−4'−methyl diphenyl iodonium cations of Rhodorsil−FABA undergo homolytic cleavage and yield 4−isopropyl phenyl iodonium radical cations and 4−phenyl methane radicals. [90] The generated 4−isopropyl phenyl iodonium radical cations then create a photo−generated acid with tetrakis(pentafluorophenyl) borate as an anion by bringing protons from the surrounding environment. [91−93] The photo−induced generated acids attack the C=O bond of the carbonate group, initiating the decomposition reaction. The applied continuous energy, either thermal or ultraviolet, triggers the formation of three intermediate states of PPC polymer, which are thermodynamically

unstable and lead to the final residue. Cyclic compounds are produced as by-products, and the tetrakis(pentafluorophenyl) borate anion acts as a catalyst for the decomposition reaction of these compounds, resulting in the formation of acetone, carbon dioxide, and other cyclic compounds that evaporate. [94]

The present study aimed to explore the chemical composition and decomposition mechanism of trigger transient materials through spectroscopic observation. The corresponding results are illustrated in Figures 23C and 23D, which demonstrate the differences in molecular structure before and after decomposition of the material. Fourier transform infrared spectroscopy (FT-IR) analysis revealed the cleavage of the PPC polymer backbone after UV and heat treatment, as evidenced by the differences between before (black line) and after (red line) peaks (Figure 23C). The decrease in peak intensities of the C=O bond peak (1738 cm^{-1}) and C-O bond peak (1225 cm^{-1}) indicated the decomposition of the PPC polymer by photo-induced generated acid and external energy.

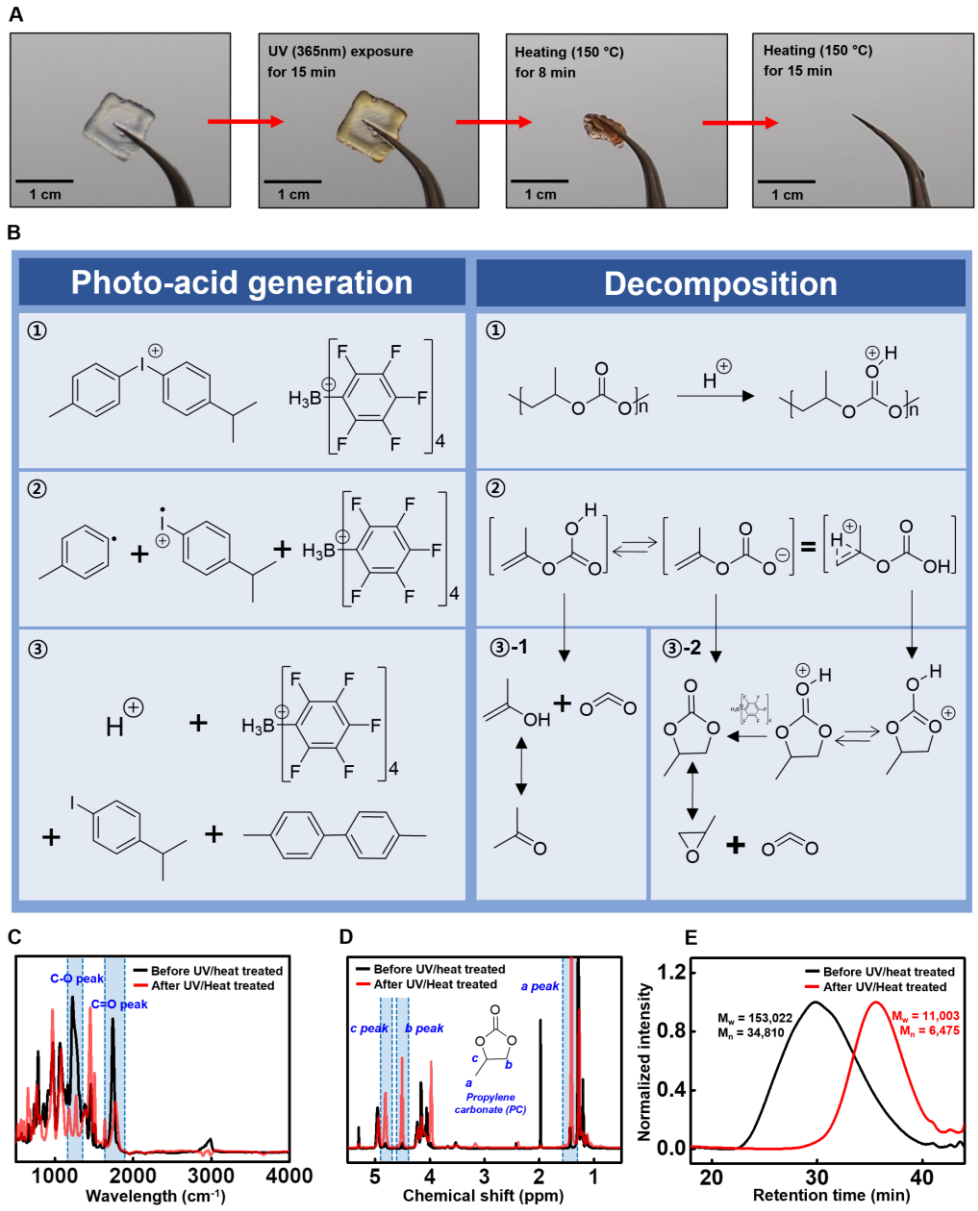

Figure 23. Structural analysis of photo-triggered decomposition of PPC polymer by PAG.

The decomposition mechanism was further confirmed by proton nuclear magnetic resonance (^{1}H−NMR) spectroscopy (Figure 23D), which revealed the formation of propylene carbonate (PC) as gas and liquid residue after decomposition. [95] The absence of PC peaks before UV and heat treatment and the appearance of new peaks at 1.50 ppm, 4.55 ppm (and 4.0 ppm), and 4.85 ppm corresponding to CH3, CH2, and CH of PC after UV and heat treatment confirmed the decomposition of the PPC polymer via PAG. [96]

The weight−average molecular weight (M_w) and number−average molecular weight (M_n) of the polymer were measured before and after the decomposition reaction using gel−permeation chromatography (GPC) (Figure 23E). The results showed that the Mw and Mn of the polymer residue were significantly reduced to 11,003 Da and 6,475 Da, respectively, after the decomposition reaction by UV light and heat treatment, indicating the irreversibility of the breakage of the PPC polymer backbone. Therefore, the spectroscopic analyses conducted in this study confirm the decomposition of the PPC polymer via PAG structurally.

4.3.2 Kinetics Analysis

The verification of the PPC/PAG polymer composite's

decomposition kinetics as a function of temperature variation was performed through mass loss analysis, as illustrated in Figure 24. Figure 24A demonstrates the thermogravimetric analysis (TGA) data used for analyzing the reaction kinetics of the PPC/PAG composite decomposition. The pure PPC polymer (black curve) undergoes decomposition at around 250℃, and complete decomposition requires a temperature higher than 250℃. However, for the PPC polymer composites with added PAG (red curve) at a weight percent of 30wt%, depolymerization occurs at 150℃ owing to the acceleration of the decomposition reaction induced by the photo-generated acids present in the polymer composites. [97] In this reaction, decomposition does not occur around 200 ℃ and can be estimated as a by-product of PAG (as shown in Figure 24B, left) after photo-acid generation due to its weight percent and temperature. [85]

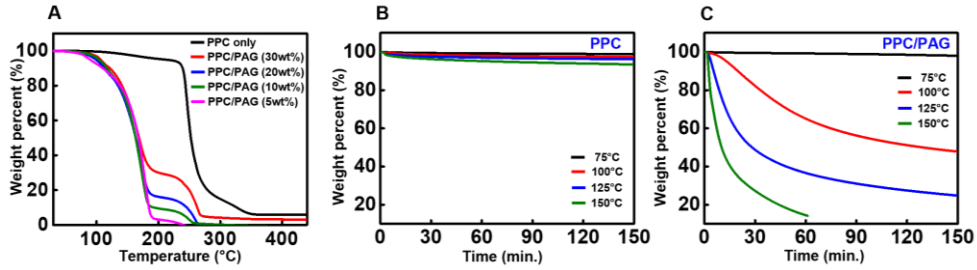

Figure 24. Decomposition reaction kinetic analysis of PPC polymer by PAG using TGA analysis.

The TGA analyses conducted with varying weight percentages of PAG (0 wt%, black; 5 wt%, pink; 10 wt%, green; 20 wt%, blue; 30wt %, red) reveal that decomposition reactions occur at 150℃ regardless of PAG weight percent. Therefore, it can be inferred from these results that the decomposition was not an acid-consuming reaction but a catalytic reaction that utilizes acid. The catalytic decomposition reaction's characteristic enables the PPC polymer to decompose with a small amount of PAG.

Through the unique attribute of the decomposition reaction, the formation of a double layer consisting of a thin PPC/PAG layer on the PPC layer can be completely disintegrated via the diffusion of photo-induced acid. The weight loss data of the PPC polymer at varying temperatures (75℃, black; 100℃, red; 125℃, blue; 150℃, green) for a period of 150 minutes is illustrated in Figure 23B. Since pure PPC polymer without PAG disintegrates at a temperature of approximately 250℃ (as shown in Figure 23A), it may be inferred that there would be no alteration in weight percentage under the experimental conditions of 75℃, 100℃, 125℃, and 150℃. As revealed in Figure 23A, the PPC polymers retain 90% of their weight. The results of the weight loss analysis at varying temperature conditions (75℃, black; 100℃, red; 125℃, blue; 150℃, green) are presented in Figure 23C, indicating the

acceleration of the PPC/PAG composite decomposition reaction. Prior to the TGA analysis, UV light (365 nm, 15 min) is utilized to trigger the decomposition reaction with a photo-induced acid. At 75°C (black), the behavior of the composite decomposition rate is not dissimilar from that of pure PPC, suggesting that the degradation energy barrier is not overcome and thus, the decomposition reaction does not occur. The decomposition reaction occurs at the 100°C (red) condition, with nearly half of the weight loss observed after 150 minutes. A complete decomposition reaction can be achieved by applying heat energy for a prolonged duration, and this prolonged duration is due to the sluggish speed of the degradation reaction. At 125°C (blue) condition, the heat energy instigates the vaporization of the majority of the composite material by decomposition, with only 30 weight percent of liquid remaining. At 125°C, a full decomposition reaction can be attained by applying heat energy for a period that is considerably shorter than at the 100°C (red) condition. When the decomposition reaction occurs at 150°C (green), the majority of the materials vaporize, and only a small amount of liquid residue remains after 60 minutes.

4.4. Robotic Applications

4.4.1 SAM capsulized magnetic particles.

The use of magnetic particles in the design of kirigami soft robots has allowed for diverse unconstrained actuation capabilities through magnetic fields. However, in order to achieve transient systems in magnetically actuated soft actuators, the formation of new chemical bonds between the polymers and reactive magnetic particle surfaces must be prevented. Figure 25 illustrates the validation of trigger transience properties and modification of magnetic particles for magnetically actuated transient kirigami robots. It is observed in Figure 25A that the PPC/PAG composite with untreated Sr−ferrite added as the magnetic particles does not decompose completely, resulting in lumps due to new chemical bond formation between the Fe atom of Sr−ferrite and the carboxylate of PPC polymer intermediate state during the decomposition reaction. [98, 99]

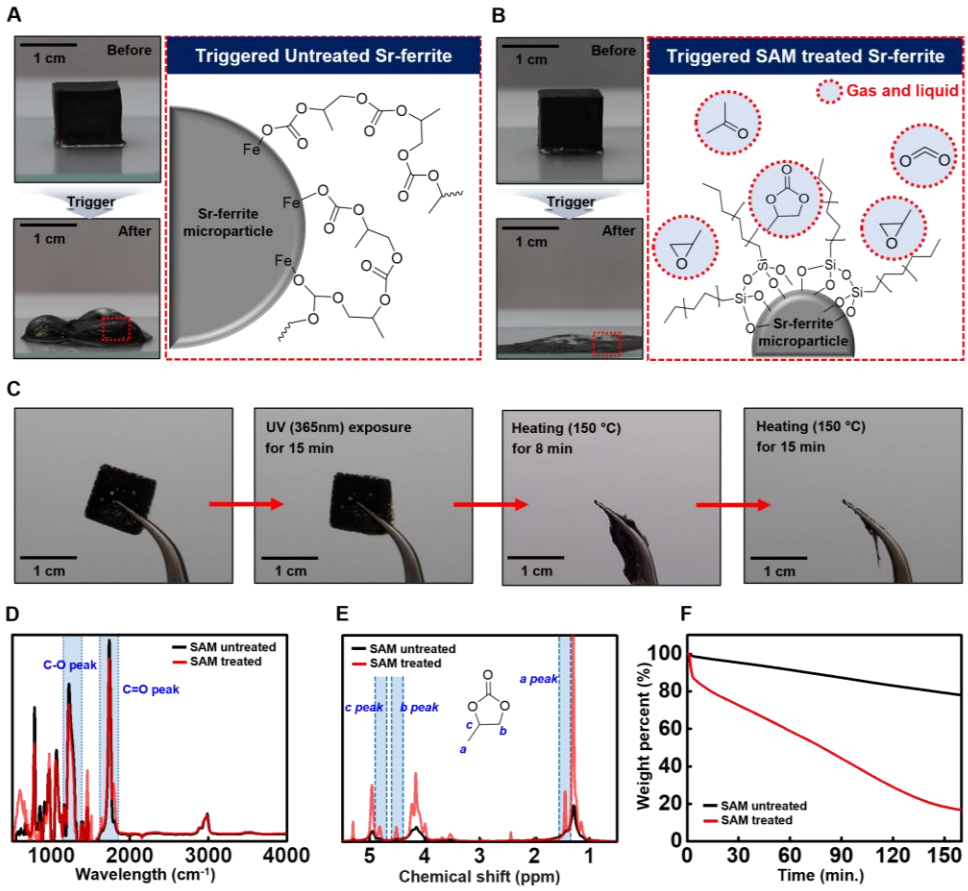

Figure 25. Magnetic particle modifications for embedding in PPC polymer and various analyses for confirming decomposition of PPC polymer.

To inhibit the formation of lumps, it is necessary to employ a specific treatment on the surface of Sr-ferrite to block the formation of Fe-O bonding. Self-assisted monolayer (SAM) treatment is used, which involves UV-ozone and specific treatment processes on the oxide surface to pack and align the alkyl layer in an edge-on state, forming a super-hydrophobic surface. [100, 101] SAM treatment is performed on Sr-ferrite using octadecyl trichlorosilane (ODTS) and n-hexane. Sr-ferrite particles without SAM treatment possess a hydrophilic surface that absorbs water, whereas Sr-ferrite with SAM treatment has a super-hydrophobic surface and shows a high contact angle. Figure 25B displays the transient polymer composites with SAM-treated Sr-ferrite and its schematics after decomposition. The composite sample with SAM-treated Sr-ferrite is nearly completely decomposed, leaving only a small amount of liquid residue and magnetic particles without lumps between the magnetic particle and PPC polymers. This is due to the super-hydrophobic passivated surface of Sr-ferrite through SAM treatment, which hinders the access of PPC polymer to the surface of the Sr-ferrite during the decomposition reaction, thus inhibiting Fe-O bonding formation. Figure 25C exhibits the transient behavior of the fabricated dual-layer composite material (PPC/Sr-ferrite layer and PPC/PAG layer) in sequential images. Since the Sr-

ferrite absorbs a significant portion of UV light (365nm wavelength), the initiation of PAG using UV light is challenging. [102, 103] To facilitate the decomposition reaction, a dual-layer structure that forms a thin PPC/PAG layer on the PPC/SAM-treated Sr-ferrite composite is designed. Upon exposure to 365 nm UV light for 15 min, the transparent PPC/PAG composite layer changes into a translucent light brown color, and decomposition is triggered owing to photo-acid generation. The application of heat energy at 150 ℃ using a heat gun accelerates depolymerization, resulting in a phase transition from solid to gas and liquid. After 15 min under 150 ℃, the decomposition of composite materials is completed, and only a small amount of liquid residue and Sr-ferrite magnetic particles remain.

An examination of the structure following the decomposition reaction through spectroscopic analysis provides evidence of the impact of surface self-assisted monolayer (SAM) treatment on preventing Fe-O bond formation. Figures 25D-25E demonstrate the spectroscopic findings of the decomposed residue before and after the SAM treatment of Sr-ferrite. In Figure 25D, the Fourier-transform infrared (FT-IR) spectra of the residue reveal the degree of decomposition with and without SAM treatment. In the sample treated with SAM, the peak intensities of the C-O bond

(1225 cm^{-1}) and C=O bond (1738 cm^{-1}) are decreased in comparison to those of the untreated sample. Further demonstration prensents the variance between the C-O bond peak and C=O bond peak before and after the decomposition reaction. While the untreated sample's C-O bond peak and C=O bond peak showed no significant difference, the SAM-treated sample exhibited an evident distinction in intensity before and after the decomposition reaction. These findings suggest that the SAM treatment of the magnetic particles has a significant impact on the decomposition reaction.

Figure 25E shows the data obtained from the proton nuclear magnetic resonance (^{1}H-NMR) analysis, which verifies the difference between the samples with and without SAM treatment. The intensity of the propylene carbonate (PC) peak indicates the degree of decomposition reaction. The PC proton peaks at positions a, b, and c are faint for the residue of the composite sample without SAM treatment. In contrast, they are apparent for the sample treated with SAM. Figure 4E display the NMR data on samples that use untreated Sr-ferrite and SAM-treated Sr-ferrite before and after the decomposition reaction. These graphs validate that the PC peaks, which were absent before the decomposition reaction, were detected after the reaction. The PC peak in the untreated sample was feeble after the reaction, while it was relatively strong in the

SAM-treated sample. These spectroscopic data indirectly support the notion that the decomposition reaction is contingent upon whether the magnetic particle underwent SAM treatment. The application of spectroscopic observation serves as a means of discerning whether a sample has undergone decomposition. Mass loss measurements can be obtained through TGA analysis to accurately quantify the extent of the decomposition reaction. As displayed in Figure 25F, the isothermal TGA mode can demonstrate the dependency of the decomposition reaction on whether SAM has been treated, where the untreated sample is depicted in black and the treated sample in red. Following exposure to UV light, a constant heat of 150℃ is applied to the sample, and the change in weight percentage is measured. The untreated sample reveals only a slight decomposition reaction after 150 minutes, with approximately 80 weight percent remaining. In contrast, the treated sample displays a much more substantial reaction, with only roughly 20 weight percent remaining after the same time interval. These results serve as a quantitative representation of the fact that most composite materials, such as PPC and PAG, undergo decomposition and vaporization into gas, excluding the magnetic particle. By employing both spectroscopic and thermodynamic analyses, it can be confirmed that SAM treatment facilitates the decomposition

reaction by impeding Fe–O bond formation, both qualitatively and quantitatively.

4.4.2 Magnetically actuated trigger transient actuators

Figure 26 illustrates the successful application of a trigger transient polymer composite in the construction of a magnetically actuated kirigami soft actuator. The pattern schematics of the kirigami soft actuator and real images of actuation experiments via homogeneous magnetic fields are presented in Figure 26A–C. The dual–layer composite consisting of PPC/SAM–treated Sr–ferrite and PPC/PAG is cut into a square shape using a laser cutter and magnetized in the desired direction using a vibrating–sample magnetometer (VSM). Each part is then assembled into a pre–made silicon mold and the transient composite material is poured into the connections to fabricate the kirigami structure through a solvent casting process. Figure 26A showcases a gripper function actuator, composed of five magnetized square composite parts, aligned in the direction of the magnetic field in an environment where homogeneous magnetic fields are applied. The actuator operates as a gripper, as demonstrated in the experiment images and Video 4. Figure 26B presents a basic rotating square–based kirigami pattern consisting of nine magnetized composite parts arranged in a zigzag

array in a silicone mold. The composite material solution is poured into the hinge sections to fabricate the kirigami actuator, which has an actuation with a negative Poison's ratio tendency that spreads out in the x and y axes when a homogeneous magnetic field is applied. The experiment images demonstrate the designed actuation of the kirigami pattern via uniform magnetic fields. The experiment in Figure 26C scales up the actuator shown in Figure 26B with a basic rotating square-based kirigami pattern consisting of 16 segments, which demonstrates an actuation with a negative Poison ratio tendency that spreads out in the x and y axes when a uniform magnetic field is applied to the actuator.

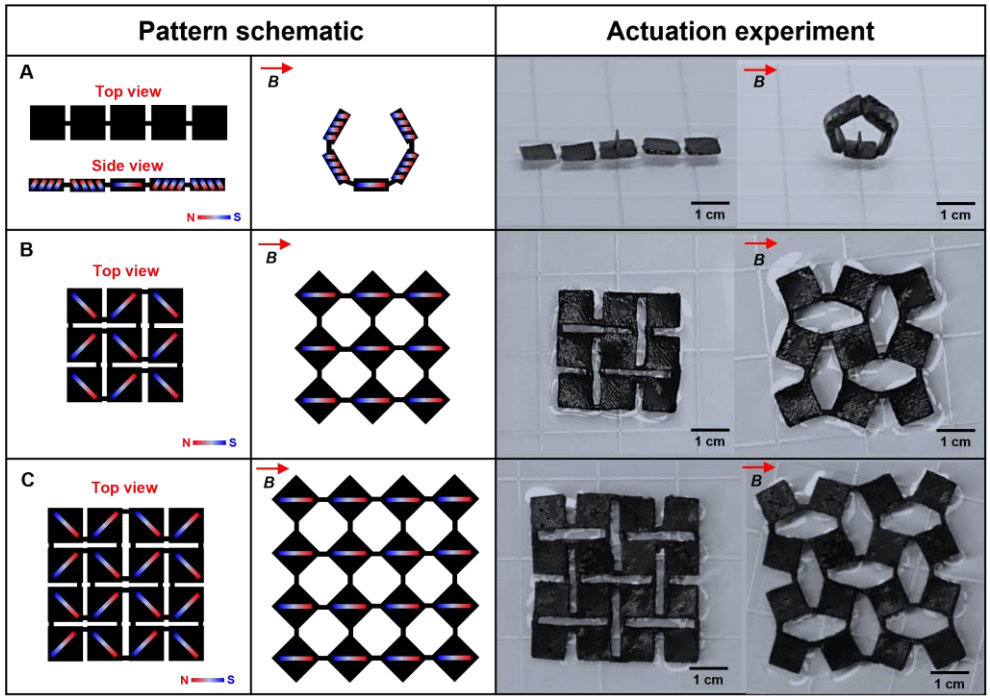

Figure 26. Application of trigger transient composites to kirigami soft robot.

The present study showcases the trigger transient properties of magnetically actuated soft actuators through degradation experiments displayed in Figure 27. These tests were conducted under the same conditions as Figure 25, whereby the PPC/PAG layer of the dual layer was irradiated with UV (365 nm) light for 15 min to create photo-induced acid and accelerate the decomposition reaction with heat at 150°C. All the samples in Figure 27A-27C disintegrated in a similar fashion: initially, the PPC/PAG layer, which comes into contact with the hot plate, decomposed due to photo-induced acid; then the acid diffused into the PPC/SAM-treated Sr-ferrite layer, which broke down sequentially. Most of the materials vaporized, leaving behind only small amounts of liquid residue and SAM-treated Sr-ferrite magnetic particles, which is consistent with the TGA outcomes presented. Thus, the transience property can be achieved in the desired time by utilizing trigger transient soft composite materials in magnetically controlled soft actuators.

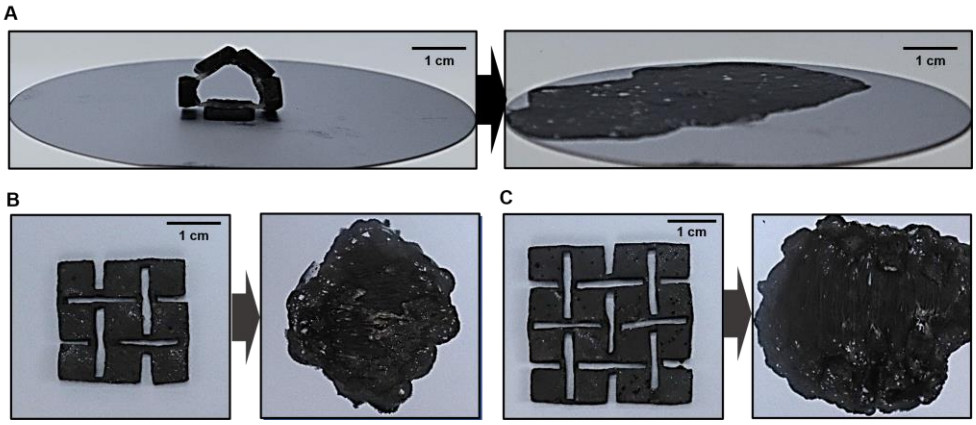

Figure 27. Photo-induced degradation of kirigami soft robot.

4.5. Experimental Verification

Preparation of PPC/PAG composites

The process of producing silicone molds involved the utilization of 3D printed polylactic acid (PLA) molds in a double-mold form. An amalgamated Ecoflex 00-30 pre-polymer (A:B = 1:1, mass ratio; Smooth-On, USA) was subsequently injected into the 3D printed PLA molds and left to cure in an oven at 60℃ for 30 min. Post-curing, the silicone mold was fabricated by immersing the product into acetone to dissolve the PLA mold, followed by cleaning with isopropyl alcohol (IPA) and drying in an oven at 60° C for 10 min. Polypropylene carbonate (PPC, Sigma-Aldrich, USA) polymer beads and 4-isopropyl-4'-methyl diphenyl iodonium tetrakis(pentafluorophenyl) borate (Rhodorsil-FABA; TCI, Japan) photo-acid generator (PAG) powder were then added to an ethyl acetate solvent and stirred using a magnetic bar. The mixture was poured into the silicone mold and allowed to cure overnight through solvent evaporation. The same method was used in preparing PPC single layer samples. To create PPC+PPC/PAG double-layer samples, the PPC/PAG solution was added onto the previously fabricated PPC layer and then allowed to cure overnight under ambient conditions.

Characterization and decomposition analysis of PPC/PAG composites

To create freestanding samples with a thickness of 1–3 mm, a width of 10–15 mm, and a length of 50 mm, cured polymer composite sheets were cut. To measure the mechanical properties of these samples, uniaxial tensile testing was conducted using an Instron 3343 universal tensile testing machine with a fixed strain rate of 10% per second. The decomposition kinetic behavior of the samples was analyzed using thermogravimetric analysis (TGA) with a heating acceleration rate of 5℃ per minute in a nitrogen atmosphere. The decomposition chemistry of the samples was analyzed using IR spectroscopy with a Nicholet iS50 FT–IR spectrophotometer. Additionally, 1H–NMR data were obtained using a 500 MHz AvanceIII–500 (Bruker, German) with dichloromethane (DCM) serving as a solvent.

Preparation of SAM treated Sr–ferrite and PPC/Sr–ferrite composite.

The process of surface treatment of Sr–ferrite, with a diameter less than 10 μm, was carried out by exposing it to ultraviolet ozone for 30 minutes using a UV–ozone cleaner (UVC–150, Omni science, Korea) to create a hydroxyl surface. Thereafter, the ozone–treated

Sr-ferrite was immersed in n-hexane solvent in a glass petri dish, and octadecyl-trichlorosilane (ODTS, Sigma-Aldrich, USA) of 200 μL was uniformly added using a pipette. After one hour of soaking, the SAM-treated Sr-ferrite was obtained by removing it from the solvent and washing it with n-hexane and isopropyl alcohol (IPA) followed by drying in an oven (60℃ for 10 min).

The desired PPC solution was prepared by adding PPC polymer beads into ethyl acetate solvent and stirring. PPC/Sr-ferrite solution was prepared by adding the SAM treated Sr-ferrite to the desired PPC solution. To obtain samples with different morphologies, the solution was thoroughly mixed using an ultrasonicator and a vortexer before pouring it into silicone molds. The curing process with solvent evaporation was performed overnight in ambient conditions. To fabricate the PPC/Sr-ferrite + PPC/PAG composite, the PPC/PAG solution was poured onto the PPC/Sr-ferrite composite layer to form the PPC/Sr-ferrite + PPC/PAG dual layer, followed by the same curing process.

Fabrications and characterization of kirigami soft robots

The PPC/Sr-ferrite + PPC/PAG dual layer composite was accurately shaped using a state-of-the-art laser cutter (MD-U1000C, Keyence, Japan). The resulting cut samples were

subjected to a uniform magnetic field region (1T, 10 min) through the employment of a vibrating sample magnetometer (VSM, VSM-7410, Lake Shore Crytronics Inc., USA) to induce magnetization along a desired direction. The magnetized polymer composites were then arranged into a specifically designed silicone mold with a designated actuation direction. The magnetically actuated kirigami robot was formed by pouring PPC/PAG solution into hinges and curing overnight in ambient conditions with solvent evaporation. This same process was utilized to create all magnetically actuated kirigami robots. Actuation testing of the magnetically actuated kirigami robot was conducted on water, with the floated kirigami soft robots being activated through uniform magnetic fields between large electromagnets under 300 mT.

4.6. Chapter Summary

In this study, we have devised a novel material system for soft actuators that is capable of magnetic actuation and trigger transience. This is achieved by incorporating PPC/PAG composites and SAM-treated Sr-ferrite particles, which respectively provide the functions of transience and magnetic actuation. We have verified the proposed material decomposition mechanism through spectroscopic analysis and confirmed the decomposition behavior of the PPC/PAG polymer composite using kinetic analysis. To prevent bonding formation between the PPC polymer and Sr-ferrite during the decomposition reaction, we have performed SAM treatment on the Sr-ferrite particle surface. By utilizing this composite material, we have successfully fabricated disposable soft actuators such as gripper and kirigami patterns that exhibit the functions of actuation and motion under a magnetic field. The actuator can be decomposed entirely in a desired time through UV light and heat exposure after the final operation. The complete degradability of this material makes it suitable for potential applications such as hardware-secure actors or robots, effective robotic waste management, and access to dangerous areas.

Chapter 5

LIFECYCLE CONFIGURABLE SOFT ROBOTS

Contents

5.1 Introduction 118

5.2 Overall strategy of research 122

5.3 Material design 126

5.3.1 Self Healing System 126

5.3.2 Self Reporting System 129

5.3.3 Self Healing, Reporting and Degrading combined System 131

5.4 Application to Soft Robotics 134

5.4.1 Soft Robot demonstration 134

5.4.2 Soft Electronics Integration 135

5.5 Chapter Summary 137

5.1. Introduction

Soft materials are attracting attention in various research fields due to not only their intrinsic soft characteristics but also their advantages such as low cost and processability, as well as their widespread use in daily life. [104] Initially, the focus was on using soft materials in the study of materials such as engineering polymers, which then evolved into their application in electronic components. Soft materials have been used not only as substrates for flexible electronic components but also as materials for organic semiconductors. [105-107] Beyond these developments, researchers have recently started studying soft robots made from soft materials. [108-110] As the use of soft materials increases in various fields, there is a growing need for research on controlling the lifespan of these materials. Furthermore, the development of polymer-based flexible materials that possess human-like or identical functionality is currently limited by the inherent properties of polymers. [111] The ultimate solution to improve the lifespan, stability, and sustainability of these materials is the development of soft composite materials with a wide range of potential applications in next-generation electronic skin, biocompatible materials for organs/tissues and muscles, and beyond.

For the production of such materials, various soft materials have been studied, such as self-reporting, self-healing, and controlled degrading materials. [112] Self-reporting materials are those that can visualize external forces or damage to the material in real-time without any external power source while maintaining the material's properties. Research using spiropyran (SP) molecules, a type of mechanophore, has been extensively conducted by synthesizing the molecules with polymer materials, allowing for stress visualization through changes in the molecule's optical properties. [113-115] At Hokkaido University, studies using rotaxane molecules to control fluorescence resonance energy transfer by molecular strain-induced luminescence have also been conducted. While this technology enables the implementation of material systems that emit light of various colors through fluorescence resonance energy transfer, it is difficult to apply to real-world scenarios due to the need to synthesize complex polymer materials. Self-healing materials have been studied using various methods, such as capsule-type self-healing, ionomers that utilize intermolecular forces, pi-pi stacking structures, hydrogen bonding structures, and reversible covalent bond structures. Recently, researchers at the University of Illinois Urbana-Champaign (UIUC) reported the implementation of self-healing

polymers using boric acid (BA), which can be easily produced by condensation reactions with hydroxyl groups and exhibits rapid self-healing properties at low temperatures. [116-118] However, the mechanical properties of self-healing materials, which are in trade-off with their self-healing properties, leave much to be desired. Controlled-degrading materials have also been studied based on various degradation mechanisms, such as acid or base hydrolysis, mechanochemical degradation, and photo-induced degradation. Research has also been conducted on structurally unstable materials with low ceiling temperatures. Autonomous lifespan control composite materials can be considered the ultimate new material concept that can enhance the lifespan, stability, and sustainability of materials by combining self-reporting, self-healing, and controlled degrading technologies into one polymer material technology. However, despite the need for a new material concept that combines all of these technologies, there are various limitations that have not yet allowed for the exploration of autonomous lifespan control composite materials. Furthermore, there are currently no reports of biomimetic material systems that can react to the environment and control their lifespan without external energy sources.

In this study, we have devised a novel self-life control

conjugated material with the capability of simultaneously implementing self-reporting, self-healing, and controlled degrading. This material is composed of a polymer composite, and each of its functions is realized through chemical reactions. When subjected to external forces, the material changes color, and when damaged by strong forces, it can be healed at low temperatures. Furthermore, by applying intense ultraviolet radiation and thermal energy at the desired moment, complete degradation of the polymer composite can be achieved.

5.2. Overall Strategy of Research

In this study, we have devised a cutting-edge next-generation compliant composite material with self-diagnostic, self-healing, and controlled degradation capabilities, based on a novel concept. Unlike conventional compliant materials that serve merely as a passive exterior or support, this technology is designed to autonomously respond to various damaging factors such as external impact, chemical corrosion, and severe heat, akin to human skin tissue, without the need for external devices. Figure 28 illustrates the overall scheme of this material. During operation, if damage occurs due to external forces applied to the material, the self-reporting system allows for the identification of the damage, followed by self-healing, using a specific amount of external energy, to restore the performance of the polymer to its initial state. To enable the material to be used indefinitely until required, we employed a strategy of controlled degradation, allowing the material to be decomposed into an irrecoverable state when its utility is reduced.

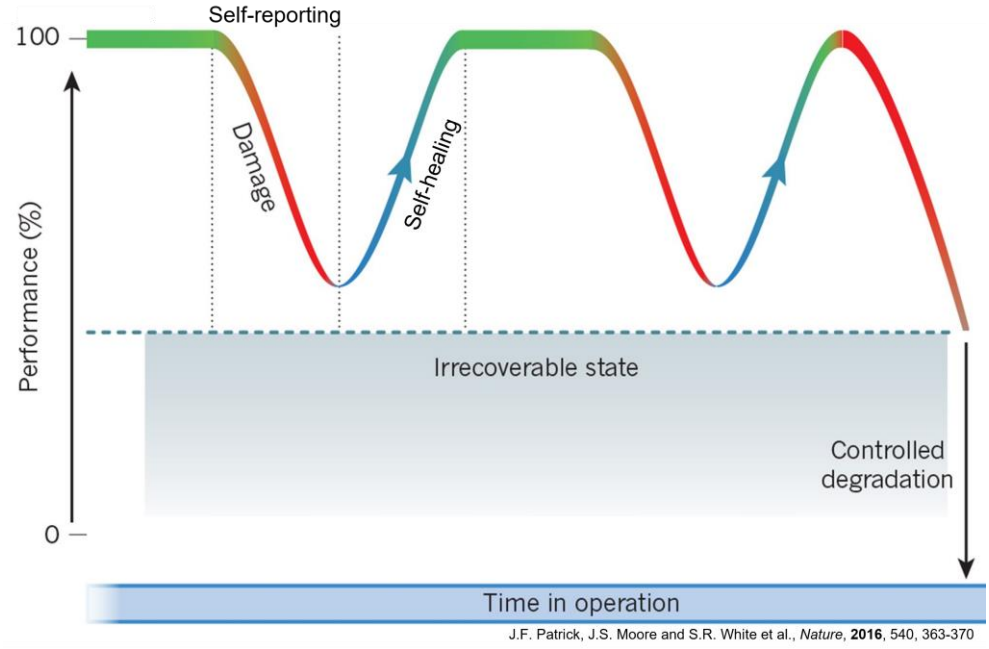

Figure 28. Scheme of autonomous lifetime-configurable soft material.

Figure 29 presents the materials chosen to implement lifetime-configurable soft materials. For self-reporting materials, we employed the well-known mechanophore material, spiropyran, which exhibits mechano-chromic properties during the polymer synthesis process. For self-healing materials, we utilized boric acid cross-linkers and hydroxyl-terminated PDMS, which require minimal activation energy, thus easily manifesting self-healing properties even at low temperatures. Finally, to achieve controlled degradation, we employed the photo-fluoride generator diphenyliodonium hexafluorophosphate (DPI-HFP) used in Chapter 3, which enables the photo-induced fluoride ion to break the polymer chains, leading to irreversible state transition. Ultimately, we implemented lifetime-configurable soft materials using this research strategy.

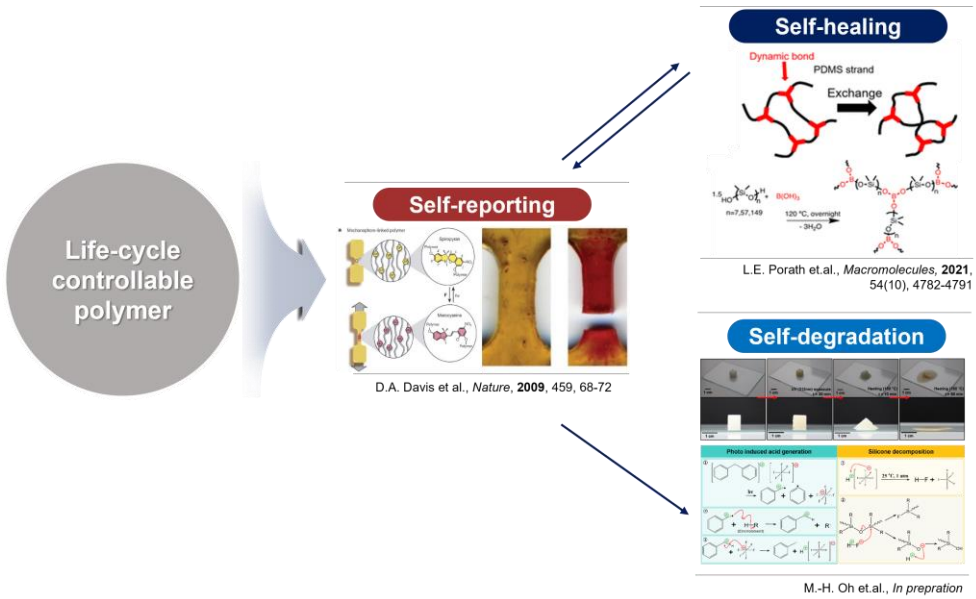

Figure 29. Overall strategy of autonomous lifetime-configurable soft material.

5.3. Material design

5.3.1 Self Reporting System

For the implementation of lifetime-configurable soft material, a self-reporting material was used that utilizes spiropyran (SP). Figure 30 illustrates the operating principle of the self-reporting system using SP and a photograph of the PDMS-based crosslinked silicone elastomer to which it was applied. Spiropyran is composed of cyclic components, including benzene, and the mechano-chromic moiety is bound to the polymer chain. When external force is applied, a force-induced 6-π electrocyclic ring-opening reaction occurs, causing a chemical structure transformation to merocyanine (MC). Unlike SP, which lacks a conjugation structure, MC's chemical structure change leads to the creation of conjugation through cleavage of the C-O bond, resulting in light absorption in the visible range and causing polymer color change. To produce clear color changes, previous studies reported the bonding of polymer chains to various parts of SP, but this study strategically bonded polymer to position 8, where stress could be preferentially applied to the central C-O bond. (Figure 30A)

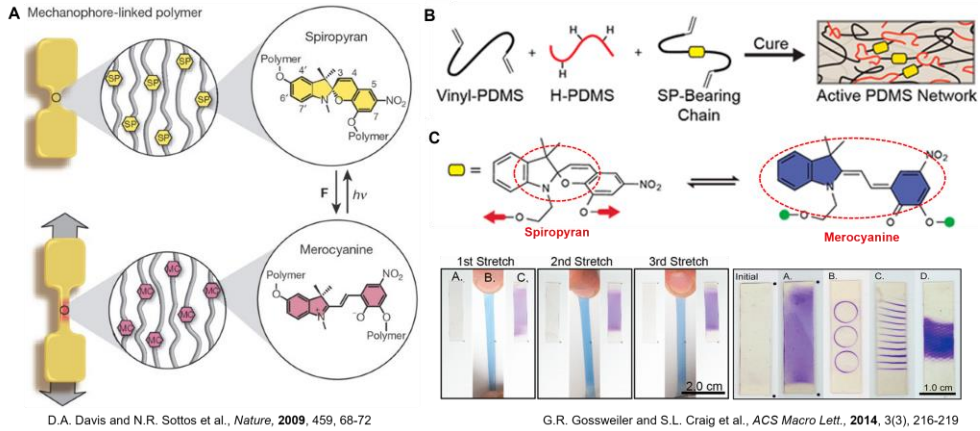

D.A. Davis and N.R. Sottos et al., *Nature*, **2009**, 459, 68-72

G.R. Gossweiler and S.L. Craig et al., *ACS Macro Lett.*, **2014**, 3(3), 216-219

Figure 30. Working mechanism of self-reporting material and polymerization strategy.

The SP molecule exhibits thermo- and photochromic response characteristics, and even when it transforms into the planar structure of MC due to external forces, the reversible C-O bond, which is cleaved by UV light or thermal energy, reunites to return to the SP structure. Figure 30B shows a simple scheme of polymerization by adding SP molecules to the actual polymer to be produced. Crosslinked PDMS is formed by solvent-free cross-linking reaction with H-PDMS, vinyl-PDMS, and Pt-catalyst. This reaction is a well-known and simple chemical reaction that occurs at room temperature simply by mechanically mixing these substances. When the self-reporting material, SP molecule, is mixed with H-PDMS, vinyl-PDMS, and Pt-catalyst and reacted, the vinyl group at positions 5 and 8 of the SP molecule reacts with H-PDMS through the Pt-catalyst to exist together in the crosslinked PDMS network. Figure 30C illustrates the operating principle and a photograph of the material produced using this method. When uniaxial strain is applied to the material, it changes color to purple, as shown in the bottom left image. When UV light or thermal energy is applied to the purple material, it returns to its original transparent color, and this reaction is reversible and can be repeated multiple times. As seen in the right photo of Figure 30C, not only uniaxial strain but also various mechanical deformations,

such as scratches, cause the mechanophore to react well, resulting in color changes. This material is intended to be used to implement a self-reporting material, one of the various functions of a lifetime-configurable soft material.

5.3.2 Self Healing System

The implementation of lifetime-configurable soft material requires the utilization of self-healing material based on dynamic bonding, employing boric acid (BA) cross-linker, in order to create self-healable PDMS. This study, which has been previously reported by UIUC in the United States, involves the use of hydroxyl-terminated PDMS and BA to perform condensation polymerization, resulting in the formation of dynamic-bonding based self-healable PDMS (as shown in Figure 31A). The dynamic bonding that constitutes the self-healing PDMS relies on chain rearrangements within the polymer network, enabled by low bonding formation activation energy. Upon subjecting the polymer to 10 minutes of thermal energy at 60 degrees Celsius using a vacuum oven, the polymer exhibits healing without any visible traces of fracture (as depicted in Figure 31B).

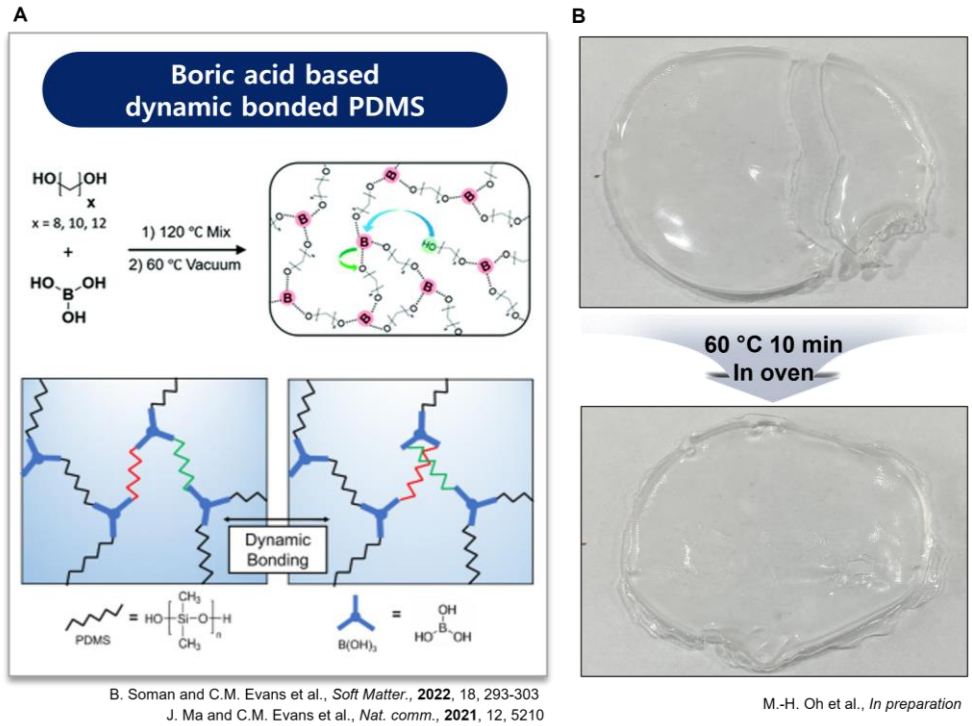

Figure 31. Healing mechanism of dynamic bond-based self-healing materials and real images.

This dynamic-bonding based self-healing polymer boasts an unparalleled advantage in terms of its unlimited healing frequency, when compared to microcapsule-based self-healing polymers. Moreover, due to its superior mechanical properties compared to hydrogen-bonding based self-healing polymers, it holds enormous potential for application in various fields. We aim to implement self-healing materials through the use of this dynamic-bonding based self-healing PDMS.

5.3.3 Self Healing, Reporting and Degrading combined System

To construct a lifetime-configurable soft material at the molecular level, the integration of self-healing and self-reporting materials poses the greatest challenge. The polymerization mechanisms of these materials differ; self-healing materials are synthesized through condensation reactions in which the hydroxyl groups at both ends of the polymer react with the hydroxyl groups of boric acid (BA), while self-reporting materials are synthesized through cross-linking reactions in which the Si-H bonds and vinyl groups react with Pt catalyst to form covalent bonds.

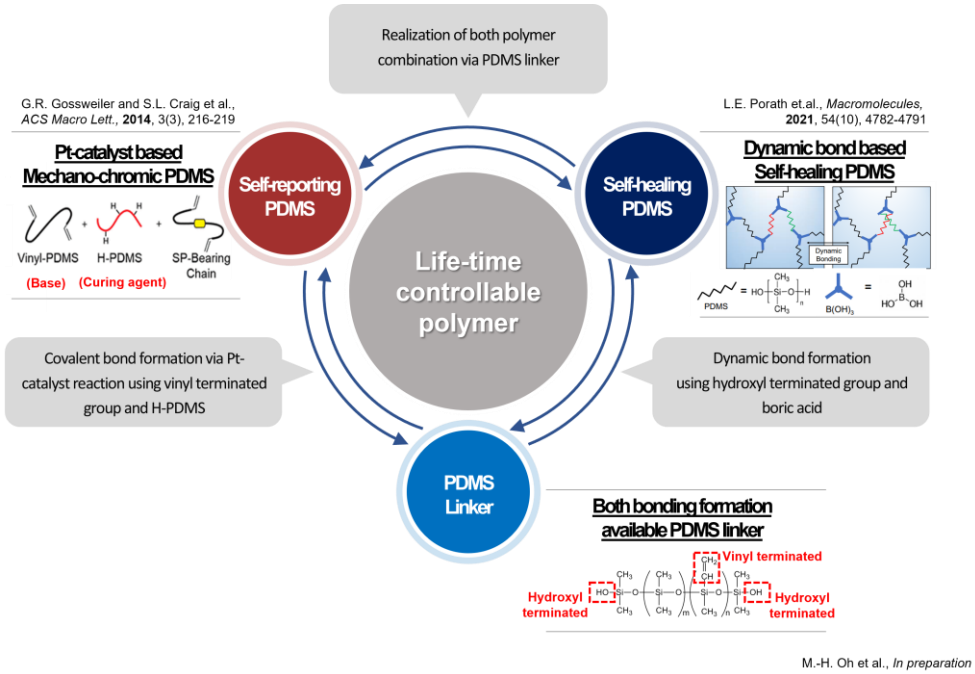

Figure 32. Integration strategy of self-healing materials and self-reporting material via PDMS linker.

To combine these two types of materials, we have introduced a new PDMS linker, as depicted in Figure 32, which has hydroxyl-terminated ends and vinyl-terminated moieties interspersed throughout the unit. The hydroxyl groups at both ends of the linker react with BA to form dynamic bonds between the linker and BA, while the vinyl groups within the unit react with H-PDMS and Pt catalyst to bind with the self-reporting material. This enables the formation of a single material from two distinct materials. Furthermore, both materials can be formed with simple thermal applications, as their reactions occur at similar temperatures around 100℃, without any complex processes. By adding a photo-fluoride generator (PFG) such as diphenyl iodonium hexafluorophosphate (DPI-HFP) during the curing process of this polymer, a degrading system can be easily implemented. This allows for the simultaneous implementation of various functions of the lifetime-configurable soft material.

5. 4. Application to Soft Robotics

5.4.1 Soft Robot demonstration

The implementation of a multi-functional, lifetime-configurable soft material with the abilities of self-healing, self-reporting, and controlled degrading has opened up a range of potential applications. In our current study, we aim to apply this material to soft robotics. The creation of a soft robot requires consideration of various factors, and the use of our proposed lifetime-configurable soft material poses challenges in terms of the constraints imposed by traditional 3D-printed molds, due to the condensation-based polymerization process involved in polymer synthesis. Therefore, we plan to produce a soft robot in the same way as previous research, utilizing the self-healing property of the lifetime-configurable soft material (as shown in Figure 32). To facilitate this process, the lifetime-configurable soft material is fabricated in thin film form, which is easier than producing a thicker material. After laser cutting the desired shape (as shown in Figure 32), the material is folded and heated in an oven at 60 degrees Celsius for 10 minutes to bond the desired parts together. This technique enables the creation of various shapes of pneumatic actuators as required. When external force is applied to the actuator or fracture

occurs, the polymer changes color to purple, and applying heat energy through healing restores both the polymer's color and transparency. Once the soft robot has reached the end of its useful life, it can be irreversibly decomposed using strong UV light and heat energy at 120℃. This enables the realization of a lifetime-configurable soft robot.

5.4.2 Soft Electronics Integration

Through the implementation of soft electronics using multi-functional lifetime-configurable soft material as a substrate, we have focused on the self-healing property among the various features of the lifetime-configurable soft material to select metal as a component for the construction of electronics. There have been numerous studies on metal particle/polymer composite based electronics and liquid metal-based electronics. Metal particle/polymer composite based electronics have the advantage of easy handling due to the inclusion of polymer in the conductor, which enhances its binding with other polymer substrates. However, it has a weakness in its electrical performance. On the other hand, liquid metal-based electronics have the advantage of superior electrical performance but suffer from the drawback of poor binding with polymer substrates, making them difficult to handle. We

propose a new concept of polymer conductor that combines both advantages by mixing polymer with liquid metal-based electronics. We added a small amount of hydrophilic polyurethane Slip C binder as a polymer binder to well-known liquid metal EGaIn, resulting in the formation of a liquid metal-polymer composite. This composite is easily coated on the PDMS-based polymer, which is the lifetime-configurable soft material. We can use doctor-blade to form a large-area conductor film, and then cut it into desired electronic shapes using a laser cutter, which allows us to produce various passive electronic components.

5.5. Chapter Summary

In this study, we have developed an advanced, resilient composite material that is capable of autonomously reporting and healing damage caused by external factors such as impact, chemical corrosion, and extreme heat, without the need for external devices. Additionally, we have implemented controlled degradation that causes irreversible changes after use. These materials were achieved through spiropyran, a mechano-chromic material, boric acid-based dynamic bonding PDMS, and DPI-HFP photo-fluoride generator.

Furthermore, we have utilized this material to create soft robots and soft electronics. For the soft robot, a simple pneumatic actuator was created using film production and origami systems. For the soft electronics, a liquid metal-polymer composite conductor was made by adding hydrophilic polyurethane Slip C binder to liquid metal EGaIn and coating it onto lifetime-configurable soft material using doctor-blade. This film was then cut into various shapes using laser cutter to create different passive electronic components. This ultimate concept of a new material technology that can improve the lifespan, stability, and sustainability of the material has broad applicability in the development of biomaterials such as electronic

skin, organs/tissues, and muscles. By presenting actual applications of soft robots and soft electronics, this study enhances the significance of our research.

Chapter 6

CONCLUSION

Conclusion

In this doctoral dissertation titled "Lifetime-Configurable Polymer Composite Systems for Soft Robotics," we have conducted research on various soft materials that can be applied to soft robotics, which is crucial for the development of soft robots. To achieve this goal, we have investigated composite material systems that are configurable in terms of their lifetime.

In the pursuit of realizing the disintegration of soft robots, various challenges have impeded progress, including mechanical properties of transient materials, instability under ambient conditions, and material degradation in operational environments. To address these issues, we have approached this problem by incorporating a type of photo-reactive material, specifically a photo-acid generator (PAG), into conventional polymers. This material not only possesses stability until exposed to intense UV light, but also exhibits excellent mechanical properties, making it highly suitable for application in highly deformable soft robots. The polymer composite was subjected to spectroscopic analyses such as FT-IR, NMR, and photo-DSC in order to identify the mechanism underlying its decomposition reaction, and to predict variables such as the rate of degradation. This photo-degradable material was

then applied to construct a pneumatic actuated walking soft robot and a magnetically actuated kirigami soft robot. Moreover, various electronic components, including UV detectors, strain sensors, and temperature sensors, were integrated into the soft robots. These electronically embedded soft robots were able to gather data by scouting virtual environments and ultimately undergo irrecoverable degradation through UV and heat exposure once their mission was complete.

In our latest research, we present a groundbreaking concept for a Lifetime-Configurable Polymer Composite that combines self-reporting materials capable of color change upon external forces, and self-healing materials that can repair damaged areas using thermal energy. This new material represents a significant advancement in the ability to simulate the true lifetime of robots, including the effects of damage. The self-reporting material, spiropyran, generates a planar conjugation structure when its central C-O bond is broken upon the application of external forces, resulting in light absorption and a purple coloration. The self-healing material utilizes boric acid to form dynamic bonds and undergoes polymerization through condensation reactions, forming a low activation energy, rapidly healing polymer structure that can be activated even at low temperatures. By linking these two materials

with a new linker, we have successfully combined both properties into one composite material. Finally, we utilize DPI-HFP to degrade the polymer irreversibly, allowing us to realize a true lifetime-configurable polymer composite. This material was also used to construct simple soft actuator and passive component-based electronics.

Through the results of these studies, the developed lifetime-configurable composite material system in this research has demonstrated great potential for application in the field of soft robotics. These research findings are expected to play a crucial role in advancing the development of soft materials and soft robotics technology. However, during the research process, several limitations were identified, and further research will be necessary to address them. Ultimately, the advancement of soft materials and soft robotics technology will open up new possibilities for application in various fields. Therefore, the material system developed in this study will have potential applications not only in the field of soft robotics but also in diverse industries such as medicine, automotive, and aerospace.

References

1. C. Majidi, Soft robotics: A perspective—current trends and prospects for the future. *Soft Robot.* **1**, 5–11 (2014).

2. M. Kovac, The bioinspiration design paradigm: A perspective for soft robotics. *Soft Robot.* **1**, 28–37 (2013).

3. G. M. Whitesides, Soft robotics. *Angew. Chem. Int. Ed. Engl.* **57**, 4258–4273 (2018).

4. P. Polygerinos, N. Correll, S. A. Morin, B. Mosadegh, C. D. Onal, K. Petersen, M. Cianchetti, M. T. Tolley, R. F. Shepherd, Soft robotics: review of fluid–driven intrinsically soft devices; manufacturing, sensing, control, and applications in human–robot interaction. *Adv. Eng. Mater.* **19**, 1700016 (2017).

5. A. Sadeghi, A. Tonazzini, L. Popova, B. Mazzolai, A novel growing device inspired by plant root soil penetration behaviors. *PLOS ONE.* **9**, e90139 (2014).

6. A. Sadeghi, A. Mondini, B. Mazzolai, Toward self-growing soft robots inspired by plant roots and based on additive manufacturing technologies. *Soft Robot.* **4**, 211-223 (2017).

7. M. Liu, S. Zhu, Y. Huang, Z. Lin, W. Liu, L. Yang, D. Ge, A self-healing composite actuator for multifunctional soft robot via photo-welding. *Compos. Part B.* **214**. 108748 (2021).

8. S. Terryn, J. Brancart, D. Lefeber, G. V. Van Assche, B. Vanderborght, Self-healing soft pneumatic robots. *Sci. Robot.* **2**, eaan4268 (2017).

9. Y. Yang, Y. Li, Y. Chen, Principles and methods for stiffness modulation in soft robot design and development. *Bio-Des. Manuf.* **1**, 14-25 (2018).

10. J. W. Boley, W. M. van Rees, C. Lissandrello, M. N. Horenstein, R. L. Truby, A. Kotikian, J. A. Lewis, L. Mahadevan, Shape-shifting structured lattices via multimaterial 4D printing. *Proc. Natl. Acad. Sci. U. S. A.* **116**, 20856-20862 (2019).

11. B. Mazzolai, C. Laschi, A vision for future bioinspired and biohybrid robots. *Sci. Robot.* **5**, eaba6893 (2020).

12. F. Hartmann, M. Baumgartner, M. Kaltenbrunner, Becoming Sustainable, The New Frontier in Soft Robotics. *Adv. Mater.* **33**, 2004413 (2021).

13. Vanishing Acts: A Call for Disappearing Delivery Vehicles (Defence Advanced Research Projects Agency (DARPA), 2015).

14. M. Lucia, Someday Disposable Drones May Deliver a Payload, Then Vanish. (NPR, 2017).

15. C. A. Aubin, S. Choudhury, R. Jerch, L. A. Archer, J. H. Pikul, R. F. Shepherd, Electrolytic vascular systems for energy-dense robots. *Nature.* **571**, 51-57 (2019).

16. R. K. Katzschmann, J. DelPreto, R. MacCurdy, D. Rus, Exploration of underwater life with an acoustically controlled soft robotic fish. *Sci. Robot.* **3**, eaar3449 (2018).

17. G. Muscato, F. Bonaccorso, L. Cantelli, D. Longo, C. D. Melita, Volcanic environments: robots for exploration

and measurement. *IEEE Robot. Automat. Mag.* **19**, 40–49 (2012).

18. . J. Huo, M. Liu, K. A. Neusypin, H. Liu, M. Guo, Y. Xiao, Autonomous search of radioactive sources through mobile robots. *Sensors (Basel).* **20**, 12, 3461 (2020).

19. R. R. Murphy, J. Peschel, C. Arnett, D. Martin, in 2012 *IEEE International Symposium on Safety, Security, and Rescue Robotics (SSRR) (IEEE, 2012),* pp. 1–4.

20. C. García–Garrido, L. A. Pérez–Maqueda, J. M. Criado, P. E. Sánchez–Jiménez, Combined kinetic analysis of multistep processes of thermal decomposition of polydimethylsiloxane silicone, *Polymer*, **153**, 558–564 (2018).

21. P. Hu, J. Madsen, A. L. Skov, One reaction to make highly stretchable or extremely soft silicone elastomers from easily available materials, *Nat. Comm.,* **13**, 370 (2022).

22. S. Walker, J. Rueben, T. V. Volkenburg, S. Hemleben, C. Grimm, J. Simonsen, Y. Mengüc ， Using an

environmentally benign and degradable elastomer in soft robotics. *Int. J. Intell. Robot. Appl.* **1**, 124–142 (2017).

23. M. Baumgartner, F. Hartmann, M. Drack, D. Preninger, D. Wirthl, R. Gerstmayr, L. Lehner, G. Mao, R. Pruckner, S. Demchyshyn, L. Reiter, M. Strobel, T. Stockinger, D. Schiller, S. Kimeswenger, F. Greibich, G. Buchberger, E. Bradt, S. Hild, S. Bauer, M. Kaltenbrunner, Resilient yet entirely degradable gelatin-based biogels for soft robots and electronics. *Nat. Mater.* **19**, 1102–1109 (2020).

24. G. Lee, Y. S. Choi, H.-J. Yoon, J. A. Rogers, Advances in physicochemically stimuli-responsive materials for on-demand transient electronic systems. *Matter*. **3**, 1031–1052 (2020).

25. O. Shelef, S. Gnaim, D. Shabat, Self-immolative polymers: an emerging class of degradable materials with distinct disassembly profiles. *J. Am. Chem. Soc.* **143**, 21177–21188 (2021).

26. A. Sagi, R. Weinstain, N. Karton, D. Shabat, Self-immolative polymers. *J. Am. Chem. Soc.* **130**, 5434-5435 (2008).

27. Q. E. A. Sirianni, E. R. Gillies, The architectural evolution of self-immolative polymers. *Polymer.* **202**, 122638 (2020).

28. J. A. Kaitz, C. E. Diesendruck, J. S. Moore, End group characterization of poly(phthalaldehyde): surprising discovery of a reversible, cationic macrocyclization mechanism. *J. Am. Chem. Soc.* **135**, 12755-12761 (2013).

29. J. L. Dektar, N. P. Hacker, Photochemistry of diaryliodonium salts. *J. Org. Chem.* **55**, 639-647 (1990).

30. Y. Yağci, I. Reetz, Externally stimulated initiator systems for cationic polymerization. *Prog. Polym. Sci.* **23**, 1485-1538 (1998).

31. S. Schlögl, M. Reischl, V. Ribitsch, W. Kern, UV induced microcellular foaming—A new approach towards the

production of 3D structures in offset printing techniques. *Prog. Org. Coat.* **73**, 54–61 (2012).

32. Y. Yagci, F. Yilmaz, S. Kiralp, L. Toppare, Photoinduced polymerization of thiophene using iodonium salt. *Macromol. Chem. Phys.* **206**, 1178–1182 (2005).

33. J. H. Simons, Academic press. *J. Fluor. Chem.* **18** (1954).

34. D. W. Davidson, S. K. Garg, The hydrate of hexafluorophosphoric acid. *Can. J. Chem.* **50**, 3515–3520 (1972).

35. M. J. Sailor, Chemical reactivity and surface chemistry of porous silicon, in Handbook of Porous Silicon, *L. Canham, Ed.*, 2014, pp. 1–24.

36. C. E. Son, S.–S. Choi, Analytical techniques for measurement of crosslink densities of rubber vulcanizates. *Elastomers Compos*. **54**, 209–219 (2019).

37. H. Hara, Y. Sano, H. Mimura, K. Arima, A. Kubota, K. Yagi, J. Murata, K. Yamauch, Novel abrasive–free

planarization of 4H-SiC (0001) using catalyst. *J. Electron. Mater.* **35**, L11-L14 (2006).

38. A. Isohashi, P. V. Bui, D. Toh, S. Matsuyama, Y. Sano, K. Inagaki, Y. Morikawa, K. Yamauchi, Chemical etching of silicon carbide in purewater by using platinum catalyst. *Appl. Phys. Lett.* **110**, 201601 (2017).

39. B. Rupasinghe, J. C. Furgal, Full circle recycling of polysiloxanes via room-temperature fluoride-catalyzed depolymerization to Repolymerizable cyclic. *ACS Appl. Polym. Mater.* **3**, 1828-1839 (2021).

40. H. M. Brothers Jr., T. Boehmer, R. A. Campbell, S. Dorn, J. J. Kerbleski, S. Lewis, C. Mund, D. Pero, K. Saito, M. Wieser, W. Zoller, Determination of cyclic volatile methylsiloxanes in personal care products by gas chromatography. *Int. J. Cosmet. Sci.* **39**, 580-588 (2017).

41. D. J. Krug, M. Z. Asuncion, R. M. Laine, Facile approach to recycling highly cross-linked thermoset silicone

resins under ambient conditions. *ACS Omega.* **4**, 3782–3789 (2019).

42. E. F. C. Griessbach, R. G. Lehmann, Degradation of polydimethylsiloxane fluids in the environment — a review. *Chemosphere.* **38**, 1461–1468 (1999).

43. S. Xu, R. G. Lehmann, J. R. Miller, G. Chandra, Degradation of polydimethylsiloxanes (silicones) as influenced by clay minerals. *Environ. Sci. Technol.* **32**, 1199–1206 (1998).

44. S. Vyazovkin, A. K. Burnham, J. M. Criado, L. A. Pérez–Maqueda, C. Popescu, N. Sbirrazzuoli, ICTAC Kinetics committee recommendations for performing kinetic computations on thermal analysis data. *Thermochim. Acta*. **520**, 1–19 (2011).

45. R. Hardis, J. L. P. Jessop, F. E. Peters, M. R. Kessler, Cure kinetics characterization and monitoring of an epoxy resin using DSC, Raman spectroscopy, and DEA. *Compos. Part A Appl. Sci. Manuf.* **49**, 100–108 (2013).

46. S.-Y. Fu, X.-Q. Feng, B. Lauke, Y.-W. Mai, Effects of particle size, particle/matrix interface adhesion and particle loading on mechanical properties of particulate-polymer composites. *Composites Part B: Engineering.* **39**, 933-961 (2008).

47. A. J. Kinloch, R. J. Young, Fracture Behaviour of Polymers (Kluwer Academic Publishers, Dordrecht, Netherlands, 1983).

48. P. Mazurek, S. Vudayagiri, A. L. Skov, How to tailor flexible silicone elastomers with mechanical integrity: a tutorial review. *Chem. Soc. Rev.* **48**, 1448-1464 (2019).

49. Y. Tang, Y. Chi, J. Sun, T. H. Huang, O. H. Maghsoudi, A. Spence, J. Zhao, H. Su, J. Yin, Leveraging elastic instabilities for amplified performance: spine-inspired high-speed and high-force soft robots. *Sci. Adv.* **6**, eaaz6912 (2020).

50. D. P. J. Cotton, I. M. Graz, S. P. Lacour, A multifunctional capacitive sensor for stretchable electronic skins. *IEEE Sens. J.* **9**, 2008-2009 (2009).

51. T. Dinh, H. Phan, A. Qamar, P. Woodfield, N. Nguyen, D. V. Dao, Thermoresistive effect for advanced thermal sensors: fundamentals, design considerations, and applications. *J. Microelectromech. Syst.* **26**, 966–986 (2017).

52. J. H. Dellinger, The temperature coefficient of resistance of copper. *J. Franklin Inst.* **170**, 213–216 (1910).

53. T. P. Pearsall, M. A. Pollack, Compound semiconductor photodiodes. *Semicond. Semimetals* (Elsevier, 1985). **22**, D, 173–245.

54. J. Y. Bae, E. J. Gwak, G. S. Hwang, H. W. Hwang, D. J. Lee, J. S. Lee, Y. C. Joo, J. Y. Sun, S. H. Jun, M. R. Ok, J. Y. Kim, S. K. Kang, Biodegradable metallic glass for stretchable transient electronics. *Adv. Sci.* **8**, 2004029 (2021).

55. N. G. Mistkawi, M. A. Hussein, M. Ziomek-Moroz, S. B. Rananavare, Copper thin-film dissolution/precipitation

kinetics in organic HF containing cleaning solution. *J. Electrochem. Soc.* **157**, 801–805 (2010).

56. I. Apsite, S. Salehi, L. Ionov, Materials for Smart Soft Actuator Systems. *Chem. Rev.* **122**, 1349–1415 (2022).

57. J. Kim, J. W. Kim, H. C. Kim, L. Zhai, H. U. Ko, R. M. Muthoka, Review of Soft Actuator Materials. *Int. J. Precis. Eng. Manuf.* **20**, 2221–2241 (2019).

58. R. V. Martinez, A. C. Glavan, C. Keplinger, A. I. Oyetibo, G. M. Whitesides, Soft Actuators and Robots That Are Resistant to Mechanical Damage. *Adv. Funct. Mater.* **24**, 3003–3010 (2014).

59. F. Hartmann, M. Baumgartner, M. Kaltenbrunner, Becoming Sustainable, the New Frontier in Soft Robotics. *Adv. Mater.* **33**: ARTN 2004413 (2021).

60. B. azzolai, C. Laschi, A Vision for Future Bioinspired and Biohybrid Robots. *Sci. Robot.* **5**: ARTN eaba6893 (2020).

61. J. W. Boley, W. M. van Rees, C. Lissandrello, M. N. Horenstein, R. L. Truby, A. Kotikian, J. A. Lewis, L. Mahadevan, Shape-Shifting Structured Lattices via Multimaterial 4D Printing. *Proc. Natl. Acad. Sci. U. S. A.* **116**, 20856–20862 (2019).

62. G. M. Whitesides, Soft Robotics. *Angew. Chem. Int. Ed. Engl.* **57**, 4258–4273 (2018).

63. P. Polygerinos, N. Correll, S. A. Morin, B. Mosadegh, C. D. Onal, K. Petersen, M. Cianchetti, M. T. Tolley, R. F. Shepherd, Soft Robotics: Review of Fluid-Driven Intrinsically Soft Devices; Manufacturing, Sensing, Control, and Applications in Human-Robot Interaction. *Adv. Eng. Mater.* **19**: ARTN 1700016 (2017).

64. R. F. Shepherd, F. Ilievski, W. Choi, S. A. Morin, A. A. Stokes, A. D. Mazzeo, X. Chen, M. Wang, G. M. Whitesides, Multigait Soft Robot. *Proc. Natl. Acad. Sci. U. S. A.* **108**, 20400–20403 (2011).

65. T. Jiralerspong, G. Bae, J. H. Lee, S. K. Kim, Wireless Control of Two- and Three-Dimensional Actuations of Kirigami Patterns Composed of Magnetic-Particles-Polymer Composites. *ACS Nano.* **14**, 17589–17596 (2020).

66. H. Song, H. Lee, J. Lee, J. K. Choe, S. Lee, J. Y. Yi, S. Park, J. W. Yoo, M. S. Kwon, J. Kim, Reprogrammable Ferromagnetic Domains for Reconfigurable Soft Magnetic Actuators. *Nano Lett.* **20**, 5185–5192 (2020).

67. V. Cacucciolo, J. Shintake, Y. Kuwajima, S. Maeda, D. Floreano, H. Shea, Stretchable Pumps for Soft Machines. *Nature*. **572**, 516–519 (2019).

68. Y. Wu, Y. Yang, X. Qian, Q. Chen, Y. Wei, Y. Ji, Liquid-Crystalline Soft Actuators with Switchable Thermal Reprogrammability. *Angew. Chem. Int. Ed. Engl*. **59**, 4778–4784 (2020).

69. J. Hu, W. Z. Wang, H. F. Yu, Endowing Soft Photo-actuators with Intelligence. *Adv. Intell. Syst.* **1**: ARTN 1900050 (2019).

70. H. Yuk, S. T. Lin, C. Ma, M. Takaffoli, N. X. Fang, X. H. Zhao, Hydraulic Hydrogel Actuators and Robots Optically and Sonically Camouflaged in Water. *Nat. Commun.* **8**, 14230 (2017).

71. N. Bira, P. Dhagat, J. R. Davidson, A Review of Magnetic Elastomers and Their Role in Soft Robotics. *Front. Robot. AI.* **7**: ARTN 588391 (2020).

72. Y. Dong, L. Wang, N. Xia, Z. X. Yang, C. Zhang, C. F. Pan, D. D. Jin, J. C. Zhang, C. Majidi, L. Zhang, Untethered Small-Scale Magnetic Soft Robot with Programmable Magnetization and Integrated Multifunctional Modules. *Sci. Adv.* **8**, eabn8932 (2022).

73. N. Ebrahimi, C. H. Bi, D. J. Cappelleri, G. Ciuti, A. T. Conn, D. Faivre, N. Habibi, A. Hošovský, V. Iacovacci, I. S. M. Khalil, Magnetic Actuation Methods in Bio/Soft

Robotics. *Adv. Funct. Mater.* 31: ARTN 2005137 (2021).

74. Y. Kim, X. H. Zhao, Magnetic Soft Materials and Robots. *Chem. Rev.* 122, 5317–5364 (2022).

75. W. Q. Hu, G. Z. Lum, M. Mastrangeli, M. Sitti, Small-Scale Soft-Bodied Robot with Multimodal Locomotion. *Nature*. 554, 81–85 (2018).

76. Y. Kim, H. Yuk, R. K. Zhao, S. A. Chester, X. H. Zhao, Printing Ferromagnetic Domains for Untethered Fast-Transforming Soft Materials. *Nature.* 558, 274–279 (2018).

77. Y. H. Wu, S. Zhang, Y. Yang, Z. Li, Y. Wei, Y. Ji, Locally Controllable Magnetic Soft Actuators with Reprogrammable Contraction-Derived Motions. *Sci. Adv.* 8, eabo6021 (2022).

78. M.-H. Oh, Y.-H. Kim, S.-M. Lee, G.-S. Hwang, K.-S. Kim, J.-Y. Bae, J.-Y. Kim, J.-Y. Lee, Y.-C. Kim, S. Y. Kim, S.-K. Kang, Lifetime-Configurable Soft Robots

via Photodegradable Silicone Elastomer Composites. *arXiv* :2302.14331. (2023).

79. M. Baumgartner, F. Hartmann, M. Drack, D. Preninger, D. Wirthl, R. Gerstmayr, L. Lehner, G. Y. Mao, R. Pruckner, S. Demchyshyn. M. Kaltenbrunner Resilient yet Entirely Degradable Gelatin-Based Biogels for Soft Robots and Electronics. *Nat. Mater.* **19**, 1102–1109 (2020).

80. A. Heiden, D. Preninger, L. Lehner, M. Baumgartner, M. Drack, E. Woritzka, D. Schiller, R. Gerstmayr, F. Hartmann, M. Kaltenbrunner. 3D Printing of Resilient Biogels for Omnidirectional and Exteroceptive Soft Actuators. *Sci. Robot.* **7**: eabk2119 (2022).

81. Y. Gao, S. Gu, F. Jia, G. H. Gao, A Skin-Matchable, Recyclable and Biofriendly Strain Sensor Based on a Hydrolyzed Keratin-Containing Hydrogel. *J. Mater. Chem. A.* **8**, 24175–24183 (2020).

82. G. Lee, Y. S. Choi, H. J. Yoon, J. A. Rogers, Advances in Physicochemically Stimuli-Responsive Materials for On-Demand Transient Electronic Systems. *Matter.* **3**, 1031–1052 (2020).

83. J. A. Kaitz, C. E. Diesendruck, J. S. Moore, End Group Characterization of Poly(Phthalaldehyde): Surprising Discovery of a Reversible, Cationic Macrocyclization Mechanism. *J. Am. Chem. Soc.* **135**, 12755–12761 (2013).

84. A. Sagi, R. Weinstain, N. Karton, D. Shabat, Self-Immolative Polymers. *J. Am. Chem. Soc.* **130**, 5434–5435 (2008).

85. O. Shelef, S. Gnaim, D. Shabat, Self-Immolative Polymers: An Emerging Class of Degradable Materials with Distinct Disassembly Profiles. *J. Am. Chem. Soc.* **143**, 21177–21188 (2021).

86. M. G. Cupta, P. J. Joseph, P. A. Kohl, Photoacid Generators for Catalytic Decomposition of

Polycarbonate. *J. Appl. Polym. Sci.* 105, 2655–2662 (2007).

87. A. Ulman, Formation and Structure of Self-Assembled Monolayers. *Chem. Rev.* 96, 1533–1554 (1996).

88. P. P. Jing, J. L. Du, J. B. Wang, J. W. Wei, L. Pan, J. A. Li, Q. F. Liu, Width-Controlled M-Type Hexagonal Strontium Ferrite ($SrFe_{12}O_{19}$) Nanoribbons with High Saturation Magnetization and Superior Coercivity Synthesized by Electrospinning. *Sci. Rep.* 5, 15089 (2015).

89. L. Wang, C. F. Guo, X. H. Zhao, Magnetic Soft Continuum Robots with Contact Forces. *Extreme Mech. Lett.* 51: 101604 (2022).

90. Y. Kim, E. Genevriere, P. Harker, J. Choe, M. Balicki, R. W. Regenhardt, J. E. Vranic, A. A. Dmytriw, A. B. Patel, X. H. Zhao, Telerobotic Neurovascular Interventions with Magnetic Manipulation. *Sci. Robot.* 7, eabg9907 (2022).

91. J. L. Dektar, N. P. Hacker, Photochemistry of Diaryliodonium Salts. J. *Org. Chem.* **55**, 639–647 (1990).

92. Y. Yağci, I. Reetz, Externally Stimulated Initiator Systems for Cationic Polymerization. *Prog. Polym. Sci.* **23**, 1485–1538 (1998).

93. Y. Yagci, F. Yilmaz, S. Kiralp, L. Toppare, Photoinduced Polymerization of Thiophene Using Iodonium Salt. *Macromol. Chem.* Phys. **206**, 1178–1182 (2005).

94. S. Schlögl, M. Reischl, V. Ribitsch, W. Kern, UV Induced Microcellular Foaming—A New Approach Towards the Production of 3D Structures in Offset Printing Techniques. *Prog. Org. Coat.* **73**, 54–61 (2012).

95. E. Uzunlar, J. Schwartz, O. Phillips, P. A. Kohl, Decomposable and Template Polymers: Fundamentals and Applications. *J. Electron. Packaging.* **138**: 020802 (2016).

96. C. Alberti, D. Rijono, M. Wehrmeister, E. Cheung, S. Enthaler, Depolymerization of Poly(1,2−Propylene

Carbonate) via Ring Closing Depolymerization and Methanolysis. *ChemistrySelect.* **7**: e202104004 (2022).

97. M. Mandal, U. Monkowius, D. Chakraborty, Synthesis and Structural Characterization of Titanium and Zirconium Complexes Containing Half–salen Ligands as Catalysts for Polymerization Reactions. *New J. Chem.* **40**, 9824–9839 (2016).

98. O. Phillips, J. M. Schwartz, P. A. Kohl, Thermal Decomposition of Poly(Propylene Carbonate): End–Capping, Additives, and Solvent Effects. *Polym. Degrad. Stabil.* **125**, 129–139 (2016).

99. M. Szekeres, I. Y. Tóth, R. Turcu, E. Tombácz, The Effect of Polycarboxylate Shell of Magnetite Nanoparticles on Protein Corona Formation in Blood Plasma. *J. Magn. Magn. Mater.* **427**, 95–99 (2017).

100. V. Socoliuc, D. Peddis, V. I. Petrenko, M. V. Avdeev, D. Susan–Resiga, T. Szabó, R. Turcu, E. Tombácz, L. Vékás, Magnetic Nanoparticle Systems for

Nanomedicine—A Materials Science Perspective. *Magnetochemistry.* **6**: 2 (2020).

101. S. A. Kulinich, M. Farzaneh, Alkylsilane Self-Assembled Monolayers: Modeling Their Wetting Characteristics. *Appl. Surf. Sci.* **230**, 232–240 (2004).

102. M. Pasquali, S. De Gendt, S. Armini, Understanding the Impact of Cu Surface Pre-treatment on Octadecanethiol-Derived Self-Assembled Monolayer as a Mask for Area-Selective Deposition. *Appl. Surf. Sci.* **540**: 148307 (2021).

103. T. P. Xie, L. J. Xu, C. L. Liu, Y. Wang, Magnetic Composite $ZnFe_2O_4/SrFe_{12}O_{19}$: Preparation, Characterization, and Photocatalytic Activity Under Visible Light. *Appl. Surf. Sci.* **273**, 684–691 (2013).

104. G. R. Whittell, M. D. Hager, U. S. Schubert, I. Manners, Functional soft materials from metallopolymers and metallosupramolecular polymers. *Nat. Mater.* **10**, 176–188 (2011).

105. A. Malik, B. Kandasubramanian. Flexible Polymeric Substrates for Electronic Applications. *Polymer Reviews.* **58**, 630–667 (2018).

106. P. W. M. Blom. Polymer Electronics: To Be or Not to Be? *Adv. Mater. Tech.* **5**, 2000144 (2020).

107. Q.-D. Ling, D.-J. Liaw, C. Zhu, D. S.-H. Chan, E.-T. Kang, K.-G. Neoh. Polymer electronic memories: Materials, devices and mechanisms. *Progress in Polymer Science.* **33**, 917–978 (2008).

108. C. Majidi. Soft-Matter Engineering for Soft Robotics. *Adv. Mater. Tech.* **4**, 1800477 (2019).

109. C. Lee, M. Kim, Y. J. Kim, N. Hong, S. Ryu, H. J. Kim, S. Kim. *International Journal of Control, Automation and Systems.* **15**, 3–15 (2017).

110. K.-J. Cho, J.-S. Koh, S. Kim, W.-S. Chu, Y. Hong, S.-H. Ahn. *International Journal of Precision Engineering and Manufacturing.* **10**, 171–181 (2009).

111. S. Kim, C. Laschi, B. Trimmer. Soft robotics: a bioinspired evolution in robotics. *Trends in Biotechnology*, **31**, 287–294 (2013).

112. J. F. Patrick, M. J. Robb, N. R. Sottos, J. S. Moore, S. R. White. Polymers with autonomous life-cycle control. *Nature*. **540**, 363–370 (2016).

113. D. A. Davis, A. Hamilton, J. Yang, L. D. Cremar, D. V. Gough, S. L. Potisek, M. T. Ong, P. V. Braun, T. J. Martínez, S. R. White, J. S. Moore, N. R. Sottos. Force-induced activation of covalent bonds in mechanoresponsive polymeric materials. *Nature*. **459**, 68–72 (2009).

114. G. R. Gossweiler, G. B. Hewage, G. Soriano, Q. Wang, G. W. Welshofer, X. Zhao, S. L. Craig. Mechanochemical Activation of Covalent Bonds in Polymers with Full and Repeatable Macroscopic Shape Recovery. *ACS Macro Lett.* **3**, 216–219 (2014).

115. T. A. Kim, B. A. Beiermann, S. R. White, N. R. Sottos. Effect of Mechanical Stress on Spiropyran–Merocyanine Reaction Kinetics in a Thermoplastic Polymer. *ACS Macro Lett.* **5**, 1312–1316 (2016).

116. L. E. Porath, C. M. Evans. Importance of Broad Temperature Windows and Multiple Rheological Approaches for Probing Viscoelasticity and Entropic Elasticity in Vitrimers. *Macromolecules.* **54**, 4782–4791 (2021).

117. B. Soman, Y. K. Go, C. Shen, C. Leal, C. M. Evans. Impact of dynamic covalent chemistry and precise linker length on crystallization kinetics and morphology in ethylene vitrimers. *Soft Matter*. **18**, 293–303 (2022).

118. J. Ma, L. E. Porath, M. F. Haque, S. Sett, K. F. Rabbi, S. Nam, N. Miljkovic, C. M. Evans. Ultra–thin self–healing vitrimer coatings for durable hydrophobicity. *Nat. Comm.* **12**, 5210 (2021).

초 록

소프트 재료는 다양한 물질군들 중 비교적 부드러운 기계적 물성을 가지는 다양한 소재들을 의미한다. 소프트 재료는 이러한 부드러운 기계적 물성으로 인하여 초기의 엔지니어링 플라스틱을 시작으로 생체 소재 분야, 전자 소자 분야, 로봇 분야 등 다양한 분야의 많은 공학자들에 의해 연구가 진행되어 왔다. 최근에 이러한 소프트 재료를 활용한 로봇 연구 분야인 소프트 로봇이라는 연구가 활발하게 이루지고 있다.

소프트 로봇은 큰 변형이 가능하기 때문에 자유로운 움직임을 가질 수 있는 장점이 있고 또한 외부의 물체들과 계면에서의 이질감 없는 접촉이 가능하다는 장점이 있다. 또한 사람의 몸과 비교적 비슷한 특성의 물질로 제작되기 때문에 생체 모방이 가능하다는 점이 있고 제작에 있어서도 3D 프린팅과 같은 가격이 저렴한 다양한 프로세스를 통해 대량 생산이 가능하다는 이점도 있다. 이러한 다양한 이점과 다양한 분야로의 적용 가능성으로 인해 전세계적으로 소프트 로봇 시장은 급속도로 성장하고 있고 실제 소프트 로봇을 제작하는 회사도 설립되어 운영 중에 있다.

이러한 소프트 로봇 연구의 궁극적인 목적은 사람 혹은 생명체의 정교한 모사에 있다. 현재 다양한 생체 모사 소프트 로봇이

연구되고 또 제작되고 있다. 간단하게는 동물의 걷는 원리를 모사한 치타 모사 로봇부터, 소금쟁이 모사로봇, 애벌레 모사 로봇 등이 생명체의 움직임을 모사한 대표적인 예시이다. 뿐만 아니라 로봇에 작은 3D 프린터를 매립하여 로봇의 성장을 모사한 연구도 최근 보고되었다. 나아가 자가치유 고분자를 이용하여 생명체의 상처 회복을 모사한 소프트 로봇까지도 연구가 되고 있다. 그러나 이러한 연구들은 각각 하나의 기능만 모사가 되고 있는 실정이다. 그렇기 때문에 미래의 소프트 로봇은 생명체의 온전한 삶 전체를 모사하는 것이 목표가 되고 있다.

우리는 그 중 로봇의 죽음 모사에 집중하여 본인의 기능을 수행하다 최종적으로 로봇의 필요성이 사라지거나, 기능을 더 이상 하지 못하는 상황에서 최종적으로 분해되어 회복 불가능한 상태로의 전환을 진행하는 분해가능형 소프트 로봇에 대한 연구를 진행하였다. 이 연구의 진행에 있어서 로봇의 몸체의 대부분을 이루는 표준물질인 실리콘 기반의 가교 고분자가 가장 큰 문제로 작용하였다. 실리콘 가교 고분자는 강한 화학 결합을 통한 우수한 기계적 성질을 가질 뿐만 아니라 고온 및 화학 물질에 대한 저항성이 매우 뛰어나 소프트 로봇 분야에 많이 활용되고 있다. 그러나 이러한 화학 구조적 특징으로 인해 분해에 대한 어려움이 많았고, 이를 극복하기 위해 사람들은 물에 녹는 생분해성 고분자를 위주로 연구를 진행하여 왔다. 이러한 고분자는 물에 취약한 특성을 가질 뿐만 아니라 사용 환경에서의 분해반응으로 인해 제작과 동시에 두께의 조절을 통해 소재의 수명을 미리 결정해야 하는

치명적인 단점이 존재하였다.

이 연구에서 우리는 기존에 존재하는 기계적 특성이 좋은 다양한 고분자에 빛에 반응하면 산을 발생시키는 다양한 광산발생제를 첨가하여 우수한 기계적 특성을 가짐과 동시에 작동하는 동안 분해반응이 일어나지 않는 작동 안정성을 확보한 소재를 연구 개발하였다. 또한 해당 소재들에 대한 화학적, 열역학적 분석을 통해 분해반응에 대한 특정 조건에서의 정성화 및 정량화를 진행하였고 분해반응에 대한 매커니즘도 제시하였다. 뿐만 아니라 고분자에 외력에 반응하여 색이 변하는 자가진단 분자와, 낮은 에너지를 통해 치유가 가능한 자가치유 분자를 첨가 및 합성하여 최첨단 소프트 복합소재를 제시하였다. 나아가 해당 고분자 시스템을 이용하여 소프트 로봇과 전자소자에 적용하고 가상의 시나리오에서 작동시켜 실제 적용 가능성을 제시하였다.

주요어: 소프트 재료, 소프트 로봇, 소프트 전자소자, 고분자 공학, 유기 분석

학번: 2019-35593

Curriculum Vitae

Min-Ha Oh

Ph.D.

Department of Materials Science & Engineering

Bio-Interfaced Electronics Lab. (BIE)

Seoul National University

Education

2011 – 2017 .....(B.S.)

Department of Applied Organic Materials Science and Engineering

Inha University

2017 – 2019 ..... (M.S.)

School of Materials Science and Engineering

Gwangju Institute of Science and Technology (GIST)

2019 – 2023 ..... (Ph.D.)

Department of Materials Science and Engineering

Seoul National University

Acknowledgement

유난히 추웠던 2019년 1월 말, 서울대학교로 첫 등교하던 날이 아직도 생생하게 기억이 납니다. 등교하는 학생들로 꽉 찬 5511번 버스를 타고 학교 정문을 통과하면서 ‘세상에 이렇게 똑똑한 사람이 많았구나’라는 생각과 동시에 ‘내가 이 사람들처럼 함께 연구하고 공부하며 무사히 박사 과정을 마칠 수 있을까?’라는 생각을 했었습니다. 막연한 걱정과 함께 시작했던 학위과정을 무사히 마치고 이렇게 추억들을 되돌아보며 박사 학위 논문의 감사의 말을 작성하는 감회는 표현하기 힘들만큼 깊고 또 뭉클합니다. 주위 여러 도움이 있었기에 생각보다 많은 경험을 할 수 있었고, 또 좋은 연구를 다양하게 할 수 있었던 것 같습니다. 비록 짧은 감사의 말이지만, 그간 감사했던 마음을 담아 조금이나마 전달해 보려 합니다.

우선, 제가 학위 과정을 무사히 마칠 수 있도록 항상 도움을 주신 지도 교수님, 강승균 교수님께 감사의 말을 전합니다. 교수님께서는 당근보다 채찍을 많이 주는 것 같아 미안하다고 항상 말씀하셨지만 되돌아보면 그렇기 때문에 가끔 받는 당근의 맛이 더 달게 느껴졌고, 또 그 당근에 대한 진정성이 느껴졌던 것 같습니다. 가끔 교수님께서 저에게 ‘회사로 가서 아쉽다’, ‘연구를 더하면 좋을 것 같다’고 말씀해주실 때마다 저는 ‘교수님께 인정받고 있구나’, ‘내가 잘 하고 있구나’라는 생각이 들면서 자신감을 얻을 수 있었고 이것이 원동력이 되어 연구에 정진할 수 있었습니다. 교수님과 연구의 최전선에서 함께 고민하며

때로는 치열하게 토론하는 귀중한 경험을 할 수 있어서 기뻤고 또 행복했습니다. 학교에서 교수님과 연구하며 얻었던 좋은 기억과 자신감을 가지고 회사에 가서도 열심히 연구해보도록 하겠습니다. 비록 저는 회사로 떠나지만, 사제의 연은 여전히 남기에 자주 연락 드리고, 또 때때로 찾아 뵙겠습니다. 항상 건강하시고 앞으로도 행복하시길 기원하고 또 응원합니다.

저의 박사학위 논문심사의 심사위원장을 맡아 주신 안철희 교수님께도 깊은 감사의 말씀을 드립니다. 교수님의 좋은 코멘트 덕분에 저의 박사학위 논문의 질이 향상될 수 있었습니다. 또한 예비심사 및 종결심사에서도 다양한 칭찬으로 분위기도 풀어주신 덕분에 제가 긴장하지 않고 발표와 질의 응답을 이어갈 수 있었습니다. 교수님께서는 기억하시지 못하겠지만 교수님께서는 저의 입학면접의 면접관 이셨습니다. 저의 대학원 생활에서 가장 의미가 깊은 시작과 끝을 함께해 주셔서 진심으로 감사드립니다. 항상 건강하시길 기원합니다.

또한 저의 박사학위 논문심사의 심사위원이신 권민상 교수님께도 감사의 말씀을 전합니다. 학위심사 뿐만 아니라 저희 연구실이 유기화학 분야에 기반이 없어 어려움을 겪고 있을 때 귀중한 시간을 내어 미팅을 해주시면 제가 궁금한 부분들을 잘 알려주시고, 또 논문을 작성하는데 있어서 직접 반응식까지 그려 주시며 저에게 많은 도움을 주신 것까지 감사한 일이 정말 많습니다. 앞으로 저도 누군가가 도움을 요청할 때 교수님이 몸소 보여주신 것처럼 도와줄 수 있는 연구자가 되겠습니다. 항상 감사했고, 또 행복하시길 기원합니다.

저의 박사학위 논문심사의 심사위원이자 제가 학위과정 동안 진행한 모든 연구들의 시작을 함께해 주신 서강대학교 김상엽 교수님께도 감사의 말을 전합니다. 교수님이 저희 교수님과 주신 아이디어 덕에 좋은 논문도 작성하였고, 또 많은 후속 연구도 진행할 수 있었습니다. 자주 뵙지는 못했지만, 종종 화상미팅이나 실제 만날 때 마다 유쾌한 모습을 보여주시며 저를 편하게 대해 주셔서 항상 감사했습니다. 회사에 가서도 종종 과제 일로 만나게 되면 반갑게 인사드리겠습니다.

마지막 저의 박사학위 논문심사의 심사위원이신 아주대학교 고제성 교수님께도 감사의 말을 드립니다. 광교에서 꽤 먼 거리임에도 저와 교수님의 요청에 학교까지 와서 저의 학위심사에 참석해 주셔서 감사합니다. 교수님께서 종결심사에 하신 질문들이 많이 기억에 남습니다. 어쩌면 제가 박사학위과정 동안 잊고 지냈던 조금은 연구에 대한 본질적인 질문이었기에 기억에 남는 것 같습니다. 앞으로 연구할 때에도 제가 어떤 일을 어떻게 하고 있는지 고민해볼 수 있는 연구자가 될 수 있게 도와주셔서 진심으로 감사드립니다.

4년 동안의 연구실 생활에서 생각해보면 가장 많은 시간을 보냈던 사람들은 다름아닌 우리 연구실 형, 친구 그리고 동생들이었습니다. 가장 먼저 우리 연구실의 맏형인 성근이형, 매일 장난친다고 놀리는데 한 번도 화내지 않고 받아줘서 고마워요. 항상 형에게 독설을 했지만, 사실 형을 보면 항상 연구에 진심인 것이 느껴져서 ‘나는 한번이라도 저렇게 진심이었던 적이 있었던가’ 라는 반성을 가끔 했었어요. 지금도 너무 잘 하고 있고 앞으로 잘 될 거니까 걱정 말고 지금처럼 열정을 잃

지 말고 연구해주세요. 항상 진심으로 응원합니다. 나의 졸업 동기이자 우리 연구실 최 고참 주용이, 궂은 일에도 내색하지 않고 무슨 일이든 열심히 하는 너를 보며 동생이지만 참 많이 배웠던 것 같아. 함께 졸업을 위해 열심히 실험하던 것이 좋은 결실을 맺어 이렇게 무사히 졸업을 할 수 있어 너무 다행이고 또 고마워. 좋은 곳에 포닥가서 하고싶은 좋은 연구 많이 해서 지스트 교수로 돌아오길 응원할게. 또 다른 나의 졸업 동기이자 입학동기인 지오, 함께 랩장 부랩장 하면서 많이 싸우고 힘들었을 텐데 그래도 졸업 전에 많이 이야기하면서 풀어갈 수 있어서 다행이야. 우리 둘 다 무사히 졸업할 수 있어서 너무 기쁘고 다른 회사로 가지만 종종 연락하며 지내자. 회사생활도 진심으로 응원할게. 교수님의 애착인형 재영이, 항상 주말에도, 평일 늦은 밤에도 자리를 지키며 연구에 집중하는 너의 모습을 보며 대단하다는 생각을 많이 했어. 남은 한 학기 동안 준비하는 논문 좋은 곳에 실려서 원하는 그룹으로 포닥가길 기원할게. 연구실 애들은 너와 내가 어색하다고 놀리지만 사실 둘이 있을 때 하나도 안어색하잖아? 나 졸업하기 전에 잘 해명해보자. 우리 연구실 꼬마신랑 재환이, 같이 GRC 학회에 갔던게 엊그제 같은데 그게 벌써 3년반 전이네. 취미가 비슷해서 함께한 시간이 많았는데, 항상 즐겁게 같이 놀아줘서 고마워. 남은 기간 얼마 남지 않았지만 지금처럼 화이팅해서 무사히 졸업하길 바래. BIE 박효신 경섭이, 연구실 생활하면서 불편하기도 하고 또 불만도 많이 생겼을 텐데 내색하지 않고 최선을 다해 연구에 집중하는 모습을 보면서 동생이지만 많이 배웠던 것 같아. 어쩌다보니 나와 연구분야가 비슷해서 여러가지 일을 맡기고 떠나게 되었

는데, 필요한 부분이 있으면 언제든 연락하고 지금처럼 열심히 해서 잘 마무리 지어보자. 연구실 랩장 승민이, 랩장 일로 바쁜 와중에도 선배들을 배려해주고 또 논문 작업도 함께 열심히 해줘서 항상 고마웠어. 삼성 장학생 면접도 좋게 흘러가고 있는 것 같은데, 얼른 졸업해서 화성에서 봤으면 좋겠다. 연구실 부랩장 지우, 부랩장을 맡으면서 복잡하고 어려운 일들을 맡아 하며 조금은 힘들어 하는 것 같아서 마음이 쓰였어. 쓴소리도 했지만 마음에 담아주지 않고 남은 기간도 힘내서 연구실 생활 잘 해 나가길 바랄 게. 콜라 준석이, 맨날 장난친다고 괴롭혔는데 항상 즐겁게 웃으며 받아줘서 고마워. 연구실 모든 구성원들과 잘 지내는 것이 보기 좋고 앞으로도 스트레스 없이 지금처럼 연구실 생활 잘해 나갔으면 좋겠다. 공대 득점왕 윤남이, 같이 축구도 하고 게임도 하면서 재밌게 지내서 좋았어. 어쩌다 보니 내가 하는 연구의 일부를 맡아서 하게 되었는데도 책임감 있게 또 재밌게 해줘서 고마워. 같이 진행하는 연구도 좋은 결과 있을 수 있게 나도 같이 고민해볼 게. 카이스트에서 돌아온 지은이, 다른 연구실에서 석사를 하고 여기로 오는 결심이 쉽지 않았을 텐데 와서도 묵묵히 열심히 연구하는 모습을 보며 대단하다는 생각을 했던 것 같아. 앞으로도 파이팅하고 같이 진행하는 연구도 잘 마무리해서 좋은 결과 내어보자. 긍정왕 영인이, 항상 웃고 긍정적으로 연구실 생활을 하는 모습이 보기 좋은 것 같아. 키스트에서 어렵사리 넘어온 만큼 좋은 연구 많이 많이 하길 바랄게. 캐나다인 영서, 석튀할거라 항상 말하지만 끝까지 남아서 박사까지 할 거 다 알아. 지금처럼 열심히 끝까지 마무리해서 학위과정 잘 마무리하길 바랄게. 재입학한 명균이, 어려

운 약물전달 연구하느라 고생이 많아. 하던 대로 침착하게 연구해서 좋은 결과 나오길 빌게. 곧 미국으로 떠나는 준민이, 유기 분야를 같이 시작하는 입장에서 많은 도움을 줘서 고마워. 미국가서도 지금처럼 연구해서 한국으로 금의환향하길 바랄게. 몸무게 30 kg 세찌, 맨날 괴롭히고 장난 쳤는데 잘 받아주고 또 재밌게 놀아줘서 고마워. 앞으론 많이 먹고 살도 찌고 졸업하기 전에 50 kg 꼭 찍자. 파이팅! 과천의 자랑 주현이, 꾸준하게 지치지 않고 집중하는 모습을 보며 많이 배운 것 같아. 주용이한테 많이 배워서 좋은 연구자가 되길 빌게. 연구실 MZ 우진이, 어린 나이에 연구실에 와서 어려움이 많았을 텐데 잘 적응하고 있는 것 같아서 보기 좋아. 열심히 사회의 톱니바퀴가 되어 보자. 연고 보다 고연 좋아하는 이정이, 지금처럼 연구에 열중해서 하고 있는 연구 좋은 결과 얻길 바랄게. 술마시면 변하는 용우, 언제나 깍듯하고 예의 있는 모습을 보여줘서 좋았어. 여러 고생을 하고 있지만 지금처럼 하면 좋은 결과 있을거야 파이팅. 4층 동지 민성이형, 늦게 시작했지만 항상 진심으로 연구에 매진하는 형의 모습을 보며 많이 배우고 갑니다. 고민이 많으시겠지만 좋은 결과 있을 것이라 믿어 의심치 않아요. 맨날 어리다고 주장하는 유정이, 나이 차이 때문에 어려울 수 있을 텐데 편하게 대해줘서 고마워. 이제 시작인 만큼 지금의 마음가짐 잊지 말고 연구에 파이팅 하길 바랄 게. 졸업해서 먼저 사회에 나가 있는 예슬누나, 태경이도 항상 즐겁게 연구실 생활을 함께 해주어 감사합니다. 그 밖에 함께 얼마 하지 못한 BIE 인턴 식구들, 유림이, 도훈이, 성우, 명준이, 수환이, 석민이, 임덕이, 그리고 같이 연구해준 미국에 간 영환이부터 경미, 주호 모두에

게 이 기회를 빌려 감사의 말을 전합니다.

항상 만날 때 마다 즐겁게 놀 수 있어 연구하는데 스트레스를 해소시켜준 성신고등학교 공부방 친구들, 오랜 기간 공부하는 친구를 위해 부담되지 않게 항상 먼저 계산해주고, 배려해준 인하대학교 나노시스템공학부 동기들, 나의 연구하며 생긴 고충들을 들어주고 이해해준 GIST 석사 동기들과 OSPL 연구실 선후배님들, 모두에게 감사드리고 앞으로 차차 감사한 이 마음 갚아가도록 하겠습니다.

학위 과정 동안 옆에서 묵묵히 응원해준 여자친구 규나에게 감사의 말을 전합니다. 항상 긍정적으로 생각하고 말해주는 규나 덕분에 어렵고 힘든 학위 과정을 조금이나마 즐겁게 보낼 수 있었던 것 같아. 결혼 준비하면서 여러가지로 스트레스 많이 받았을 텐데 전혀 티 내지 않고 항상 배려해줘서 진심으로 고마워. 이제 정말 결혼이 얼마 남지 않았는데, 앞으로 함께할 날들도 지금처럼 많이 웃고 즐겁게 지내보자. 아직 미래가 정해지지도 않은 학위 과정 동안 규나와 만나는데도 한 번도 싫은 소리 않으시고 항상 격려와 응원을 아끼지 않고 해 주신 아버님, 어머님께도 감사의 말씀을 드립니다. 아버님과 어머님의 조건 없는 배려와 응원 덕분에 학위 과정 동안 편안하게 연구를 진행할 수 있었습니다. 앞으로 규나와 잘 살아 가면서 감사한 마음을 갚아가도록 하겠습니다. 항상 감사합니다.

멀리서 저를 응원하고 계실 친할아버지, 할머니께도 감사의 말씀 전합니다. 저에게 항상 힘이 되어 주신 외할머니, 그리고 하늘에 계신 외할아버지, 아주 어릴 적부터 항상 챙겨주시고 또 응원해 주셔서 감사

합니다. 생각해보면 할머니, 할아버지가 공부하는 저를 자랑스러워하실 때 마다 힘들었던 마음을 다잡고 원동력으로 삼아 앞으로 나아갔던 것 같습니다. 할아버지께 제가 졸업하는 모습을 보여드리지 못해 너무나 아쉽고 슬프지만, 하늘에서 지켜보고 계신다 생각하고 앞으로도 더욱 열심히 나아가 보겠습니다. 할머니, 저의 효도는 이제 겨우 시작이니 부디 건강하게 오래 곁에 계셔 주세요. 항상 감사하고 또 사랑합니다. 내 동생 나혜, 원하던 직업도 얻고 결혼도 하고 심지어 오빠 용돈도 주는 너를 보면 너가 나보다 더 어른인 것 같다는 생각을 많이 하고 또 그게 많이 미안했던 것 같아. 우리 둘 다 가정이 생겨서 자주 보지는 못하겠지만, 언제든 필요한 게 있으면 연락하고 사회로 나가는 이제부터는 오빠 노릇을 제대로 시작해 볼게. 애정하고 또 응원한다. 제부, 제가 어린 형님인 데도 항상 존중해주셔서 감사해요. 앞으로도 나혜 잘 부탁드리고, 또 회사 생활 선배로써 많은 조언 부탁드리겠습니다. 항상 응원합니다.

마지막으로 30년이라는 긴 세월 동안 아들의 뒷바라지하시느라 가장 고생이 많으셨던 아버지 그리고 어머니, 어떠한 말도 저의 감사함을 표현하기에는 부족한 것 같습니다. 태어나서부터 박사학위를 받는 이 순간까지 매 순간에는 어머니, 아버지의 희생이 있었고 헌신이 있었고 또 사랑이 있었습니다. 항상 어떤 부분이든 지원해주시고 공부에 전념할 수 있는 환경을 만들어 주신 덕에 지금의 제가 있을 수 있었습니다. 혼자 한 것은 아무것도 없다는 사실을 잊지 않고 지금의 감사한 마음을 차차 갚아가도록 하겠습니다. 건강하게 또 행복하게 오래오래 곁에 있어 주세요. 항상 감사하고 또 마음 속 깊이 사랑합니다.